NASA CONTRACTOR REPORT

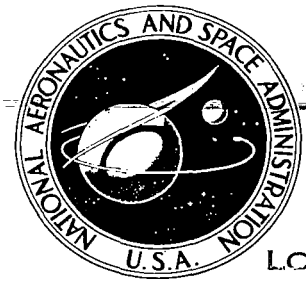

NASA CR-2826

ATMOSPHERIC ENERGETICS IN REGIONS OF INTENSE CONVECTIVE ACTIVITY

Henry E. Fuelberg

Prepared by
TEXAS A&M UNIVERSITY
College Station, Tex. 77843
for George C. Marshall Space Flight Center

NATIONAL AERONAUTICS AND SPACE ADMINISTRATION • WASHINGTON, D. C. • MARCH 1977

1. REPORT NO.	2. GOVERNMENT ACCESSION NO.	3. RECIPIENT'S CATALOG NO.
NASA CR-2826		

4. TITLE AND SUBTITLE	5. REPORT DATE
Atmospheric Energetics in Regions of Intense Convective Activity	March 1977
	6. PERFORMING ORGANIZATION CODE

7. AUTHOR(S)	8. PERFORMING ORGANIZATION REPORT #
Henry E. Fuelberg	M-213

9. PERFORMING ORGANIZATION NAME AND ADDRESS	10. WORK UNIT NO.
Center for Applied Geosciences College of Geosciences Texas A&M University College Station, Texas 77843	11. CONTRACT OR GRANT NO. NAS8-31773

12. SPONSORING AGENCY NAME AND ADDRESS	13. TYPE OF REPORT & PERIOD COVERED
National Aeronautics and Space Administration Washington, D. C. 20546	Contractor
	14. SPONSORING AGENCY CODE

15. SUPPLEMENTARY NOTES

16. ABSTRACT

Synoptic-scale budgets of kinetic and total potential energy are computed using 3- and 6-h data at nine times from NASA's fourth Atmospheric Variability Experiment (AVE IV) conducted on 24-25 April 1975. Two intense squall lines occurred during the period.

Energy budgets for areas as small as 8.0×10^{11} m^2 that enclose regions of intense convection are shown to have systematic changes that relate to the life cycles of the convection. Some of the synoptic-scale energy processes associated with the convection are found to be larger than those observed in the vicinity of mature cyclones.

Volumes enclosing intense convection are found to have large values of cross-contour conversion of potential to kinetic energy and large horizontal export of kinetic energy. Although small net vertical transport of kinetic energy is observed, values at individual layers indicate large upward transport. Transfer of kinetic energy from grid to subgrid scales of motion occurs in the volumes. Latent heat release is large in the middle and upper troposphere and is thought to be the cause of the observed cyclic changes in the budget terms. Total potential energy is found to be imported horizontally in the lower half of the atmosphere, transported aloft, and then exported horizontally. Although local changes of kinetic energy and total potential energy are small, interaction between volumes enclosing convection with surrounding larger volumes is quite large.

Spatial fields of terms in the energy budget equations are shown at three times. These have good continuity and are closely related to the locations and intensities of the two squall lines.

17. KEY WORDS	18. DISTRIBUTION STATEMENT
	47

19. SECURITY CLASSIF. (of this report)	20. SECURITY CLASSIF. (of this page)	21. NO. OF PAGES	22. PRICE
Unclassified	Unclassified	148	$6.00

* For sale by the National Technical Information Service, Springfield, Virginia 22161

FOREWORD

This report is one of several to be published from research conducted under NASA Contract NAS8-31773 entitled, "Relationships Between Severe Storms and Their Environment." This effort is sponsored by the NASA Office of Applications under the direction of Marshall Space Flight Center's Aerospace Environment Division. The results presented in this report represent only a portion of the total research effort. Data used in the report were taken from the AVE IV Experiment conducted during the period beginning at 0000 GMT on 24 April 1975 and ending at 1200 GMT on 25 April 1975.

TABLE OF CONTENTS

TABLE OF CONTENTS (Continued)

TABLE OF CONTENTS (Continued)

LIST OF FIGURES

LIST OF FIGURES (CONTINUED)

LIST OF FIGURES (CONTINUED)

LIST OF TABLES

LIST OF SYMBOLS

SCALARS

A	horizontal cross-sectional area of an atmospheric volume, i.e., $dA = dxdy$
A''	dummy variable of integration that corresponds to A
b	any arbitrary scalar defined in the atmosphere
c_p	specific heat at constant pressure
c_v	specific heat at constant volume
C_A	conversion between kinetic energy and potential energy due to vertical redistribution of mass, A-conversion
C_K	conversion between kinetic energy and potential energy due to cross-contour flow, K-conversion
$\frac{dH}{dt}$	diabatic heating per unit mass
D	dissipation of kinetic energy
F	arbitrary function
g	acceleration due to gravity
G	generation of total potential energy due to diabatic effects
HF_K	horizontal boundary flux of kinetic energy
HF_Π	horizontal boundary flux of total potential energy
I	internal energy of a limited atmospheric volume
K	kinetic energy of a limited atmospheric volume
K'	kinetic energy of the atmospheric volume surrounding the limited volume
p	atmospheric pressure
P	gravitational potential energy of a limited atmospheric volume

PW	pressure work at the boundary which also represents the interaction of the limited atmospheric volume with the surrounding volume
R	gas constant
T	temperature
V	a limited volume of the atmosphere
V"	a dummy variable of integration for volume integrals
VF_K	vertical boundary flux of kinetic energy
VF_Π	vertical boundary flux of total potential energy
w	vertical component of $\vec{V}$, $w = \frac{dz}{dt}$
w_R	vertical velocity in a hydrostatic atmosphere
(x,y,z)	Cartesian coordinates
X,Y,Z	arbitrary variables
α	specific volume
Π	total potential energy of a limited atmospheric volume, $\Pi = P+I$
Π'	total potential energy of the atmospheric volume surrounding the limited volume
ρ	density
σ	RMS error
ω	vertical velocity, $\omega = \frac{dp}{dt}$

LIST OF SYMBOLS (CONTINUED)

VECTORS

$\vec{F}$	three-dimensional frictional force
$\vec{F}_2$	two-dimensional frictional force with the vertical component excluded
$\vec{V}$	three-dimensional wind vector
$\vec{V}_2$	two-dimensional wind vector with the vertical component excluded
$\vec{\nabla}$	three-dimensional del operator
$\vec{\nabla}_2$	two-dimensional del operator with the vertical component excluded
$\vec{\nabla}_p$	two-dimensional del operator on a constant pressure surface

ATMOSPHERIC ENERGETICS IN REGIONS OF INTENSE CONVECTIVE ACTIVITY

By Henry E. Fuelberg[1]
Center for Applied Geosciences, Texas A&M University

1. STATEMENT OF THE PROBLEM

a. Introduction

A knowledge of atmospheric energetics is basic to an understanding of the atmosphere. All atmospheric processes, ranging from the largest circulation systems down to the smallest turbulent motions, are accompanied by changes in energy. An understanding of the interaction of the energy of these various scales of motion will help explain and forecast many weather phenomena that presently are not understood. Thunderstorms are important daily weather producers which generate large quantities of energy, but the role of thunderstorms in the atmospheric energy budget is not understood well. This research assesses the impact of two large, intense squall lines on the synoptic-scale budgets of potential and kinetic energy during stages of squall line development. The use of rawinsonde data at 3- and 6-h intervals permits the temporal resolution of features that ordinarily would be unresolvable with the 12-h data that are routinely available.

b. Previous studies

The literature reveals that most research in atmospheric energetics has focused on large-scale systems, but suggests that small-scale systems, such as convective areas, may be important features of the large-scale energy budgets.

1) The energetics of large-scale areas

Oort (1964), after reviewing the work of previous investigators, described the atmosphere's primary energy cycle as beginning with the creation of mean available potential energy due to diabatic processes, which is then converted to eddy available potential energy, eddy kinetic energy, and finally to mean kinetic energy. The annual cycle of atmospheric energetics in the northern hemisphere over a 5-year period has been described by Oort and Peixóto (1974), and Peixóto and Oort (1974). Numerous studies have considered average energy conditions over specific large

---

[1] Graduate Assistant

areas of the earth and/or for time periods shorter than five years; some of these are the available potential energy budget over the tropical Atlantic Ocean (Vincent, 1974), the kinetic energy balance over the tropical Pacific Ocean (Kung, 1974), and the energetics over North America (Kung, 1970).

2) The energetics of limited areas

Individual synoptic-scale systems with wavelengths of several thousand kilometers and lifetimes of several days are important components of the average energy budget computed over large areas and long time periods. Energetics research for such limited areas of the atmosphere is complicated by the presence of boundary-flux terms which vanish when the entire atmosphere is under consideration.

Numerous studies dealing with the kinetic energy budgets of individual cyclones have been conducted. A summary of this work is provided by Kung and Smith (1974) who noted that a single mature cyclone system can account for 1/4 to 1/3 of the middle-latitude energetics. Recent studies of individual cyclones have been made by Ward and Smith (1976) and Kornegay and Vincent (1976). A major conclusion reached by Vincent et al. (1974) in their kinetic energy study of Hurricane Celia was that the energy budget was dependent on the volume size used to contain the area of interest. This problem is overcome when values of terms in the energy budget equations are presented throughout the spatial and temporal extent of a cyclone instead of presenting them in terms of averages only. Such results have been given by West (1973) and Ward and Smith (1976) who could track in both time and space the important energetic processes of developing cyclones. Smith (1973a) studied the kinetic energy budget of an anticyclone and found it to be a tranquil circulation system when compared to cyclones.

Several studies have considered various aspects of the potential energy budget of limited areas. Smith and Horn (1969) described the complete available potential energy budget for North America during March 1962, while West (1973) studied the budget of total potential energy during two cases of cyclogenesis. Gommel (1973) presented values of terms describing the conversion of

available potential energy in Hurricane Celia, while Kung (1974) has done the same for an area over the tropical Pacific Ocean. The effect of geographical heat sources and sinks on the generation of available potential energy has been studied by such authors as Gall and Johnson (1971), Bullock and Johnson (1971), and Anthes and Johnson (1968).

3) The energetics of areas of convection

Research indicates that areas of intense convection produce effects on the surrounding atmospheric volumes that can be detected using synoptic-scale data. Aubert (1957) showed that latent heat release associated with thunderstorms produced increases in large-scale horizontal convergence below the level of maximum condensation and enhanced horizontal divergence above that level. He found decreases in values of geopotential height in the lower troposphere and increases in the upper troposphere. Ninomiya (1971a and b), using satellite pictures, found that the pre-existing flow at the cirrus level over tornado-producing thunderstorms changed into outflow as the thunderstorms developed. The existence of a midtropospheric warm core and a significant field of convergence below 700 mb was observed using synoptic-scale rawinsonde data, and the downward convective transport of horizontal momentum was shown to intensify the low-level jet stream. Each of these phenomena was attributed to latent heat release. Fankhauser (1971) indicated that mature thunderstorms may divert and distort mid-tropospheric air motion in a manner similar to that of solid objects. While several authors have indicated that latent heat release is important in offsetting the frictional effects in a developing cyclone (Bullock and Johnson, 1971; Danard, 1964, 1966), Tracton (1973) and West (1973) have suggested that latent heat release plays a critical role in initiating cyclogenesis in some instances.

Since research has shown that areas of convection affect synoptic-scale fields of kinematic and thermodynamic quantities, the energy budget should be affected also, but surprisingly little work has been conducted to describe the energy changes. Danard

(1964, 1966) used numerical methods with and without the inclusion of latent heat to compute the effects of a large precipitation area on certain energy budget terms. The production of kinetic energy due to rising air and cross-contour flow was enhanced considerably by latent heat release whose effect was of the same order of magnitude as that caused solely by dry adiabatic processes. The kinetic energy budget of atmospheric volumes surrounding trade wind cloud clusters in the Pacific Ocean has been investigated by Williams (1970) who found them to be vertical transporters of kinetic energy with little internal generation or dissipation. Kinetic energy was found to be imported in the lower half of the troposphere, transported upward within the convective clouds, and exported in the upper tropospheric outflow. The kinetic energy budget for clear areas was considerably different from that of the clusters.

The kinetic energy budget of volumes enclosing areas of convection within the central United States has been presented by McInnis and Kung (1972) using data from the rawinsonde network operated by the National Severe Storms Laboratory (NSSL). Their results were reported in terms of spatial averages for the entire NSSL area at various pressure levels and times. Kinetic energy generation and dissipation were found to be maxima in the lower troposphere and at the jet stream level. Horizontal inflow and vertical outflow occurred in the lower and middle troposphere while horizontal outflow and vertical inflow were found near the jet stream level.

Much remains to be learned about the energetics of all scales of motion, but additional studies dealing with scales smaller than synoptic, such as convection, would appear to be especially useful.

c. Objectives

The objective of this research was to test the hypothesis that systematic changes occur in the synoptic-scale energy budgets of atmospheric volumes enclosing areas of intense convection, and that these changes are related to the life cycle of the convective

areas and can be tracked in space and time.

To accomplish the objective it was necessary to:

1) Use energy budget equations that define energetics in a limited region of the atmosphere and that allow the computation of boundary fluxes of energy and the interaction of the convective area with its surroundings.

2) Develop analytical procedures for evaluating the energy equations that yield accurate results without requiring excessive smoothing that would destroy significant features.

3) Compute spatial fields of terms in the energy budget equations at various pressure levels during the formation, maintenance, and dissipation of areas of intense convection. This was done to relate the locations and magnitudes of the energetic processes to the locations and life cycles of the convective activity and other weather systems.

4) Compute average energy budgets for volumes of various sizes that enclose areas of convection and nonconvection so that results of this investigation could be compared with those of meteorological systems of large scales. The influence of intense convection on these systems could then be assessed.

2. THEORETICAL DEVELOPMENT

The energy budget equations used in this study were proposed by West (1973) based on suggestions by Smith (1970). Individual terms of the equations represent physical processes that lead to changes in atmospheric energy and provide a means to study the interaction of the limited volumes under consideration with larger volumes. Highlights of West's (1973) derivation of these equations along with certain modifications are given in this section.

A limited atmospheric volume, V, possesses internal energy, I, due to its temperature, T; gravitational potential energy, P, due to its height, z; and kinetic energy, K, due to its vector velocity, $\vec{V}$. These forms of energy are given by

$$I = \int_V c_v \rho T dV", \tag{1}$$

$$P = \int_V g\rho z dV" \qquad \text{and,} \tag{2}$$

$$K = \int_V \rho \frac{\vec{V}\cdot\vec{V}}{2} dV", \tag{3}$$

where c_v is specific heat at constant volume, ρ is density, g is the acceleration of gravity, and V" is a dummy variable of integration for volume integrals.

Wiin-Nielsen (1968), using the equation of mass continuity, presented the following equation that is applicable for a volume extending over a limited region of the atmosphere:

$$\int_V \frac{\partial(b\rho)}{\partial t} dV" = \int_V \rho \frac{\partial b}{\partial t} dV" + \int_V b \frac{\partial \rho}{\partial t} dV"$$

$$= \int_V \rho \frac{\partial b}{\partial t} dV" - \int_V b\vec{\nabla}\cdot(\rho\vec{V}) dV", \tag{4}$$

where b is any arbitrary scalar defined in the atmosphere, t is time, and $\vec{\nabla}$ is the three-dimensional del operator. This equation may also be written as

$$\int_V \frac{\partial (b\rho)}{\partial t} dV'' = \int_V \rho \frac{\partial b}{\partial t} dV'' - \int_V \vec{\nabla} \cdot (b\rho \vec{V}) dV'' + \int_V \rho \vec{V} \cdot \vec{\nabla} b dV'', \qquad (5)$$

or

$$\int_V \frac{\partial (b\rho)}{\partial t} dV'' = \int_V \rho \frac{db}{dt} dV'' - \int_V \vec{\nabla} \cdot (\rho b \vec{V}) dV''. \qquad (6)$$

The last term in (6) is a boundary term that would vanish if integration were performed over the entire atmosphere.

When (6) is applied to (1) and the boundary of the volume is fixed in space, the time rate-of-change of internal energy is given by

$$\frac{\partial I}{\partial t} = \int_V c_v \rho \frac{dT}{dt} dV'' - \int_V \vec{\nabla} \cdot (\rho c_v T \vec{V}) dV''. \qquad (7)$$

An expression for $c_v \frac{dT}{dt}$ can be obtained by combining the thermodynamic equation with the continuity equation. Equation (7) can then be written as

$$\frac{\partial I}{\partial t} = \int_V \rho \frac{dH}{dt} dV'' - \int_V p \vec{\nabla} \cdot \vec{V} dV'' - \int_V \vec{\nabla} \cdot (\rho c_v T \vec{V}) dV'', \qquad (8)$$

where $\frac{dH}{dt}$ is diabatic heating per unit mass and p is atmospheric pressure.

When (6) is applied to (2), the time rate-of-change of potential energy for a fixed volume is given by

$$\frac{\partial P}{\partial t} = \int_V g\rho w dV'' - \int_V \vec{\nabla} \cdot (g\rho z \vec{V}) dV'', \qquad (9)$$

where w is the vertical component of $\vec{V}$.

Finally, when (6) is applied to (3) and substitutions are made from the vector equation of motion, the time rate-of-change of kinetic energy for a fixed volume can be written as

$$\frac{\partial K}{\partial t} = -\int_V \vec{V}\cdot\vec{\nabla}p\,dV" - \int_V \rho g w\,dV"$$

$$+ \int_V \vec{V}\cdot\vec{F}\,dV" - \int_V \vec{\nabla}\cdot\left[\rho\,\frac{\vec{V}\cdot\vec{V}}{2}\,\vec{V}\right] dV", \qquad (10)$$

where $\vec{F}$ is the three-dimensional frictional force.

The first term on the right hand side of (10) and the second term on the right hand side of (8) represent the conversion between I and K in a limited volume if there is no boundary effect. These two "conversion" terms and the boundary term are related by

$$\int_V p\vec{\nabla}\cdot\vec{V}\,dV" + \int_V \vec{V}\cdot\vec{\nabla}p\,dV" = \int_V \vec{\nabla}\cdot p\vec{V}\,dV". \qquad (11)$$

The term on the right hand side of (11) usually is referred to as the pressure work term or the boundary work term and vanishes when integration is performed over the entire atmosphere if the lower boundary is rigid. Smith (1970) has shown that the boundary term also can be interpreted as the interaction of a limited volume with the surrounding volume. When (11) is substituted into (8), one obtains

$$\frac{\partial I}{\partial t} = \int_V \rho\,\frac{dH}{dt}\,dV" + \int_V \vec{V}\cdot\vec{\nabla}p\,dV" - \int_V \vec{\nabla}\cdot p\vec{V}\,dV"$$

$$- \int_V \vec{\nabla}\cdot(\rho c_v T\vec{V})\,dV". \qquad (12)$$

The hydrostatic approximation is applied since it already has been used in computing the rawinsonde data that serve as input for the budget equations. The assumption is a potential source of distortion in this research since convective cells undergo non-hydrostatic vertical accelerations, but steps were taken to lessen this potential problem (see Section 3).

The vertical component of K becomes irrelevant in the energy

budgets when the hydrostatic approximation is made and may be neglected (Wiin-Nielsen, 1968) such that the symbol K now represents only the horizontal component of kinetic energy. The vertical velocity required to maintain hydrostatic equilibrium is then denoted by w_R. With this assumption the equations for I, P, and K become

$$\frac{\partial I}{\partial t} = \int_V \rho \frac{dH}{dt} dV'' + \int_V \vec{V}_2 \cdot \vec{\nabla}_2 p dV'' + \int_V w_R \frac{\partial p}{\partial z} dV'' - \int_V \vec{\nabla} \cdot p\vec{V} dV'' - \int_V \vec{\nabla} \cdot (\rho c_v T \vec{V}) dV'', \tag{13}$$

$$\frac{\partial P}{\partial t} = \int_V \rho g w_R dV'' - \int_V \vec{\nabla} \cdot (g \rho z \vec{V}) dV'', \quad \text{and} \tag{14}$$

$$\frac{\partial K}{\partial t} = - \int_V \vec{V}_2 \cdot \vec{\nabla}_2 p dV'' + \int_V \vec{V}_2 \cdot \vec{F}_2 dV'' - \int_V \vec{\nabla} \cdot \left[\rho \frac{\vec{V}_2 \cdot \vec{V}_2}{2} \vec{V} \right] dV'', \tag{15}$$

where

$$K = \int_V \rho \frac{\vec{V}_2 \cdot \vec{V}_2}{2} dV'', \tag{16}$$

$\vec{\nabla}_2$ is the two-dimensional del operator, $\vec{F}_2$ is the two-dimensional frictional force, and $\vec{V}_2$ is the horizontal wind vector. The potential and internal energies for the entire vertical column of a hydrostatic atmosphere remain in a constant ratio (Petterssen, 1956) and are given by $P = \frac{R}{c_v} I$ where R is the gas constant.

Total potential energy, Π, is defined as the sum of internal energy and gravitational potential energy and is given by

$$\Pi = \int_V \rho T c_p dV''. \tag{17}$$

When (13) and (14) are added, one obtains the time rate-of-change of total potential energy for a fixed volume,

$$\frac{\partial \Pi}{\partial t} = \int_V \rho \frac{dH}{dt} dV'' + \int_V \vec{V}_2 \cdot \vec{\nabla}_2 p dV'' - \int_V \vec{\nabla} \cdot p\vec{V} dV'' - \int_V \vec{\nabla} \cdot (\rho c_v T \vec{V}) dV'' - \int_V \vec{\nabla} \cdot (\rho g z \vec{V}) dV''. \tag{18}$$

The sum of the last two terms on the right hand side of (18) was approximated by the term $\int_V \vec{\nabla}\cdot(\rho c_p \vec{T}\vec{V})\,dV''$, where c_p is specific heat at constant pressure. Sample calculations indicate that values obtained using the last two terms of (18) are smaller than those obtained using the approximation in the lower and middle troposphere and are larger than the approximate values in the upper troposphere and stratosphere. However, values obtained from the two methods generally differ less than 25% so that conclusions based on the approximation are not affected significantly.

Transformation into the x, y, p, t system provides the final equations for the horizontal component of kinetic energy and total potential energy of a fixed volume which are, respectively,

$$K = \frac{1}{g}\int_A\int_p \frac{\vec{V}_2\cdot\vec{V}_2}{2}\,dpdA'', \tag{19}$$

and

$$\Pi = \frac{c_p}{g}\int_A\int_p T\,dpdA'', \tag{20}$$

where A is the horizontal cross-sectional area of V and A" is a dummy variable of integration corresponding to A.

When (18) with its approximation and (15) are transformed into the x, y, p, t system, terms of the type $b\vec{V}_2\cdot\vec{\nabla}_p\rho$, $\frac{\partial(\rho b\vec{V}_2)}{\partial z}\cdot\vec{\nabla}_p z$, and $b\omega\frac{\partial\rho}{\partial p}$ occur, where b is an arbitrary scalar. These terms can be neglected because they are generally two to four orders of magnitude smaller than the remaining terms. Equations (18) and (15) then become, respectively,

$$\frac{\partial\Pi}{\partial t} = \overbrace{\frac{1}{g}\int_A\int_p \frac{dH}{dt}\,dpdA''}^{G} + \overbrace{\int_A\int_p \vec{V}_2\cdot\vec{\nabla}_p z\,dpdA''}^{C_K} - \overbrace{\frac{R}{g}\int_A\int_p \left[\vec{\nabla}_p\cdot T\vec{V}_2 + \frac{\partial}{\partial p}(T\omega)\right]dpdA''}^{PW} - \overbrace{\frac{c_p}{g}\int_A\int_p \vec{\nabla}_p\cdot T\vec{V}_2\,dpdA''}^{HF_\Pi} - \overbrace{\frac{c_p}{g}\int_A\int_p \frac{\partial}{\partial p}(T\omega)\,dpdA''}^{VF_\Pi}, \tag{21}$$

and

$$\frac{\partial K}{\partial t} = \overbrace{-\int_A \int_p \vec{V}_2 \cdot \vec{\nabla}_p z \, dp dA''}^{C_K} + \overbrace{\frac{1}{g} \int_A \int_p \frac{1}{\rho} \vec{V}_2 \cdot \vec{F}_2 dp dA''}^{D} \tag{22}$$

$$\overbrace{-\frac{1}{g} \int_A \int_p \vec{\nabla}_p \cdot \left[\frac{\vec{V}_2 \cdot \vec{V}_2}{2} \vec{V}_2 \right] dp dA''}^{HF_K} \overbrace{- \frac{1}{g} \int_A \int_p \frac{\partial}{\partial p} \left[\frac{\vec{V}_2 \cdot \vec{V}_2}{2} \omega \right] dp dA''}^{VF_K}$$

where $\omega = \frac{dp}{dt}$ and $\vec{\nabla}_p$ is the two-dimensional del operator on a constant pressure surface.

The terms in (21) and (22) represent the following physical processes. The terms are denoted by symbolic notation which does not include negative signs. Term G in (21) represents generation of potential energy due to diabatic effects. Conversion between kinetic and total potential energy due to cross-contour flow is denoted by term C_K in (21) and (22). Term PW of (21) defines pressure work at the boundary which also represents interaction of the limited volume with the surrounding volume. The horizontal and vertical components of the boundary flux of total potential energy are given by terms HF_Π and VF_Π of (21). Finally, $\frac{\partial \Pi}{\partial t}$ is the local change of total potential energy that results from the processes just described. Sample calculations indicated that term $\frac{\partial \Pi}{\partial t}$ generally was several orders of magnitude smaller than the largest terms in (21). It will therefore not be included in subsequent discussions.

Local changes in the horizontal component of kinetic energy, $\frac{\partial K}{\partial t}$, in (22) are due to four processes. Term C_K has been described previously as conversion between the two forms of energy. The dissipation of kinetic energy is denoted by term D. The exact interpretation of this term is dependent on its method of computation and is described in greater detail in Section 3. Terms HF_K and VF_K represent the horizontal and vertical boundary fluxes of kinetic energy.

Another quantity that is of interest is the release of available potential energy which is given by

$$C_A = \int_A \int_p \frac{\omega \alpha}{g} \, dp dA" \quad ,$$

where α is specific volume. This term, which Smith (1969) calls A-conversion, represents changes in available potential energy due to the vertical redistribution of mass within the volume. Many published papers have used this term to represent energy conversion instead of the term C_K, which Smith (1969) calls K-conversion. Term C_A represents direct conversion between potential and kinetic energy only if there is no boundary effect. The interaction between the limited volume and the surrounding volume can be inferred by comparing the values of terms C_A and C_K.

Figure 1 is a schematic representation of the energy processes that are described in (21) and (22); it is a modified version of a figure presented by Smith (1970). The solid boxes represent the limited atmospheric volume while the dashed boxes denote the surrounding volume.

Equations (19) to (22) are the energy budget equations that were used to investigate the relationship between energy processes and areas of intense convection.

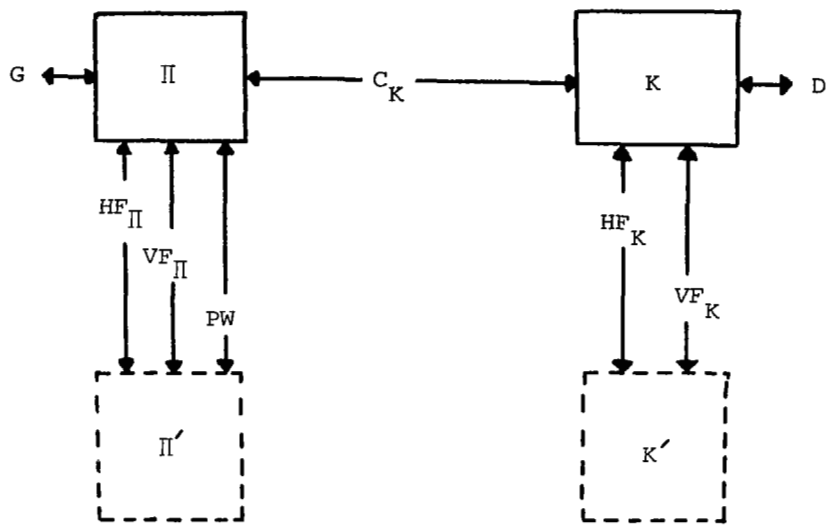

Fig. 1. Energy transformations for a limited volume.

3. DATA AND ANALYTICAL PROCEDURES

a. AVE IV experiment

A data set at time intervals smaller than the usual 12-h interval and encompassing a period of intense convective activity was needed for this study. Data from the fourth Atmospheric Variability Experiment (AVE IV) conducted on 24-25 April 1975, and sponsored by the National Aeronautics and Space Administration (NASA) met these requirements.

1) Rawinsonde data

Forty-two rawinsonde stations participated in the AVE IV experiment; these are shown in Fig. 2 and listed in the Appendix. Soundings were taken at nine times--24 April at 0000 GMT, 0600 GMT, 1200 GMT, 1500 GMT, 1800 GMT, and 2100 GMT, and on 25 April at 0000 GMT, 0600 GMT, and 1200 GMT.

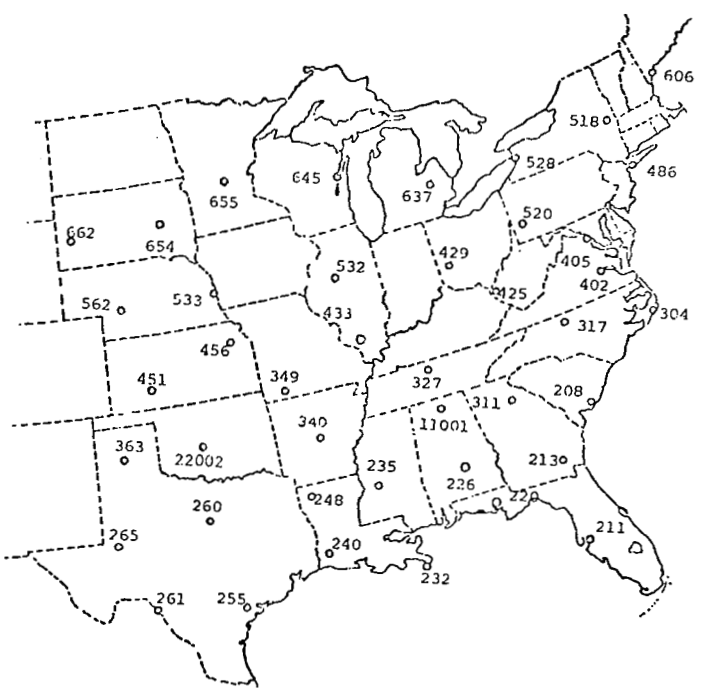

Fig. 2. Rawinsonde stations participating in the AVE IV experiment.

Data reduction procedures used to process the AVE IV rawinsonde data were designed to obtain the most accurate results possible (Fuelberg, 1974). The raw angle and ordinate data were checked for errors prior to calculating the soundings, and computed soundings then were rechecked with corrections made as required. Data were given at 25-mb intervals by Fucik and Turner (1975). Estimates of RMS errors of the thermodynamic quantities are given in Table 1 (Scoggins and Smith, 1973; Fuelberg, 1974).

Table 1. RMS errors of thermodynamic quantities for the AVE IV data.

Parameter	Approximate RMS error
Temperature	1°C
Pressure	1.3 mb surface to 400 mb 1.1 mb between 400 and 100 mb 0.7 mb between 100 and 10 mb
Humidity	10%
Pressure Altitude	10 gpm at 500 mb 20 gpm at 300 mb 50 gpm at 50 mb

Recent studies have indicated that errors in the thermodynamic quantities may be even smaller than those given in Table 1 (Lenhard, 1973; Brousaides, 1975).

An error analysis conducted by Fuelberg (1974) gave RMS errors of scalar wind speed and wind direction for the AVE IV baroswitch contact data. Table 2 presents these RMS errors for elevation angles of 40° and 20°. RMS errors for the smoothed 25-mb data that were used in this study would be somewhat smaller.

Original strip charts from all rawinsonde soundings were checked carefully to determine if sondes entered thunderstorm updrafts or downdrafts. Data for four soundings were removed from the original data set because the sondes apparently had entered violent updrafts. The potential for distorted results due to nonhydrostatic accelerations was thereby considerably reduced.

Table 2. RMS errors of baroswitch contact wind data for the AVE IV data at elevation angles of 40° and 20°.

Level	Elevation Angle 40° RMS Direction Error	Elevation Angle 20° RMS Direction Error	Elevation Angle 40° RMS Speed Error	Elevation Angle 20° RMS Speed Error
700 mb	1.8°	3.8°	0.5 m s^{-1}	1.0 m s^{-1}
500 mb	2.5°	5.6°	0.8 m s^{-1}	2.0 m s^{-1}
300 mb	3.1°	7.5°	1.0 m s^{-1}	3.8 m s^{-1}
100 mb	6.2°	15.0°	2.0 m s^{-1}	5.7 m s^{-1}

2) Surface data

All available surface data for the AVE IV experiment were obtained from the National Climatic Center. Figure 3 shows locations of the 310 surface stations used. Vector wind, temperature, dew point temperature, and surface pressure were read, keypunched, and checked carefully for errors.

Fig. 3. Locations of surface stations for the AVE IV area.

3) Digital radar data

Manually Digitized Radar (MDR) data were obtained from NOAA's Techniques Development Laboratory to determine accurately the intensity and position of the radar-observed convection during the AVE IV experiment. The MDR grid network is shown in Fig. 4. MDR data are coded with a single digit from 0 to 9 to indicate areal coverage and echo intensity within blocks that are approximately 83 km on a side. Table 3 is an explanation of the MDR code given by Foster and Reap (1973).

Table 3. Manually digitized radar (MDR) data code (Foster and Reap, 1973).

Code No.	Maximum Observed VIP[1] Values	Coverage In Box	Maximum Rainfall Rate (in h^{-1})	Intensity Category
0	No Echoes			
1	1	Any VIP1	<0.1	Weak
2	2	≤ 50% of VIP2	0.1-0.5	Moderate
3	2	> 50% of VIP2	0.5-1.0	Moderate
4	3	≤ 50% of VIP3	1.0-2.0	Strong
5	3	> 50% of VIP3	1.0-2.0	Strong
6	4	≤ 50% of VIP3 and 4	1.0-2.0	Very Strong
7	4	> 50% of VIP3 and 4	1.0-2.0	Very Strong
8	5 or 6	≤ 50% of VIP3, 4, 5, and 6	>2.0	Intense or Extreme
9	5 or 6	> 50% of VIP3, 4, 5, and 6	>2.0	Intense or Extreme

[1]Video Integrator Processor

Plots of the MDR data were made each hour for 3-h periods centered on each of the nine rawinsonde observation times. The three plots were then combined into a single chart for each of the nine times by using the highest coded value reported for each block.

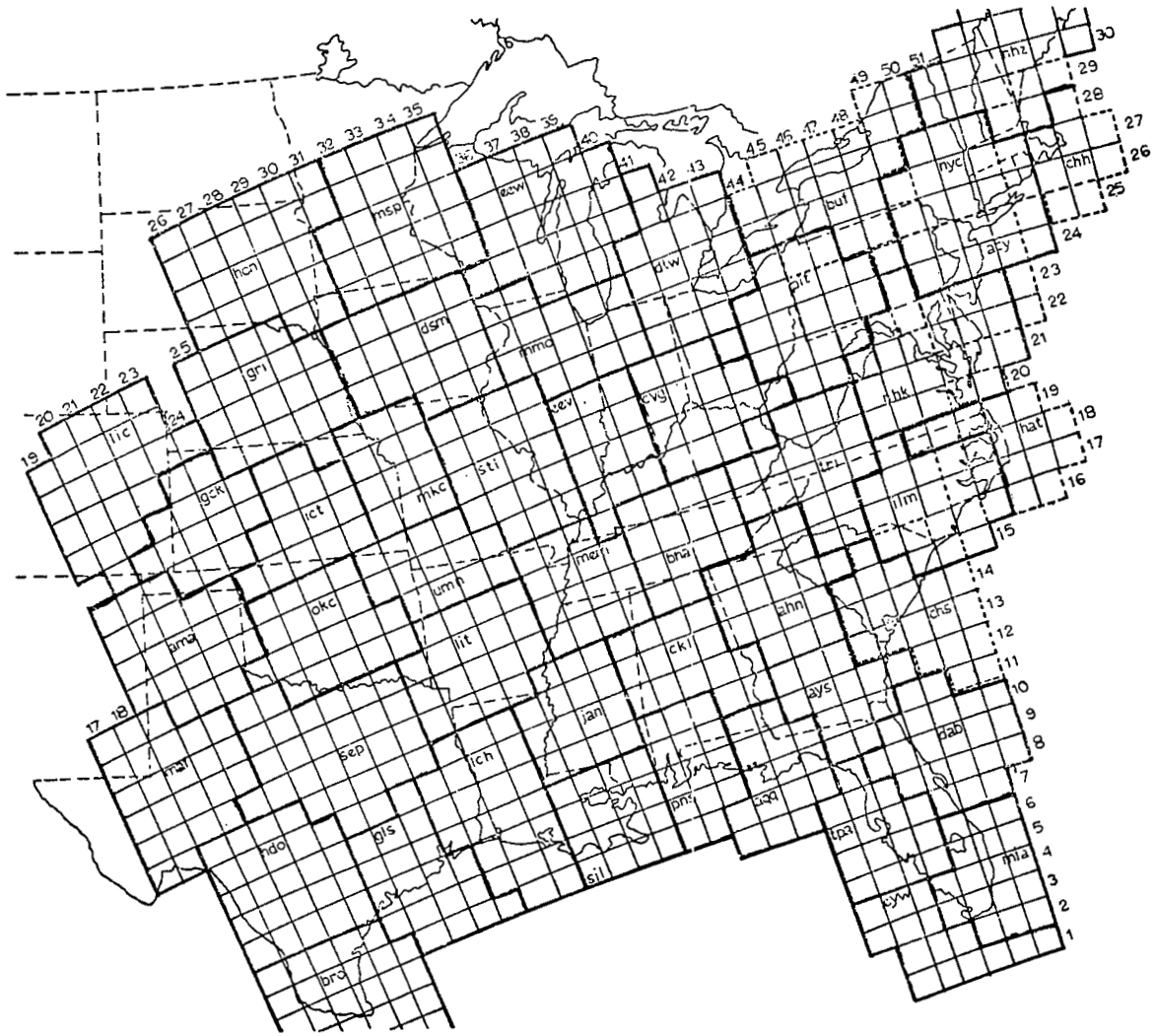

Fig. 4. Manually Digitized Radar (MDR) grid network.

b. Analytical procedures

Analytical procedures can determine the success or failure of an experiment and, therefore, must be considered carefully. This section describes the procedures that were judged most advantageous for this study and briefly discusses error estimates of terms in the budget equations using these procedures.

1) Objective analysis and smoothing

The computation of terms in the energy budget equations is simplified if data are interpolated from randomly-spaced rawinsonde stations to equally-spaced grid points. The grid network used (Fig. 5) is centered over the AVE IV data area and has a spacing of 158 km. Barr et al. (1971) have shown theoretically that a 169-km grid interval incorporates as much detail as is justified from the rawinsonde network over the United States.

Human analysis of data is still preferable to any objective scheme that has been devised, but the number of analyses required rendered hand analysis unfeasible for this study. There were several considerations in the choice of an objective analysis and smoothing procedure from the several that are described in the literature. Such a procedure should interpolate data accurately from stations to the grid without creating fictitious waves or destroying real waves present in the data. Also, the desired results of the procedure should be considered carefully with respect to the input data density. Since the average spacing of rawinsonde stations over the United States is about 400 km, features with wavelengths shorter than 800 km can never be described completely by any objective analysis scheme. Barr et al. (1971) concluded that consistent qualitative evaluation of features with wavelengths less than 1700 km is unlikely.

An objective analysis scheme by Barnes (1964) was used in this investigation. The procedure is commonly referred to as successive corrections to a first-guess field. Data from each rawinsonde station were allowed to influence grid points within a scan radius of three grid distances while four iterations were allowed.

To suppress small waves which cannot be tracked consistently,

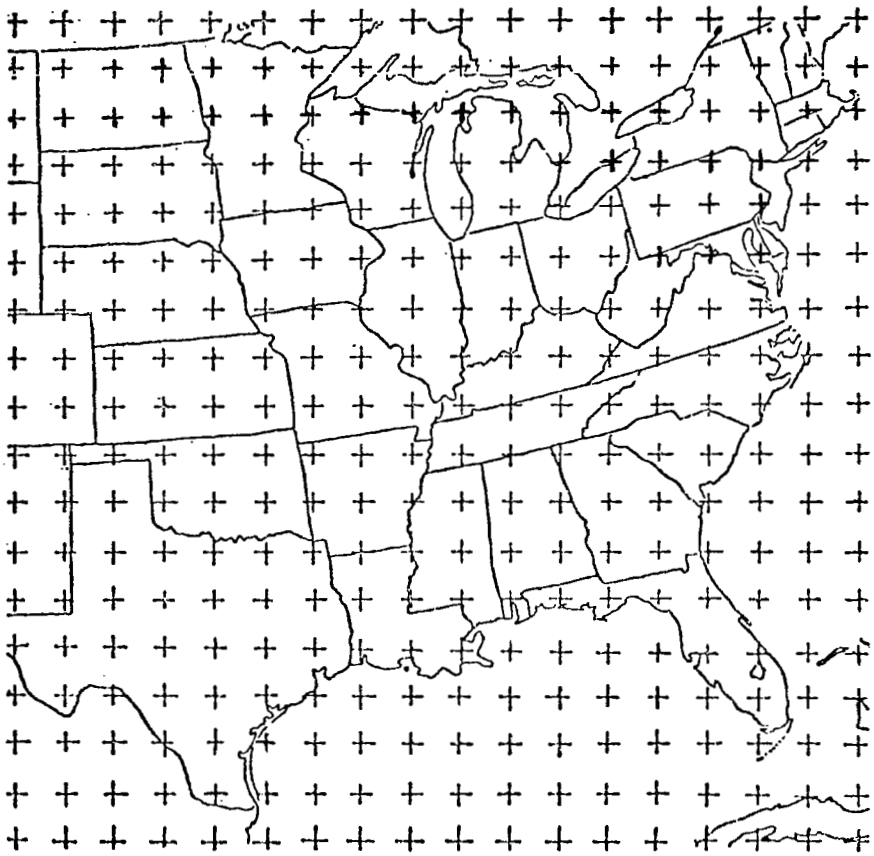

Fig. 5. Grid used for numerical computations.

as well as those which might arise due to the analysis scheme and to reduce random errors, a nine-point filter by Shuman (1957) was applied to the analyzed fields. The final result retained approximately 90% of the amplitudes of wavelengths of 1600 km, while retention of wavelengths equal to 800 km and 400 km was approximately 63% and 17%, respectively. These fields appear to retain as much detail as can be justified from the input data and have shown very good agreement with hand analyses.

The surface data were analyzed using a scan radius of 2 grid units with four iterations. This produced smooth fields from the high density surface data that meshed with the larger-scale rawinsonde data.

Gridded analyses of height, temperature, wind components, and moisture content were produced at 18 levels, i.e. the surface and at 50-mb intervals from 900 mb to 100 mb, for each of the nine time periods. Winds at the 18 levels were averages over 50 mb to reduce further random errors. These gridded values were stored on a computer disk and formed the working data set for all phases of the research.

2) Numerical evaluation of equations

i. Finite differencing and integration. Centered finite differences were used to compute horizontal derivatives, and all vertical derivatives except those at the surface where forward differences were used and at 100 mb where backward differences were used. Time derivatives also were evaluated using centered differences where possible, but forward differences at the first period and backward differences at the last period were required.

Terms in the energy budget equations (19) to (22) were computed at each of the 18 levels previously described. These results then were integrated over 50-mb layers from the surface to 100 mb using the trapezoidal rule. Integrated results were stored on a computer disk for future use. Printed spatial fields of the energy budget terms were made for the layers surface to 700 mb, 700 to 400 mb, 400 to 100 mb, and surface to 100 mb by integrating over these layers. Numerical evaluations were performed on the Amdahl 470/V6 computer at Texas A&M University.

ii. Error estimates. Random errors in input data lead to errors in computed terms of the energy budget equations. Estimates of RMS errors expected in the results were made using the propagation of error method (Young, 1962).

The propagation of error method is briefly derived as follows. If F is a function of X, Y, and Z, and if these are in error by ΔX, ΔY, and ΔZ, then F is in error by an amount ΔF which is given by the Taylor's series as:

$$\Delta F = \frac{\partial F}{\partial X} \Delta X + \frac{\partial F}{\partial Y} \Delta Y + \frac{\partial F}{\partial Z} \Delta Z. \qquad (23)$$

The equation is valid if ΔX, ΔY, and ΔZ are small compared with $\frac{\partial F}{\partial X}$, $\frac{\partial F}{\partial Y}$, and $\frac{\partial F}{\partial Z}$; it is assumed that all terms involving squares, higher powers, and cross products of ΔX, ΔY, and ΔZ are negligible, and that higher derivatives are small in value. After squaring both sides of (23) and replacing each term by its average value, the following equation is obtained when one assumes that errors in X, Y, and Z are independent and normally distributed:

$$\sigma_F^2 = \left(\frac{\partial F}{\partial X}\sigma_X\right)^2 + \left(\frac{\partial F}{\partial Y}\sigma_Y\right)^2 + \left(\frac{\partial F}{\partial Z}\sigma_Z\right)^2, \qquad (24)$$

where σ denotes RMS error.

Although the best estimates of RMS errors for the rawinsonde contact data were used to compute error estimates of the energy budget terms, several considerations suggest that the results probably should be used only in terms of order of magnitude. First, RMS errors for objectively analyzed and smoothed fields of data are difficult to determine. Secondly, the effect of finite difference and integration procedures on errors is difficult to describe. Finally, the extent to which the input data agree with the assumptions of the propagation of error technique is not known fully. Valuable insight into the error problem was obtained in spite of the difficulties involved in error estimation.

The RMS error of each term in the kinetic energy equation, (22), was compared with the range of values expected for the term. The RMS errors of all terms were found to be less than the expected values in the lower and middle troposphere. The cross-contour flow term, C_K, is the most sensitive at all levels, and its error approaches the expected values near the jet stream level. The errors of the remaining terms of the kinetic energy equation near the jet stream level are small compared to expected values.

Recent results by Vincent and Chang (1975) and Kornegay and Vincent (1976) indicated that random errors in input data do not affect seriously the results of kinetic energy studies. After kinetic energy budgets were computed using real data, random errors approaching the extremes to be expected were introduced into the

wind and height data and the budgets were recomputed. Sign uncertainty was found to be greatest when the original result was near zero, but percentage changes between real and erroneous results decreased as the original values become larger. Values of individual terms using erroneous data rarely exceeded original values by a factor of two. Finally, the trends of results and their interpretations almost always remained the same regardless of the errors introduced. These findings suggest that results based on the carefully checked AVE data will be valid.

Random error estimates of most terms in the potential energy budget equation, (21), are relatively small near the surface when compared to expected values, but increase with altitude. In the upper atmosphere, terms HF_{Π}, VF_{Π}, C_K, and C_A possess relatively large errors compared to the expected values of the terms, but based on the results of Vincent and Chang (1975) and Kornegay and Vincent (1976), no problems in interpreting the results should occur. The RMS error of the pressure work term, PW, in (21) is about two orders of magnitude larger than its expected value. The problem occurs because this term is the sum of two component terms which are of nearly equal magnitude but opposite sign. Great caution must be used in reaching conclusions based on term PW.

The difficulty in estimating errors for this type of energy study again should be emphasized. McInnis and Kung (1972) stated that judgements on validity of results usually are based on the systematic nature of those results and comparisons with other investigators. Kung and Smith (1974) pointed out that the effect of random errors can be reduced by averaging results over a large number of points. Further comments on error and interpretation of results will be made in later sections.

iii. Computation of vertical motion. Large-scale vertical motion cannot be measured directly, and no method currently available for determining vertical motion is completely accurate. The kinematic method was used in this research because it involved the least stringent assumptions and produces good results. Details of the procedures were given by Wilson and Scoggins (1976). Terrain-induced

vertical motion was included, and a correction scheme by O'Brien (1970) was applied so the values of vertical motion at 100 mb would equal the values obtained by the adiabatic method. Wilson and Scoggins adjusted values of vertical motion to zero at 100 mb. The adjustment factor significantly affects vertical motion in levels above about 500 mb. Application of an adjustment factor is necessary because the accuracy of wind data and resulting divergence calculations decrease with altitude. Adiabatic values at 100 mb were chosen because they are obtained independently of kinematic values and are more realistic than an assumption of zero at each grid point.

The kinematic method has been used widely in previous research. Vincent et al. (1976) suggested that it is better than the quasi-geostrophic form of the omega equation. Further support for the kinematic method has been given by such investigators as Chien and Smith (1973), Smith (1971), Fankhauser (1969), and Kung (1973). An unpublished study by Wilson at Texas A&M University indicated that values of kinematic vertical velocity relate better to areas of precipitation during the AVE IV experiment than do values of adiabatic vertical velocity.

iv. Frictional dissipation of kinetic energy. Term D in (22) was determined as a residual. Since dissipation of kinetic energy in large-scale circulations is not understood fully (Smith and Adhikary, 1974), computation as a residual is the only objective way to compute it without employing specific theories regarding its nature (Kung and Smith, 1974). While D conceptually represents thermodynamic frictional processes, Kung and Smith pointed out that when computed as a residual, it represents the sink of energy from the larger grid scales of motion which should serve as input to the smaller subgrid scales. It also contains errors accumulated from other terms. Computation of dissipation as a residual has been used by McInnis and Kung (1972) in their kinetic energy study of convective areas and by most other investigators of energetics.

v. Diabatic heating. Diabatic heating, term G in (21), is composed of latent heat release, sensible heat transfer, and radiational effects. The literature suggests procedures for estimating

each of these components, but each procedure requires specific assumptions which may or may not be true at a particular point in space and time. Term G was evaluated from the thermodynamic equation

$$\frac{dH}{dt} = c_p \frac{\partial T}{\partial t} + c_p \vec{V}_2 \cdot \vec{\nabla}_p T + \left(c_p \frac{\partial T}{\partial p} - \alpha \right) \omega , \qquad (25)$$

which gives the net effect of the various components of diabatic heating. This procedure has been used by Smith and Horn (1969) and West (1973).

4. SYNOPTIC CONDITIONS

Although no outstanding pressure or frontal activity occurred during the AVE IV experiment, two large areas of intense convective activity made the period ideally suited for this study. The synoptic analyses used in the following discussion are taken from Fucik and Turner (1975) and are similar to facsimile analyses made by the National Weather Service.

Two air mass types were distinguishable at the surface over the AVE IV network at the beginning of the experiment at 0000 GMT on 24 April (Fig. 6). Warm, moist, maritime tropical (mT) air was moving northward over the network with strong southerly flow around a high pressure center located about 500 km off the coast of the Carolinas. This air mass covered almost two-thirds of the network extending from central Texas and Oklahoma eastward through all of the Gulf Coast and Middle Atlantic States and northeastward into the Ohio Valley.

A cold front, extending southwestward into Kansas from a moderately strong cyclone (1000 mb center) over northern Michigan, separated the mT air from the cooler and drier continental polar (cP) air moving southward over the Northern Plains States. A warm front, extending southeastward from the cyclone into Pennsylvania, separated cP air over New England from mT air in the Ohio Valley. A second cyclone (1000 mb center) was located in central Kansas with a cold front extending southward into west Texas. Surface temperatures over the AVE IV network ranged from about 25°C along the Gulf Coast to about 10°C in the Northern Plains States, and dew point temperatures ranged from about 20°C to about -10°C.

The middle and upper tropospheric flow pattern was basically zonal during the entire experiment with the polar jet stream extending roughly west-east from the Northern Plains States to New England and the subtropical jet stream being located along the Gulf Coast States. Two clearly distinguishable short wave perturbations with wavelengths of about 1500 km moved through the zonal flow during the experiment period and were responsible for

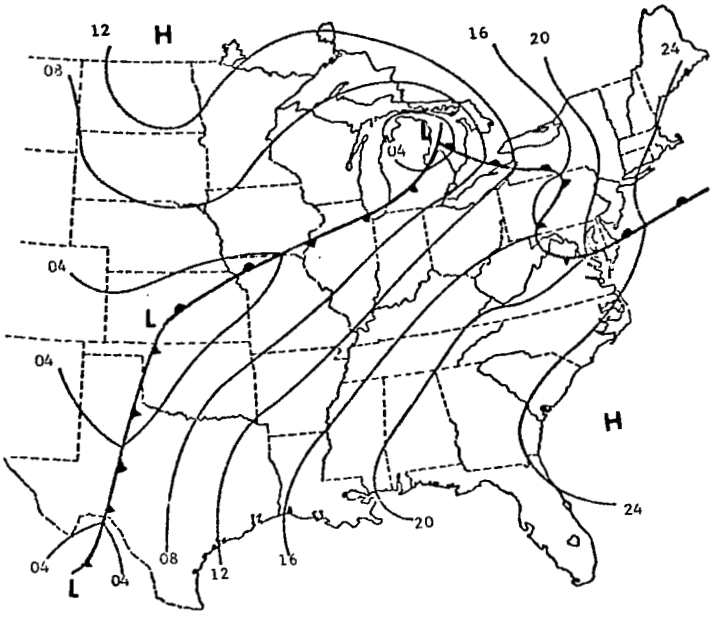

(a) Surface.

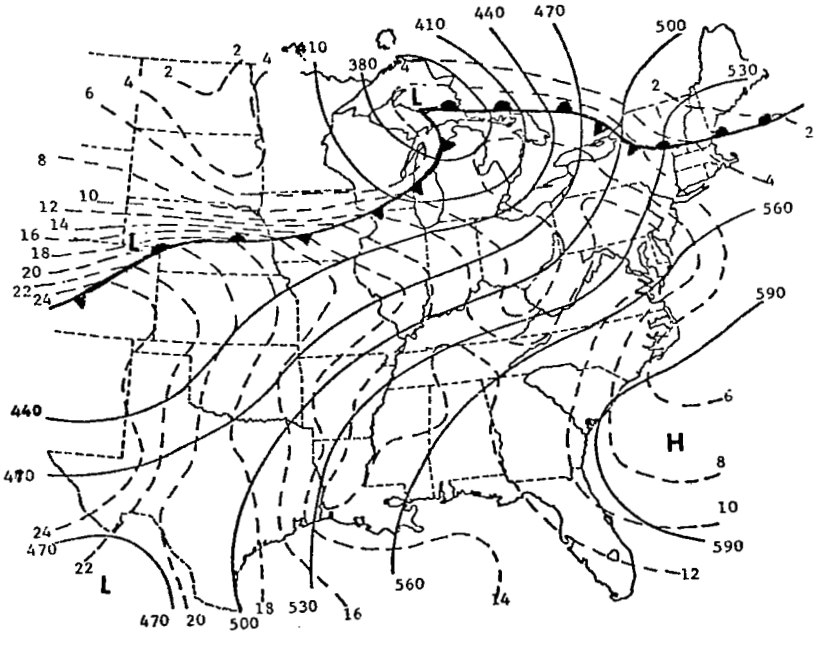

(b) 850 mb.

Fig. 6. Synoptic charts for 0000 GMT, 24 April 1975 (Fucik and Turner, 1975).

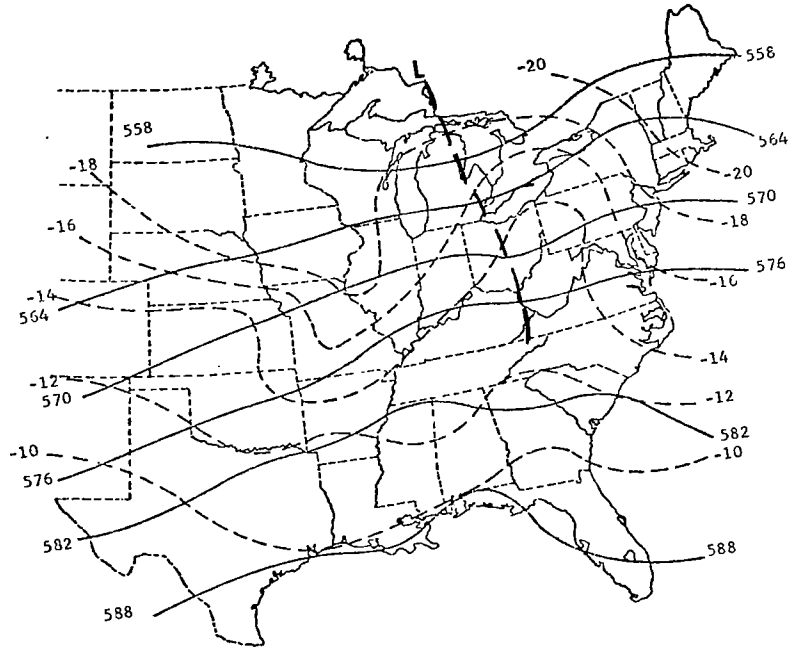

(c) 500 mb.

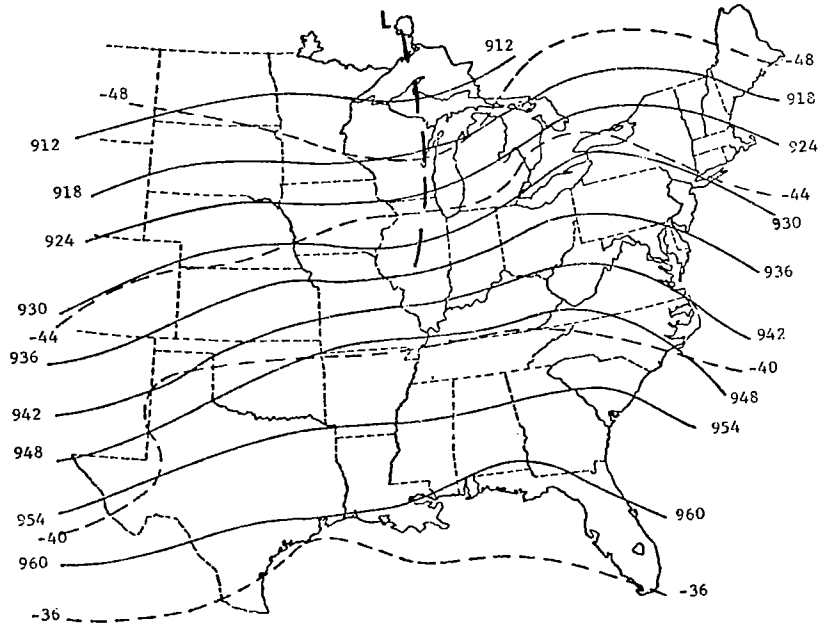

(d) 300 mb.

Fig. 6. (Continued)

much of the significant weather. There were also numerous shorter waves (750-1000 km) which could be resolved only partially by the data network. The first well-defined short wave was associated with the cyclone over northern Michigan at the beginning of the period. The second wave was still west of the AVE IV network at that time.

The first major outbreak of severe weather began just prior to the start of the AVE IV experiment and was associated with the cyclone in central Kansas and the warm front extending northeastward into northern Missouri. Maps of MDR data are given in Fig. 7 for the nine time periods. The area grew rapidly in strength and intensity so that tornado watches were issued for the area at 0000 GMT on 24 April. Radar tops extended as high as 18.3 km (60,000 ft) with MDR values as high as 9 in this unstable area where values of the K index were as high as 38. The convective area or squall line reached maximum intensity at about 0600 GMT while moving southeastward. The area decreased in intensity to shower activity by 1500 GMT while the cyclone in central Kansas remained stationary. There were numerous reports of hail and tornadoes associated with this convective system.

Light rain and rain showers with radar tops below 7.6 km (25,000 ft) occurred along and above the warm front associated with the first short wave as it moved eastward as a stable wave to a position about 250 km off the coast of Maine at the end of the experiment.

The cyclone in central Kansas began to intensify and move southeastward into northeast Oklahoma with the eastward movement of the second short wave that was located in the Dakotas by 2100 GMT on 24 April (Fig. 8). The second major squall line began to develop at this time in eastern Kansas within the intensifying low and southwestward along the trailing cold front. Values of the K index were as high as 42 in the area, indicating extreme instability. The squall line stretched from central Illinois to central Texas with maximum radar tops reaching 17.1 km (56,000 ft) at 0000 GMT on 25 April. Severe weather watches were issued as the squall line moved

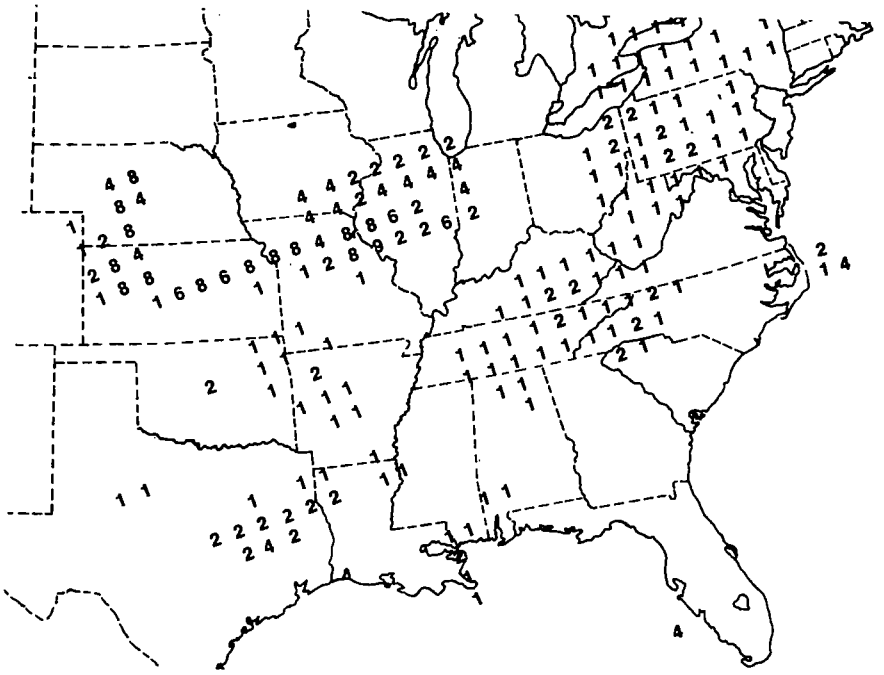

(a) 0000 GMT, 24 April.

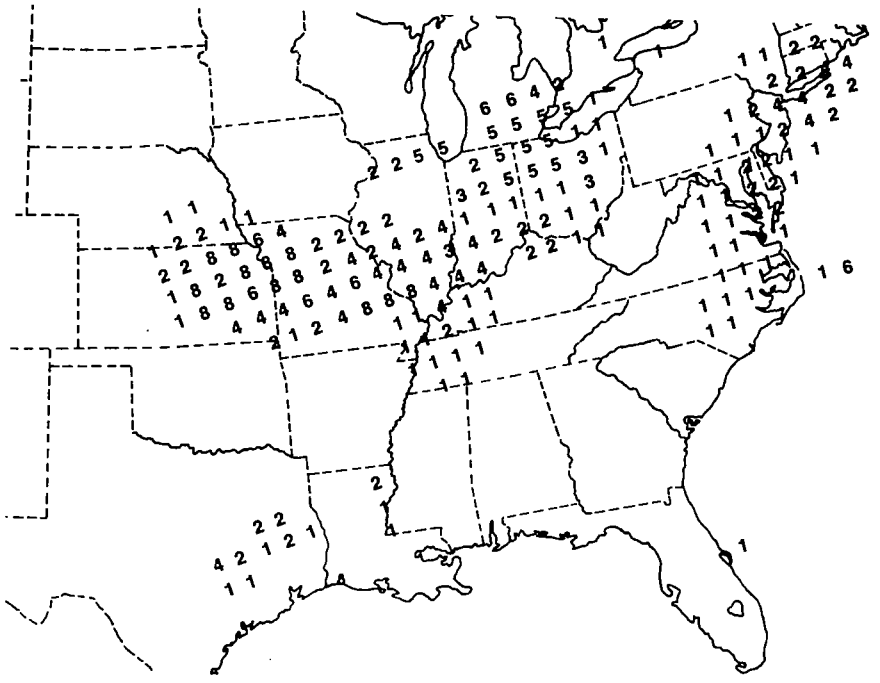

(b) 0600 GMT, 24 April.

Fig. 7. MDR data for the AVE IV experiment.

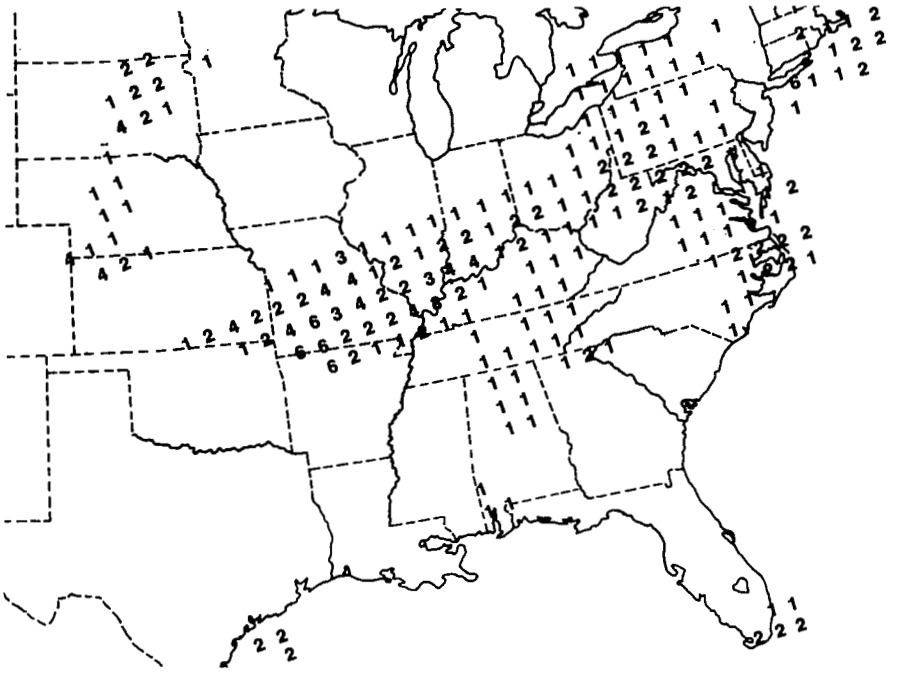

(c) 1200 GMT, 24 April.

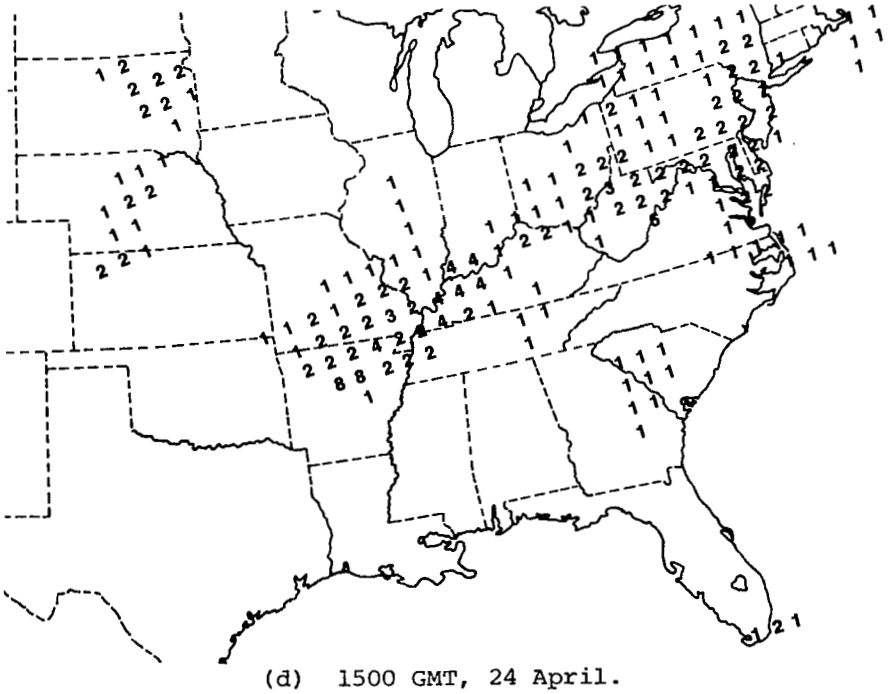

(d) 1500 GMT, 24 April.

Fig. 7. (Continued)

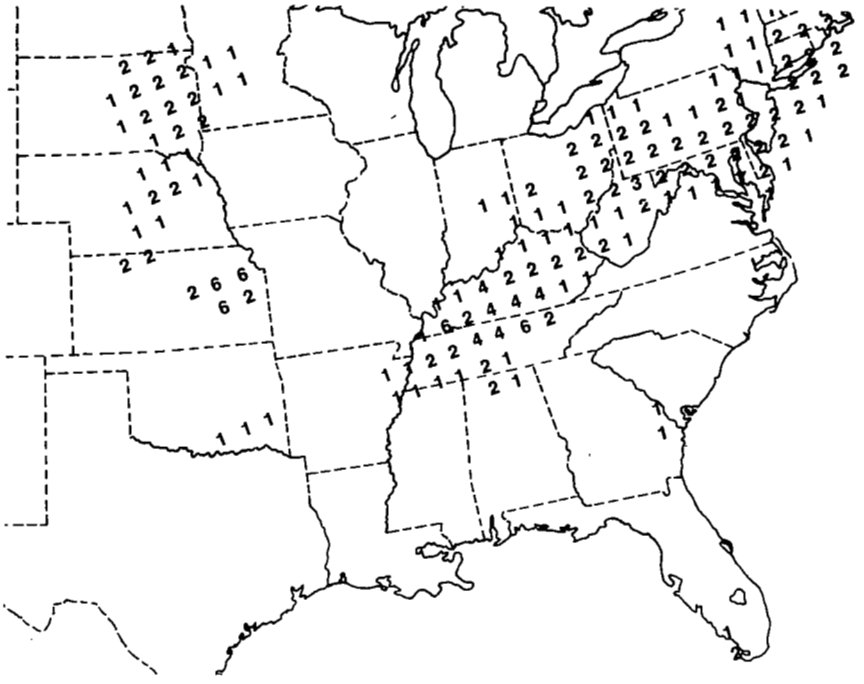

(e) 1800 GMT, 24 April.

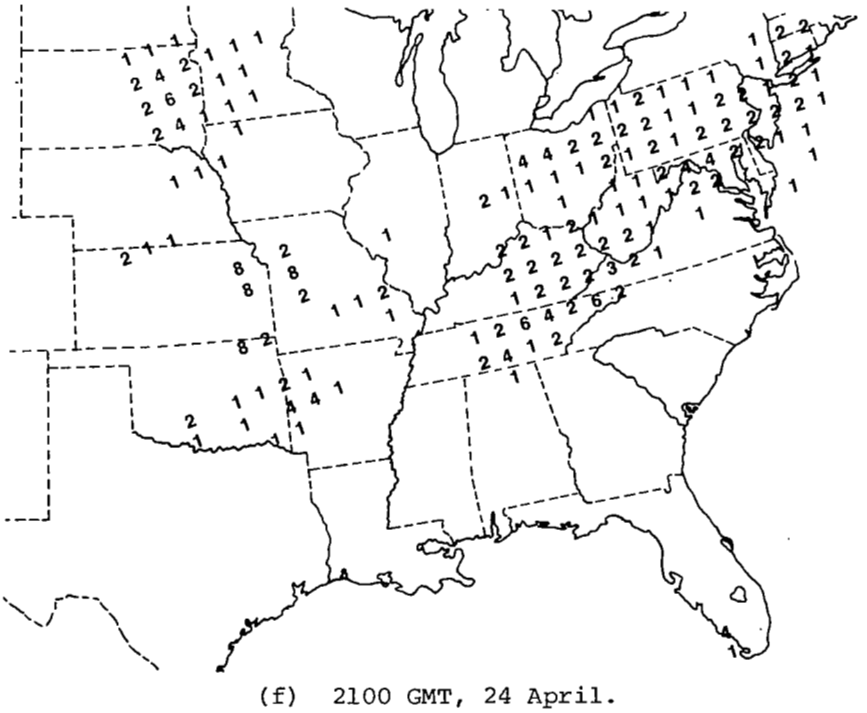

(f) 2100 GMT, 24 April.

Fig. 7. (Continued)

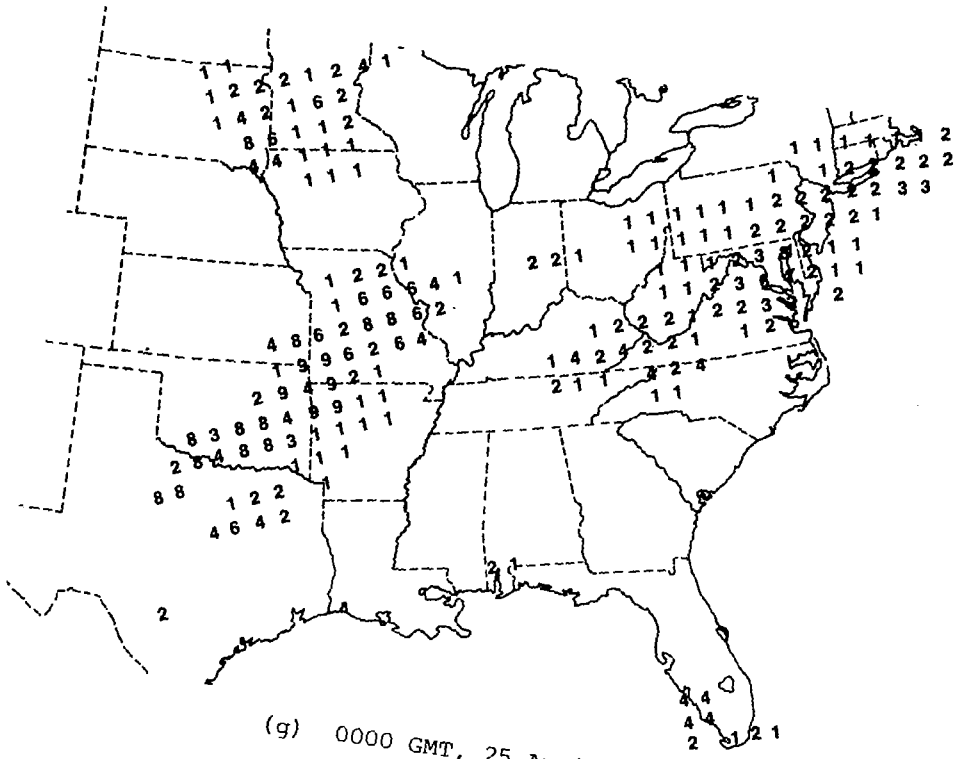

(g) 0000 GMT, 25 April.

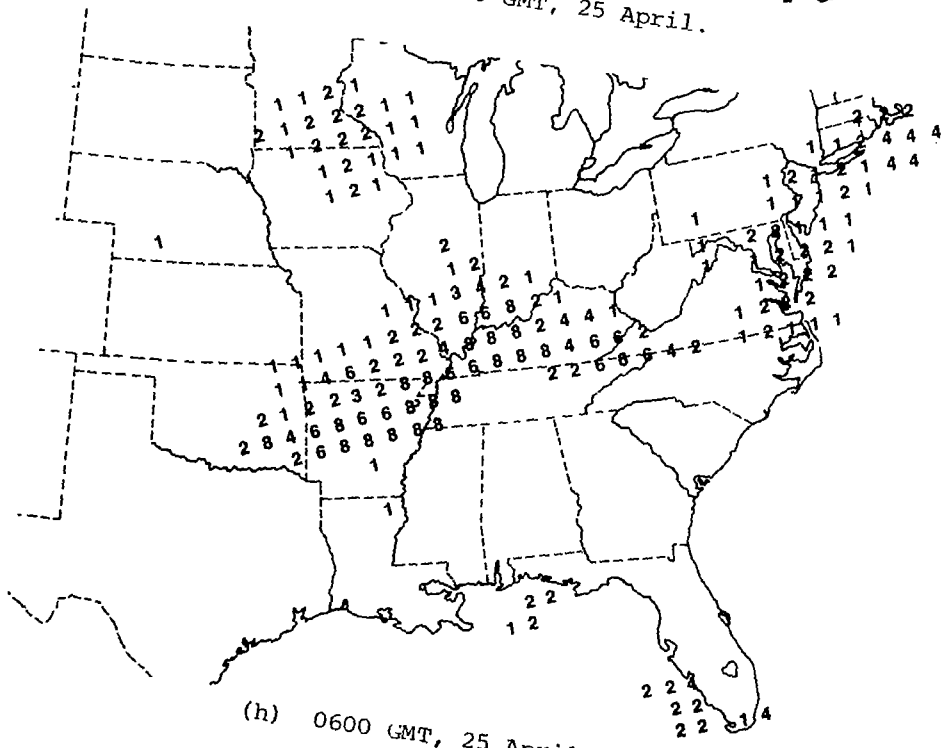

(h) 0600 GMT, 25 April.

Fig. 7. (Continued)

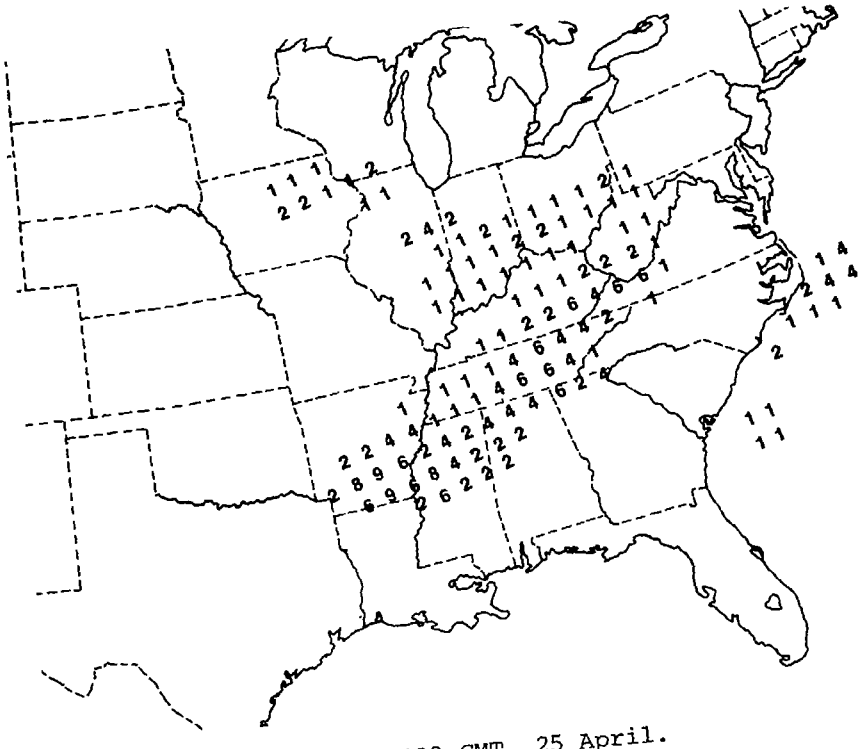

(i) 1200 GMT, 25 April.

Fig. 7. (Continued)

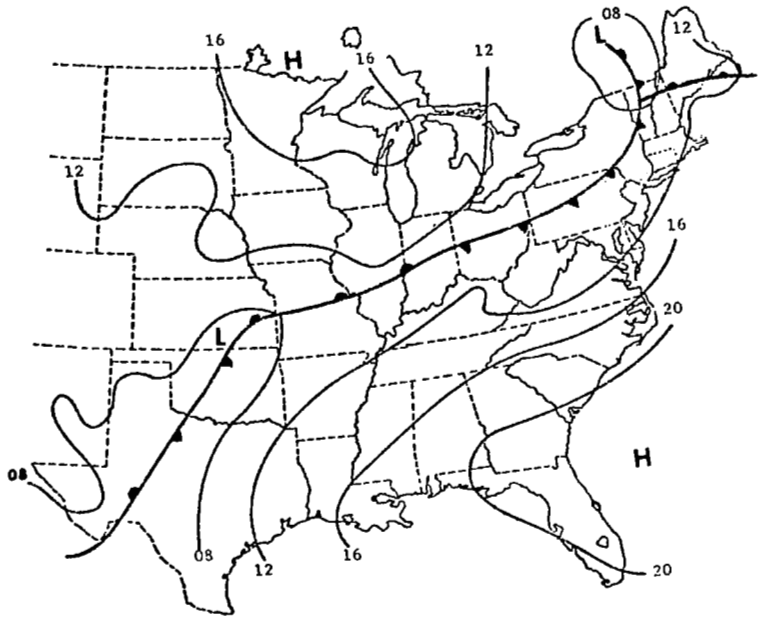

(a) Surface.

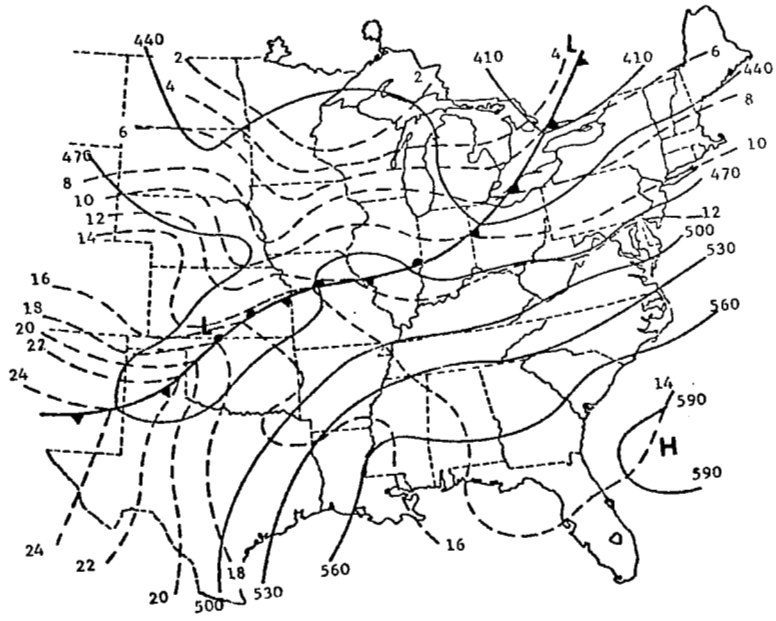

(b) 850 mb.

Fig. 8. Synoptic charts for 2100 GMT, 24 April 1975. (Fucik and Turner, 1975).

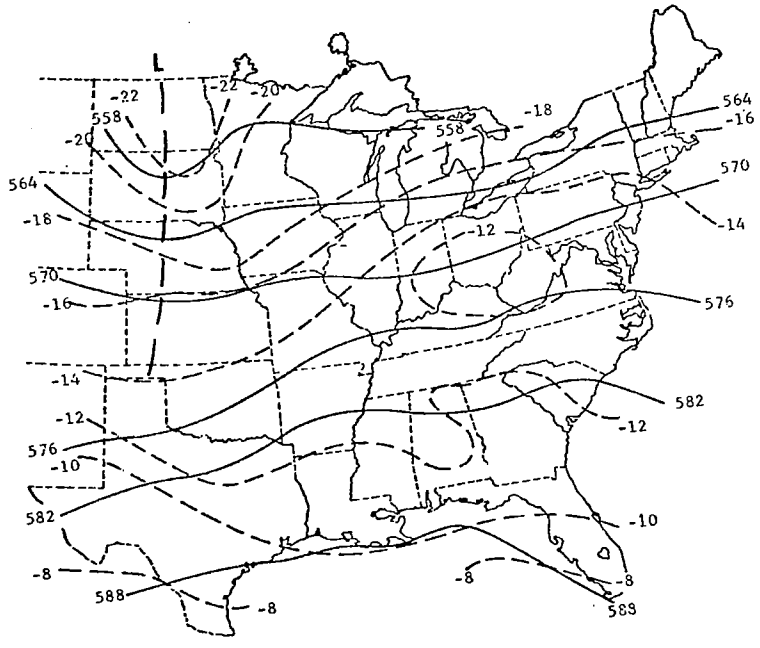

(c) 500 mb.

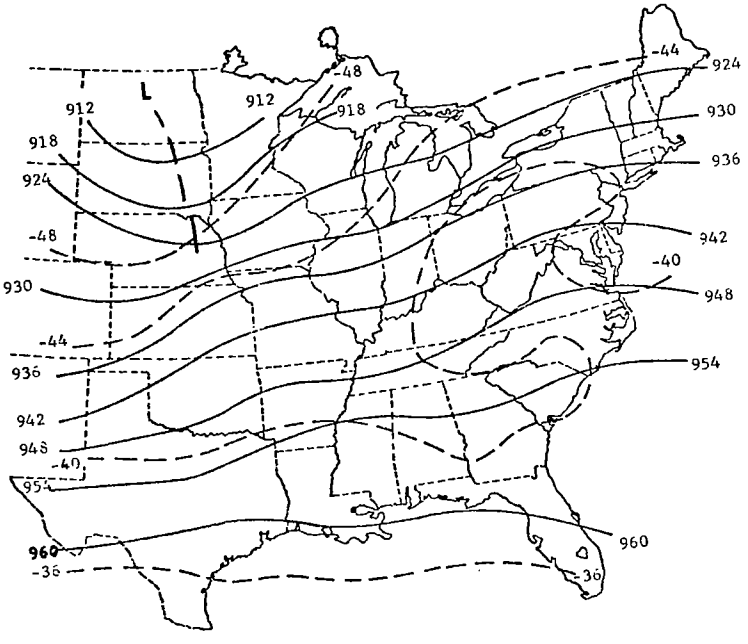

(d) 300 mb.

Fig. 8. (Continued)

southeastward.

Between 2100 GMT and 1200 GMT (Fig. 9) on 25 April the cyclone moved from Kansas eastward into Kentucky with the eastward movement of the second short wave perturbation while the associated cold front extended southwestward into Texas. The severe squall line continued to grow in intensity and length with maximum radar tops exceeding 19.8 km (65,000 ft) and, at 1200 GMT on 25 April, extended along an arc almost 1000 km long from eastern Kentucky southwestward into northern Alabama and westward into Arkansas (Fig. 7). Both hail and tornadoes were reported with the squall line.

The strong squall line moving southeastward into the southeastern United States was the major weather feature at the end of the experiment at 1200 GMT on 25 April. The second trough ran north-south through the Northern Plains. The surface anticyclone off the Carolinas had moved farther eastward out into the Atlantic, and cP air was replacing mT air in the Ohio Valley and the southeast United States with the movement of the cold front.

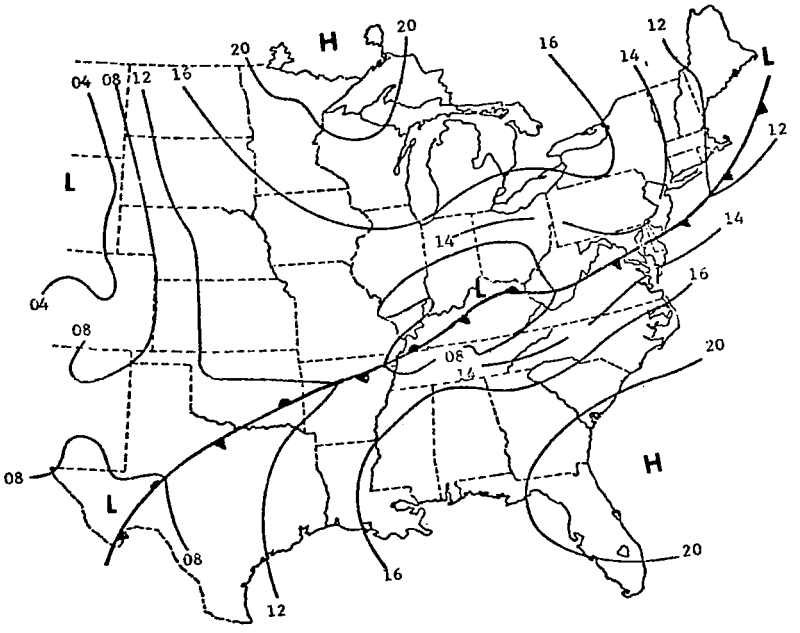

(a) Surface.

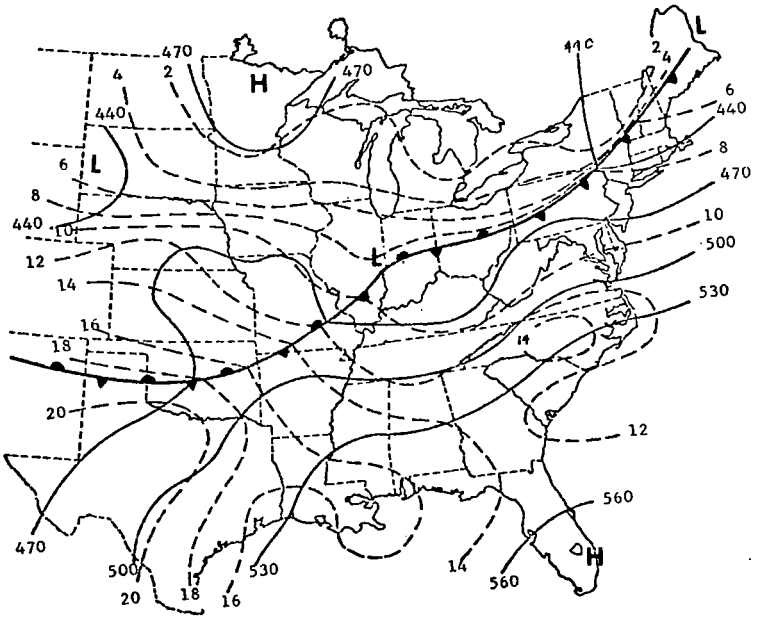

(b) 850 mb.

Fig. 9. Synoptic charts for 1200 GMT, 25 April 1975. (Fucik and Turner, 1975).

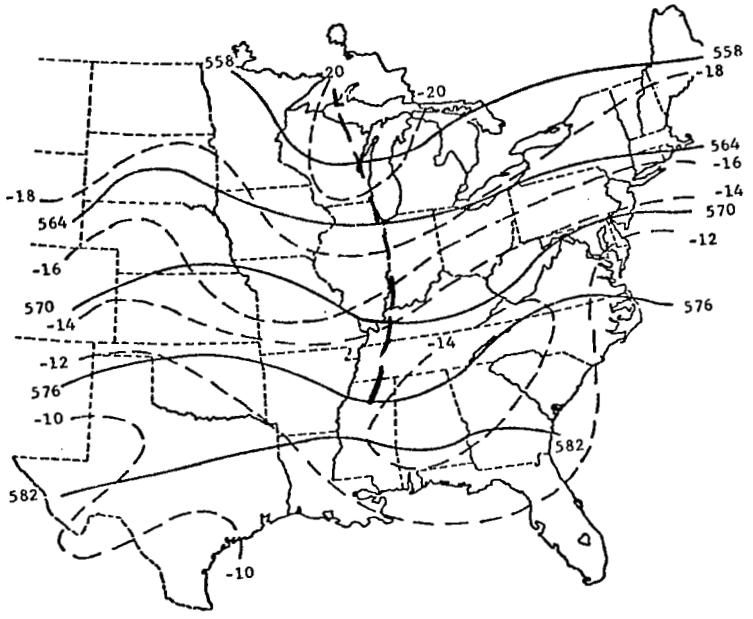

(c) 500 mb.

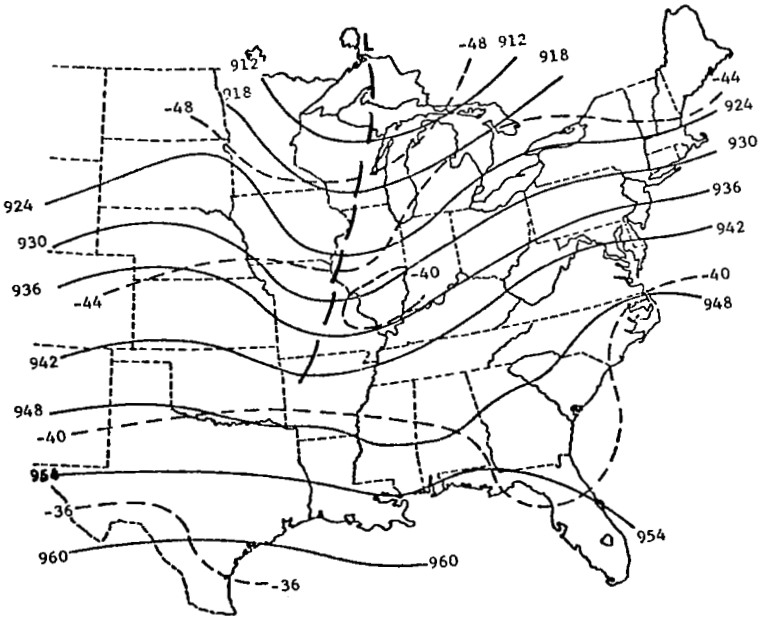

(d) 300 mb.

Fig. 9. (Continued)

5. RESULTS

A "telescoping" approach will be taken in the presentation of results. First, the energy budget for the entire experiment area will be examined. Next, synoptic-scale energy budgets of smaller volumes enclosing two squall lines will be presented to show the relation of these budgets to the overall budget. Finally, spatial maps of selected terms in the budget equations will be examined to describe features which are lost in the averaging process. In addition to the "telescoping" approach, the relation between MDR values and energy parameters will be considered.

These observational results will verify the hypothesis made in the objectives--systematic changes do occur in synoptic-scale energy budgets of atmospheric volumes enclosing areas of intense convection.

a. Average energetics of the experiment period

The energetics of the entire AVE IV area, averaged over all nine time periods, indicates rather tranquil conditions, but later sections will show that this is deceiving. The average kinetic energy budget and average total potential energy budget (Table 4) were obtained by averaging values of budget terms for 168 central grid points, an area of 49.0×10^{11} m^2, over all time periods, for a total of 1512 points.

The kinetic energy budget of the surface- to 700-mb layer is characterized by conversion from potential to kinetic energy due to cross-contour flow, term $-C_K$; near the ground this process is enhanced by frictional effects. Weak horizontal and vertical outflow of kinetic energy occur along with negative dissipation, indicating transfer of energy from grid to subgrid scales of motions. The net effect of these processes is a local reduction of kinetic energy in the surface- to 700-mb layer.

Kinetic energy is being converted to potential energy in the 700- to 400-mb layer due to air moving across height contours from low to high values. Horizontal and vertical outflow occur in this

Table 4. Average energy budget for the AVE IV experiment with comparisons to previous research. The AVE area is 49.0 x 10^{11} m^2.

Pressure Layer mb	K 10^5 J m^{-2}	$\frac{\partial K}{\partial t}$ W m^{-2}	HF_K W m^{-2}	VF_K W m^{-2}	$-C_K$ W m^{-2}	D W m^{-2}	G W m^{-2}	C_K W m^{-2}	PW W m^{-2}	HF_{II} W m^{-2}	VF_{II} W m^{-2}	C_A W m^{-2}
200-100	4.4	-1.2	0.1	-0.5	-3.0	1.4	-30.4	3.0	150.4	649.8	-123.2	17.1
300-200	5.4	-0.5	1.8	-1.7	-2.2	1.8	4.3	2.2	48.9	1037.9	-866.9	-58.7
400-300	3.4	-0.3	-0.4	-0.1	-1.5	0.8	25.8	1.5	3.3	427.2	-415.4	-103.7
500-400	2.2	-0.3	-0.3	0.2	-0.8	0.5	27.2	0.8	38.6	201.2	-66.1	-92.2
600-500	1.5	-0.4	0.1	0.3	-0.4	0.5	13.1	0.4	32.8	173.0	-58.0	-78.0
700-600	1.1	-0.4	0.3	0.5	0.2	0.2	-1.8	-0.2	8.8	58.9	-28.4	-68.8
800-700	0.8	-0.3	0.1	0.4	0.1	0.1	-9.4	-0.1	-31.6	-540.8	429.9	-54.5
900-800	0.7	-0.4	-0.1	0.4	1.4	-1.5	-24.7	-1.4	-43.8	-787.7	634.0	-26.2
sfc-900	0.4	-0.2	0.0	0.2	2.2	-2.2	-21.0	-2.2	-107.8	-525.9	147.8	-7.4
Vertical total	19.8	-4.0	1.6	-0.1	-4.0	1.5	-16.9	4.0	99.6	693.6	-346.4	-472.3
Mature cyclone vicinity, surface to tropopause, (Kung and Smith, 1974).	-	14.0	-24.4	0.5	27.4	-37.3	-	-	-	-	-	-
North America during short wave development, surface to 100mb, (Ward and Smith, 1976).	19.6	0.5	-5.2	0.0	-4.4	-0.3	-	-	-	-	-	-
Anticyclone vicinity, surface to 200mb, (Smith, 1973a).	-	-12.3	12.7	0.0	0.4	0.0	-	-	-	-	-	-
Mature cyclone vicinity, surface to 100mb, (West, 1973).	-	-	7.3	-2.5	17.4	-	40.8	2.5	227.3	-1261.6	460.0	-

layer as in the lower troposphere, but in this layer kinetic energy is being transferred from subgrid scales of motion to larger scales. A local decrease in kinetic energy is the overall result.

The kinetic energy budget near the jet stream, the 400- to 100-mb layer, is characterized by maximum conversion to potential energy; term $-C_K$ equals -3.0 W m^{-2} in the layer from 200 to 100 mb. Maximum transfer of kinetic energy from subgrid to grid scales of motion occurs in the 300- to 200-mb layer. Vertical inflow and horizontal outflow of kinetic energy is occurring with both processes reaching their greatest magnitudes in the 300- to 200-mb layer. These combined processes again lead to a local decrease in kinetic energy through the layer.

The kinetic energy budget of the total volume (surface to 100 mb) can be characterized by conversion from kinetic to potential energy, outward horizontal transport of kinetic energy, inward vertical transport, the creation of synoptic-scale kinetic energy from subgrid-scale motion, and a local decrease of kinetic energy with time.

Table 4 compares the kinetic energy budget for the AVE IV experiment with the budgets of previous investigators. The average kinetic energy budget for the AVE IV experiment is quite unlike budgets obtained for cases of cyclones. For example, the vertical total of term $-C_K$ in the vicinity of an average mature cyclone is 27.4 W m^{-2} (Kung and Smith, 1974) compared to -4.0 W m^{-2} for this study. Results of Smith's (1973a) study of an anticyclone are more similar to the present results. Smith reported values of 0.4 W m^{-2} for term $-C_K$ and 12.7 W m^{-2} for term HF_K in the surface- to 200-mb layer. The budget for North America during a period of short wave development (Ward and Smith, 1976) is also more similar.

Positive values of dissipation often are viewed with skepticism, and the computational uncertainties associated with this residual term always should be acknowledged, but several reports of positive values occur in the literature. Vincent and Chang (1975) reported a vertical total of 27.4 W m^{-2} during the developing stage of an extratropical cyclone for an area about 1.15×10^{12} m^2 using

moving coordinates. Smith (1973b) gave a value of 1.0 W m^{-2} for the surface- to 200-mb layer over North America prior to cyclogenesis; he noted that since smaller waves had a tendency to dampen out during the period, perhaps their kinetic energy was contributed to the larger scales of motion. Kornegay and Vincent (1976) gave a vertical total of 1.9 W m^{-2} when a tropical storm interacted with an extratropical frontal system.

While positive values of dissipation are often attributed to errors in the input data, Vincent and Chang (1975) and Kornegay and Vincent (1976) concluded that realistic errors alone would not produce positive values of dissipation for their studies. They suggested that subgrid-scale energy sources that are not completely detectable using synoptic-scale energy data, such as convection or eddy momentum transfer, require compensating mechanisms for dissipation which if detectable or capable of parametrization would reduce or eliminate positive values. It is clear from the synoptic discussion that convection and associated turbulence and wave phenomena, which cannot be completely resolved in time or space with the available data, are widespread and intense during this period of study. The topic of dissipation is discussed further in following sections.

Terms of the total potential energy budget during the AVE IV experiment are given in Table 4. Since average vertical motion over the area is upward, values of C_A are negative throughout most of the atmosphere, indicating conversion from potential to kinetic energy. The value of $|C_K|/|C_A|$ for the surface- to 100-mb layer is about 1% which indicates that the limited region exhibits major interaction with the surrounding atmosphere. The value of 1% is similar to values obtained by other investigators (Gommel, 1973; Smith and Horn, 1969).

The lower troposphere, from the surface to 700 mb, contains vertical outflow and horizontal inflow of total potential energy while the 700- to 100-mb layer is exporting energy horizontally and importing energy vertically. The values of diabatic effects (term G)

show a small range throughout the vertical profile. Diabatic cooling occurs in the lower troposphere, but generation of potential energy due to diabatic heating occurs in the 600- to 200-mb layer.

The literature contains few studies on total potential energy which can be compared with the current study, but West's (1973) investigation of cyclogenesis over the eastern United States is a notable exception (Table 4). His values of terms G, HF_{Π}, and VF_{Π} were larger than those presently observed, and shapes of vertical profiles of the terms were considerably different.

Based on the previous results, the atmosphere may appear tranquil during the AVE IV experiment, but significant energy processes in both time and space have been lost due to averaging. These important events are described in later sections.

b. Vertical motion and squall line development

A first indication of systematic changes in meteorological parameters that relate to areas of intense convection can be found in fields of vertical motion. Vertical motion fields at 500 mb for the nine AVE IV time periods, with superimposed areas of MDR values greater than or equal to 4, are given in Fig. 10. More detailed maps of MDR values are found in Fig. 7 (p. 30). The first major squall line is already well developed and stretches from central Illinois to western Nebraska at 0000 GMT on 24 April, but the area of maximum upward vertical motion is small and located slightly to the rear of the convective area. The area of upward motion associated with the surface low and short wave can be seen over the northeastern United States. The area of upward motion increases greatly in size and intensity by 0600 GMT when the squall line is at its maximum intensity. Values as great as -15.0 $\mu b\ s^{-1}$ are located over central Missouri, immediately behind the area of strongest convection. The area of upward motion at this time is the dominant feature in the experimental area.

The squall line decreases in areal coverage and intensity after 0600 GMT. The most intense convection is occurring over southern Missouri and northern Arkansas by 1200 GMT while the area

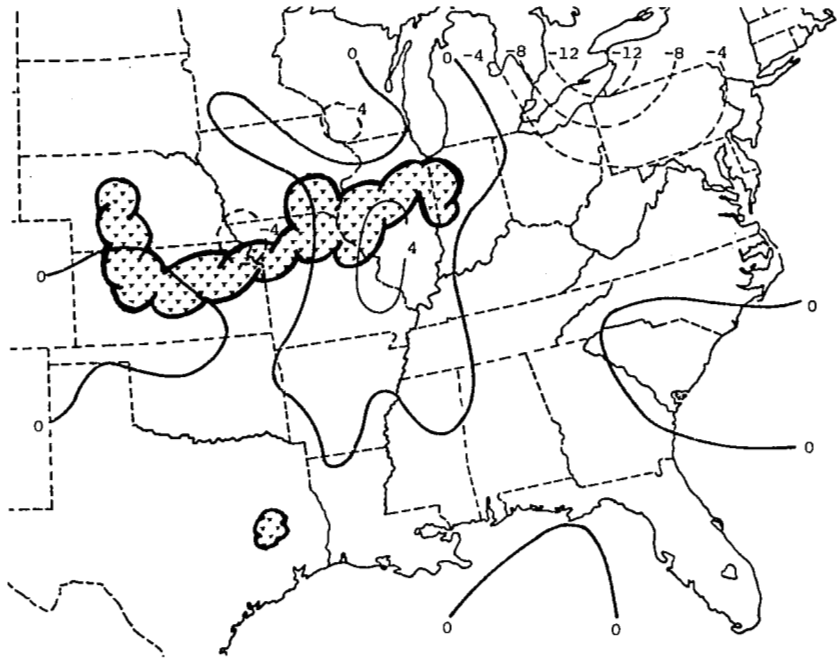

(a) 0000 GMT, 24 April.

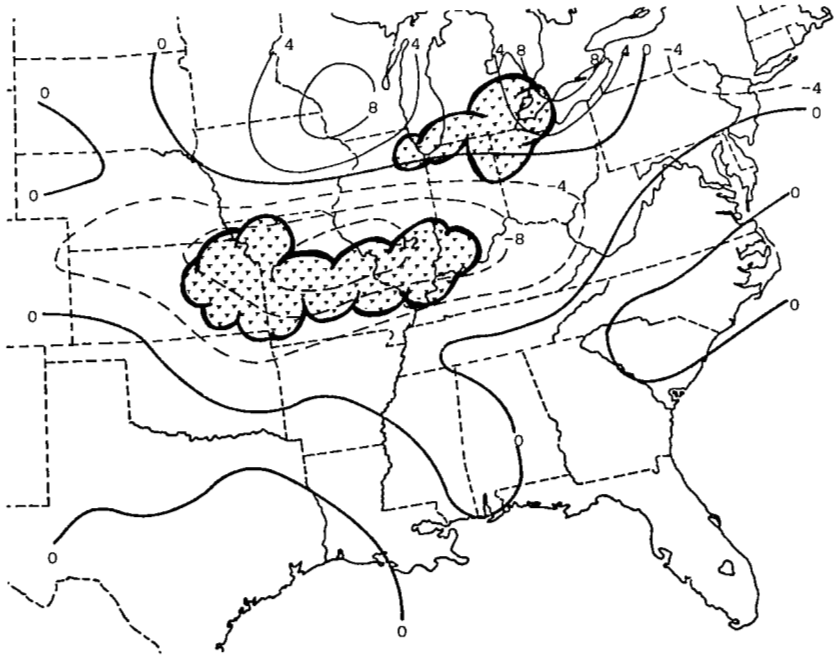

(b) 0600 GMT, 24 April.

Fig. 10. Vertical velocity at 500 mb (μb s^{-1}). Superimposed are areas of MDR values ≥ 4.

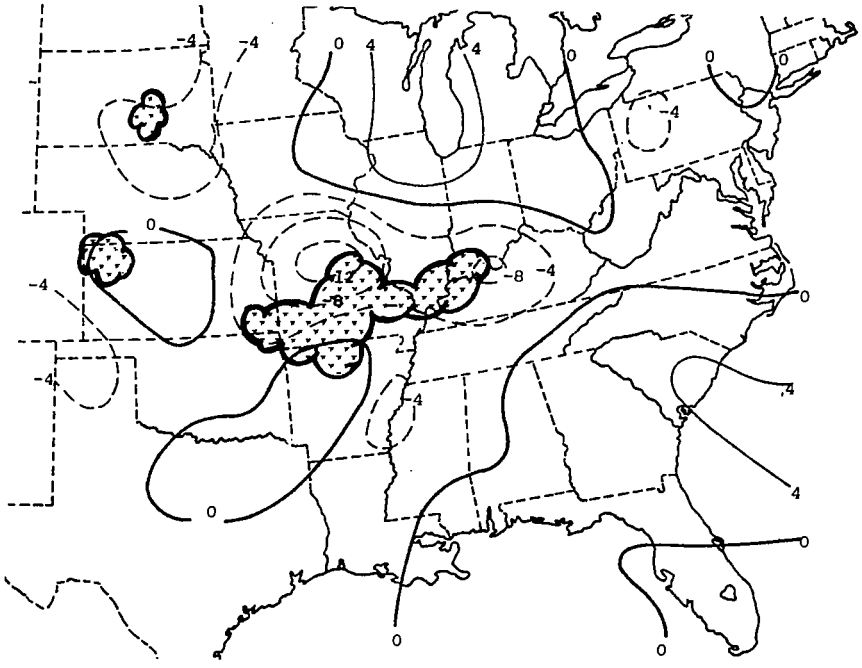

(c) 1200 GMT, 24 April.

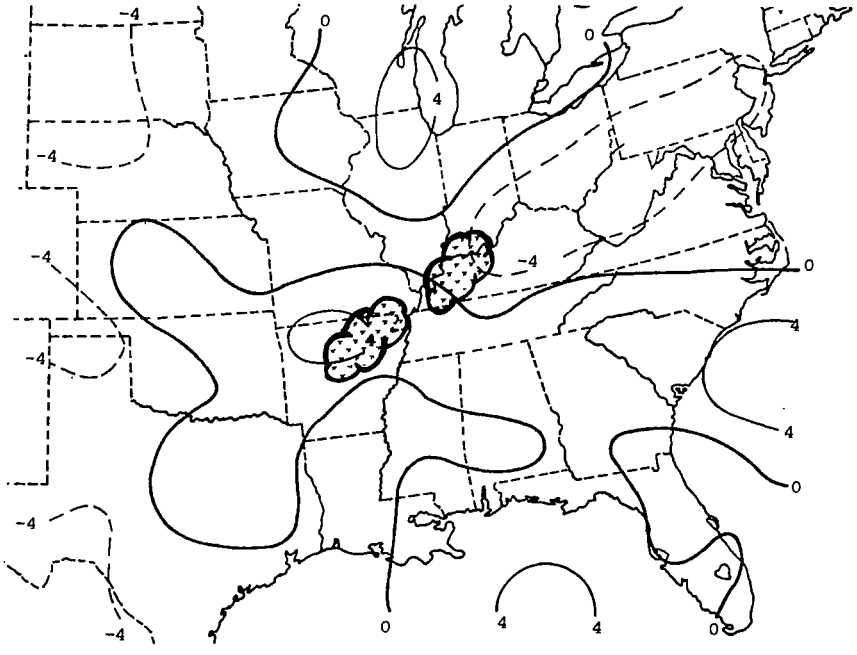

(d) 1500 GMT, 24 April.

Fig. 10. (Continued)

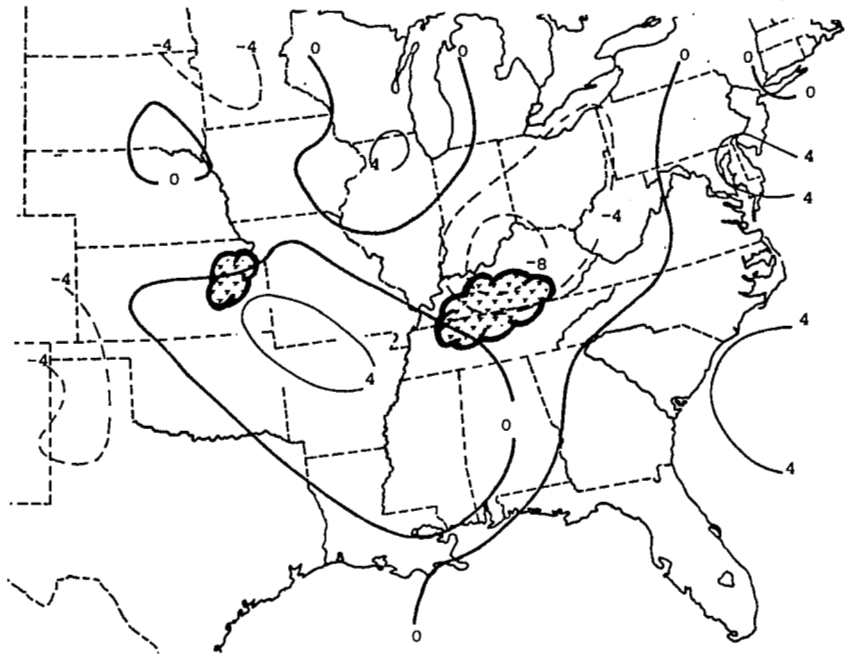

(e) 1800 GMT, 24 April.

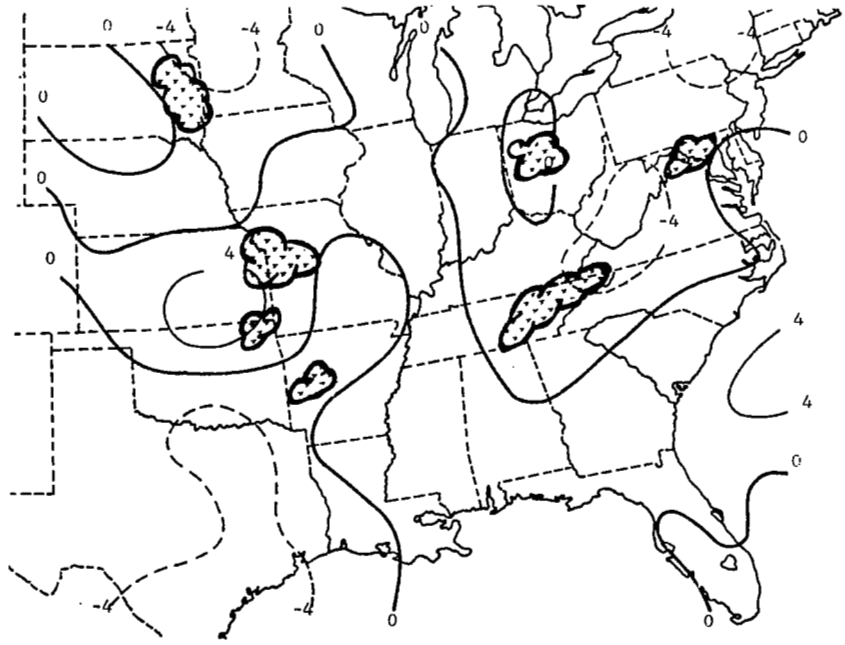

(f) 2100 GMT, 24 April.

Fig. 10. (Continued)

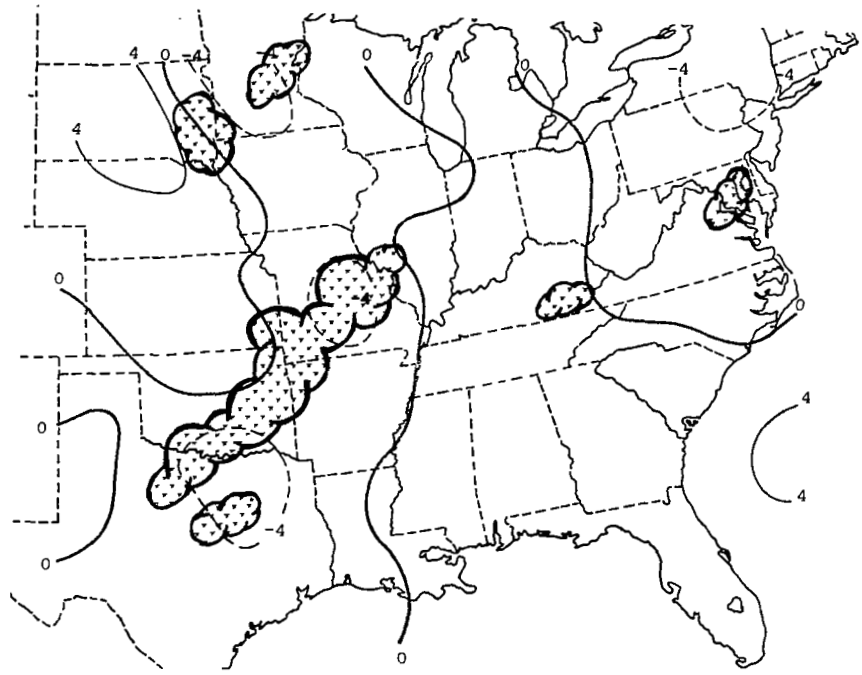

(g) 0000 GMT, 25 April.

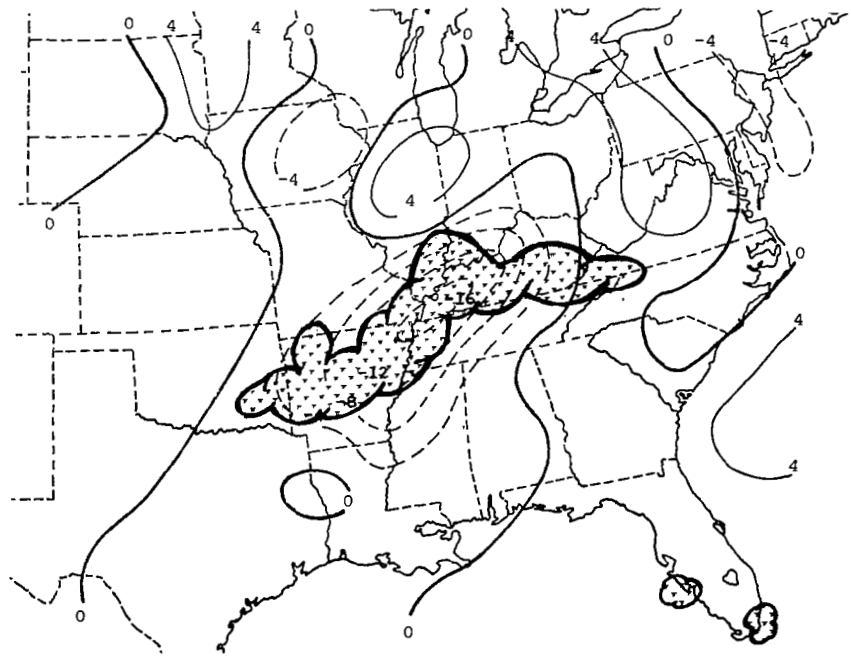

(h) 0600 GMT, 25 April

Fig. 10. (Continued)

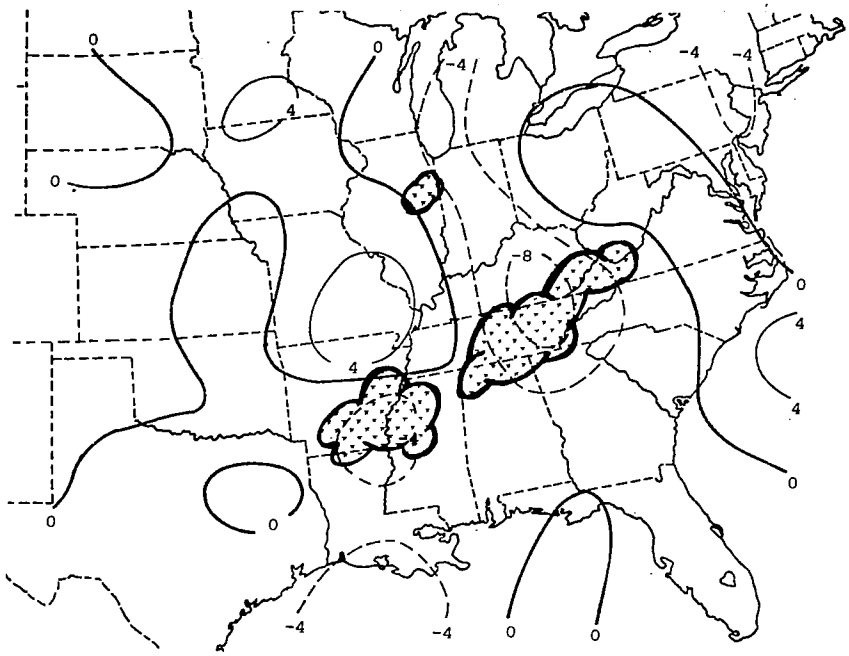

(i) 1200 GMT, 25 April.

Fig. 10. (Continued)

of strongest upward motion, reduced to -12.0 μb s^{-1} at 500 mb, is located over central Missouri. Downward vertical motion is associated with the remnants of the squall line over Missouri and Arkansas at 1500 GMT. Positive vertical motion along the Ohio River Valley and New England States at 1500 GMT is associated with rainshower activity in those areas with MDR values less than 4.

When the second major squall line develops over eastern Kansas between 1800 GMT and 2100 GMT on 24 April, part of the area is experiencing slight upward motion less than -4.0 μb s^{-1}; areas of downward motion also are in the vicinity, but are weak as well. An organized squall line, stretching from Illinois to Texas, forms by 0000 GMT on 25 April. Increases in upward vertical motion to values of -6.5 μb s^{-1} accompany this development. Peak intensity of the second squall line occurs at 0600 GMT at which time upward vertical motion at 500 mb reaches a value of -16.5 μb s^{-1} over the southern tip of Illinois. Upward vertical motion decreases in magnitude by 1200 GMT as the squall line decreases in intensity.

These results indicate that areas of upward vertical motion develop and decay as areas of convection develop and decay, with vertical motion somewhat lagging the convection. As suggested by Aubert (1957), Danard (1964), and Ninomiya (1971 a and b), diabatic heating associated with convection probably is responsible for inducing the systematic changes in these vertical motion patterns. Since systematic changes in vertical motion are associated with areas of convection in the AVE IV experiment, such changes should also occur in terms C_A, VF_K, and VF_Π of the energy budget equations because these are functions of vertical motion. Since horizontal divergence is related to vertical motion, systematic changes are expected in terms HF_K and HF_Π of the energy equations as well. This first indication that systematic changes should occur in the synoptic-scale energy budgets of volumes enclosing areas of convection will be examined in much greater detail in following sections.

c. The energy budget of a developing squall line

Energy budgets of relatively small atmospheric volumes enclosing the squall line that formed at 1800 GMT on 24 April are examined in this section. The approach is designed to describe better the nature of synoptic-scale energy processes occurring in the vicinity of intense convection. These budgets at five time periods are compared with each other and to budgets for much larger areas. The formation, mature, and initial dissipation stages of development are studied using this squall line case while an additional squall line case is used later to investigate further the mature and dissipation stages.

1) Selection of area boundaries

The relatively small atmospheric volumes were chosen such that they just enclosed the squall line based on MDR values and moved as the squall line moved. Vertical dimensions were from the surface to 100 mb while horizontal boundaries were defined using the grid points on which numerical calculations were performed (Fig. 5, p. 20). The budget for each area and each 50-mb pressure layer was computed as the average of all grid points on or within the boundary. It should be emphasized that selection of horizontal boundaries was based solely on MDR data; spatial fields of the budget terms were not considered in the selection process. As spatial fields of the terms will reveal, a different boundary location could affect significantly computed averages in some cases. Figures 11 and 12 show two examples of the boundary selection procedure while Table 5 gives the number of grid points and associated areas for the boundaries used in this squall line case. The convection in Ohio and Michigan at 0600 GMT on 24 April (Fig. 12) was not included in the volume because it was found to have a much shorter life than the remainder of the squall line and appeared to be a separate system. While the goal was to barely enclose areas of convection, at least 20 grid points were used at each time. This meant that during initial development, the horizontal boundary was centered over the much smaller area of convection. Volumes used in this study are approximately the

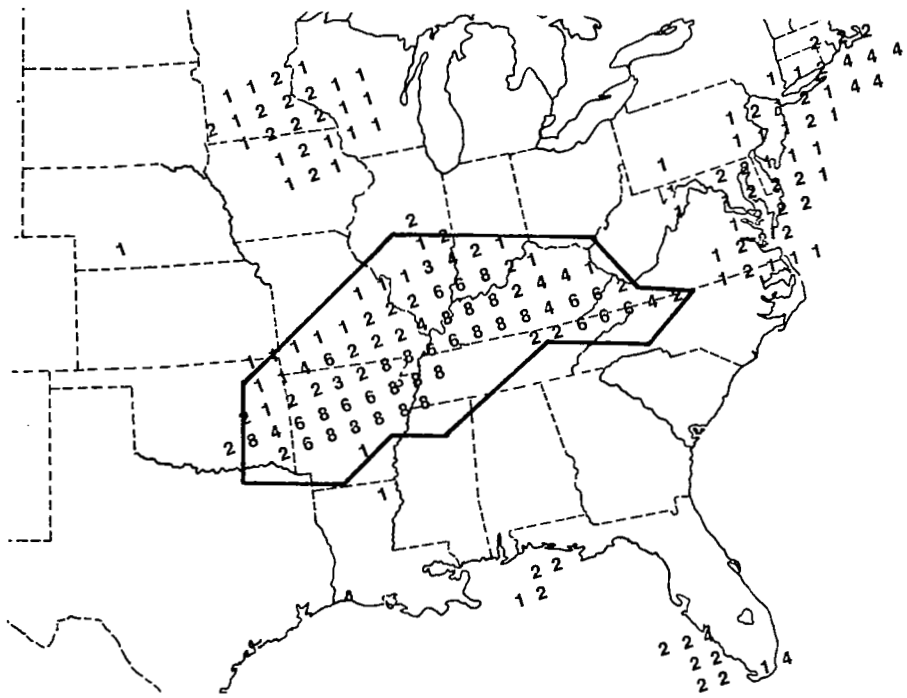

Fig. 11. Example of the limited volume used to enclose the squall line at 0600 GMT on 25 April. The area enclosed is 12.2×10^{11} m^2.

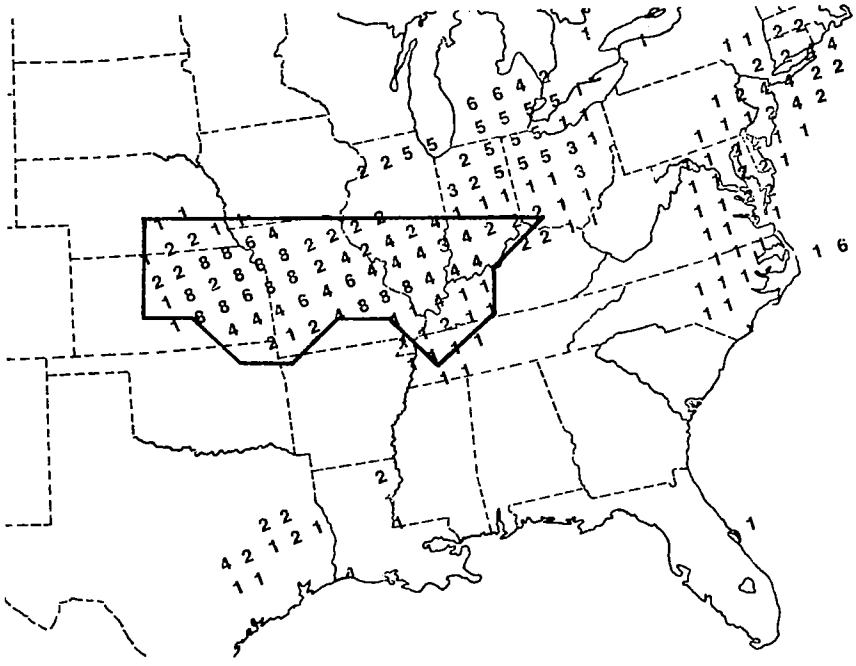

Fig. 12. Example of the limited volume used to enclose the squall line at 0600 GMT on 24 April. The area enclosed is 10.6×10^{11} m^2.

Table 5. Areas for which average energy budgets were computed for the squall line forming at 1800 GMT on 24 April.

Time	Number of points	Area (m^2)
1800 GMT, 24 April	24	8.8×10^{11}
2100 GMT, 24 April	24	8.8×10^{11}
0000 GMT, 25 April	30	10.6×10^{11}
0600 GMT, 25 April	35	12.2×10^{11}
1200 GMT, 25 April	39	13.4×10^{11}

same size as those used by such authors as Kung and Smith (1974), Kornegay and Vincent (1976), and Vincent and Chang (1975) and are much smaller than those used by numerous other investigators. They retain the desirable aspects of averaging and still enable consideration of a limited volume.

2) Average energetics in the vicinity of the squall line

Vertical profiles of energy budget terms are examined in this section. Values for several time periods are plotted on the same diagram to show the systematic nature of energy changes occurring in the vicinity of the squall line. To this author's knowledge, this is the first time that such results have been presented in the literature for most terms of the equations of total potential and kinetic energy. The tabulated energy budget of the squall line at peak intensity is examined in a later section.

i. Diabatic processes. Vertical profiles of generation of total potential energy by diabatic processes (term G) show a cyclic nature during the life cycle of the squall line (Fig. 13). Radiative effects dominate near the surface with diabatic heating occurring through 2100 GMT and diabatic cooling afterwards. The upper and middle troposphere exhibit a large increase in heating through 0600 GMT and a decrease in heating at 1200 GMT with maximum values occurring at approximately 450 mb. The time of maximum heating, 0600 GMT, corresponds to the time of maximum convective

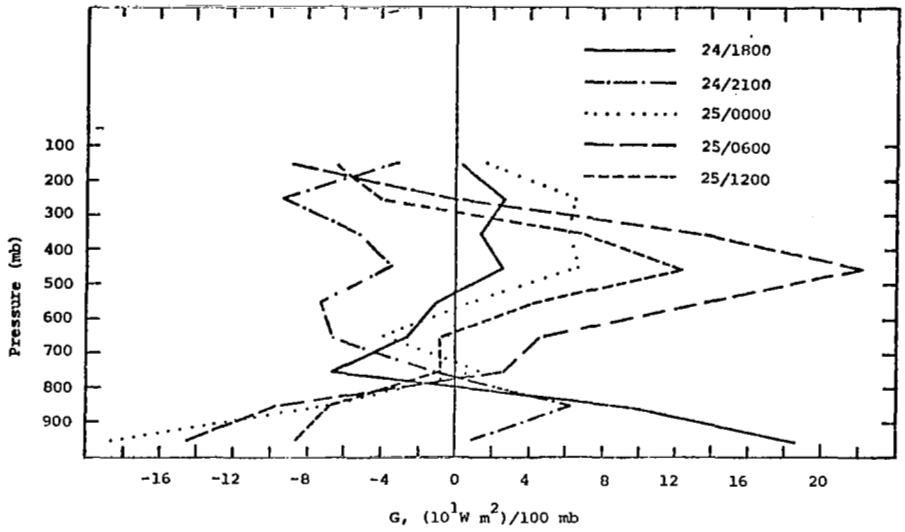

Fig. 13. Vertical profiles of term G for the squall line of 25 April.

activity; the 450-mb value at 0600 GMT is approximately three times the value observed at 0000 GMT. Latent heat release associated with convection is almost surely the cause for the observed profile in this portion of the atmosphere. Cooling at about 200 mb at 0600-1200 GMT is probably due to radiational losses above the cirrus shields of cumulonimbus clouds; such cooling has been observed by Anthes and Johnson (1968) in their study of Hurricane Hilda.

ii. Energy conversion terms. Values of A-conversion (term C_A) exhibit a remarkable systematic nature (Fig. 14). Since specific volume is always positive, the sign of the term is related directly to the sign of vertical motion. Slight conversion from potential to kinetic energy is observed near the surface and near the jet stream level at 1800 GMT when the squall line is beginning to form. This situation changes rapidly as the convection intensifies to strong conversion from potential to kinetic energy at all levels with a maximum at about 400 mb.

Conversion decreases somewhat by 1200 GMT as the convection

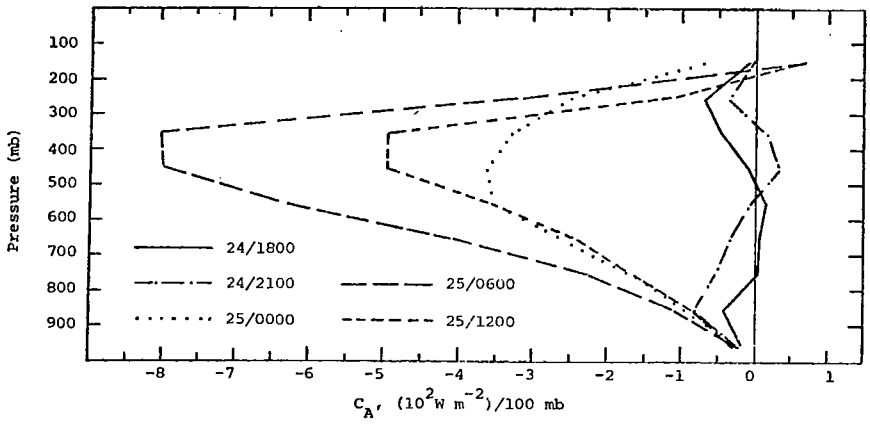

Fig. 14. Vertical profiles of term C_A for the squall line of 25 April.

decreases in intensity. Strong similarity between the vertical profiles of terms C_A and G in the middle and upper troposphere is evident. The shape of the profile of C_A is consistent with that suggested in a numerical study by Danard (1964).

The shapes of vertical profiles of term $-C_K$ (Fig. 15) are considerably different from those of term C_A, and values of $-C_K$ are much smaller than those of C_A. The ratio of $|-C_K|/|C_A|$ in the surface- to 100-mb layer remains approximately 1% at each of the five times. Positive values of term $-C_K$ indicate conversion from potential energy to kinetic energy due to cross-contour flow. Conversion to kinetic energy decreases with storm development and becomes conversion to potential energy at 0600 GMT near the 800- to 600-mb layer. The opposite occurs above 600 mb where conversion to kinetic energy increases with storm development, reaches a maximum value at 0600 GMT near 250 mb, and decreases at 1200 GMT. Results of McInnis and Kung (1972) for term $-C_K$ do not appear as cyclic in nature as the present results.

Variations in term $-C_K$ can result from changes in the vector wind and/or changes in the height gradient. Convection has been related to changes in both parameters in a way that helps explain

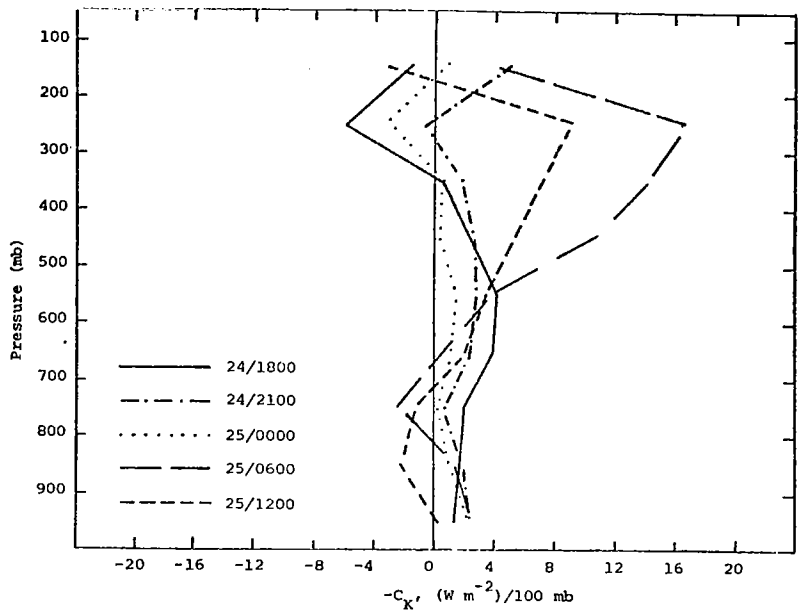

Fig. 15. Vertical profiles of term $-C_K$ for the squall line of 25 April.

the variation observed in this term. Increases in values of geopotential height in the middle and upper troposphere and decreases near the ground together with enhanced convergence in lower levels and enhanced divergence in upper levels have been associated with thunderstorm activity (Aubert, 1957; Danard, 1964; Ninomiya 1971a and b). These combined effects would lead to enhanced flow across height contours from high to low values near the surface producing enhanced conversion to kinetic energy. In the middle troposphere, increased cross-contour flow from low to high values leads to enhanced conversion to potential energy. Enhanced conversion to kinetic energy would occur in the upper atmosphere due to increased flow across height contours from high to low values. While the effect of tilting pressure systems has not been considered in this explanation, their presence generally should enhance the effects described above (Danard, 1964). Even if no height changes occur due to convection, results similar to the above could result

from wind changes associated with convection together with tilting pressure systems.

Kung (1967, 1974) has shown that conversion to kinetic energy is slightly greater at 0000 GMT than at 1200 GMT; the cause is not fully understood. Kung's results are opposite the present results in the upper atmosphere while at 750 mb Kung found only a small diurnal effect. It is doubtful that the systematic nature of term $-C_K$ in this study is caused to any great extent by diurnal effects.

iii. Boundary fluxes of kinetic energy. Significant systematic changes occur in terms HF_K and VF_K during the life cycle of the squall line. Horizontal outflow in the lower half of the atmosphere and strong horizontal inflow in the upper half of the atmosphere occur during the initial formation of the storm (Fig. 16). The horizontal inflow aloft is due largely to horizontal advection of kinetic energy since the storms form immediately downwind of a jet maximum. The profile reverses as the squall line reaches peak intensity at 0600 GMT such that weak inflow in the lower half of the atmosphere and strong outflow aloft occur. The jet maximum had moved to the northeast of the area of convection by this time. At 250 mb the range of HF_K between 1800 GMT and 0600 GMT is 44 W m^2/100 mb while in the lower troposphere the range is about one order of magnitude smaller. Magnitudes of HF_K decrease by 1200 GMT as the squall line decreases in intensity.

Values of VF_K are near zero as the convective area forms but change to vertical outflow of kinetic energy below about 400 mb and vertical inflow above about 400 mb with further development (Fig. 17). Kinetic energy is being transported to higher levels during the times of strongest convective activity since upward vertical motion is taking place over the area.

iv. Dissipation of kinetic energy. Vertical profiles of term D, given in Fig. 18, indicate that transfer of kinetic energy from subgrid to larger scales of motion generally increases with storm development below approximately 600 mb while enhanced transfer from grid to subgrid scales of motion occurs above 600 mb. While some cyclic nature is apparent, it certainly is not as pronounced as for

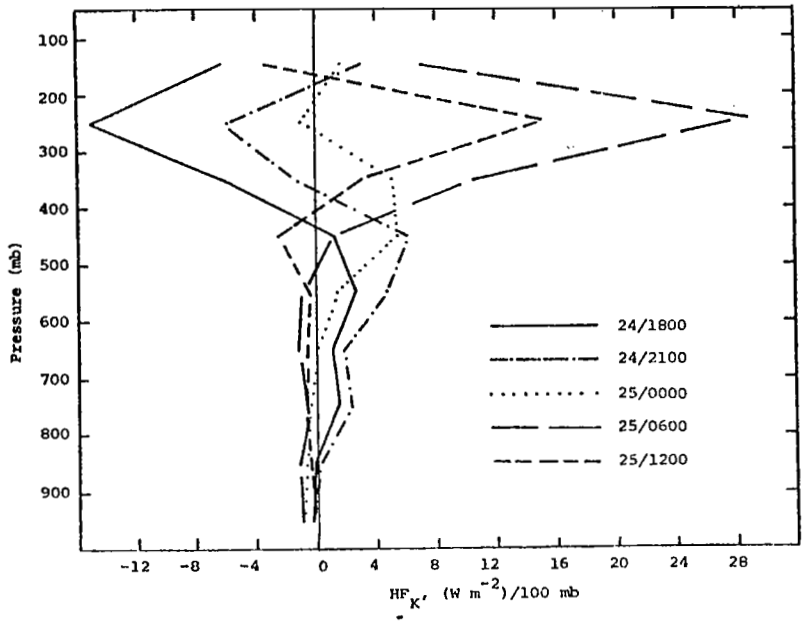

Fig. 16. Vertical profiles of term HF_K for the squall line of 25 April.

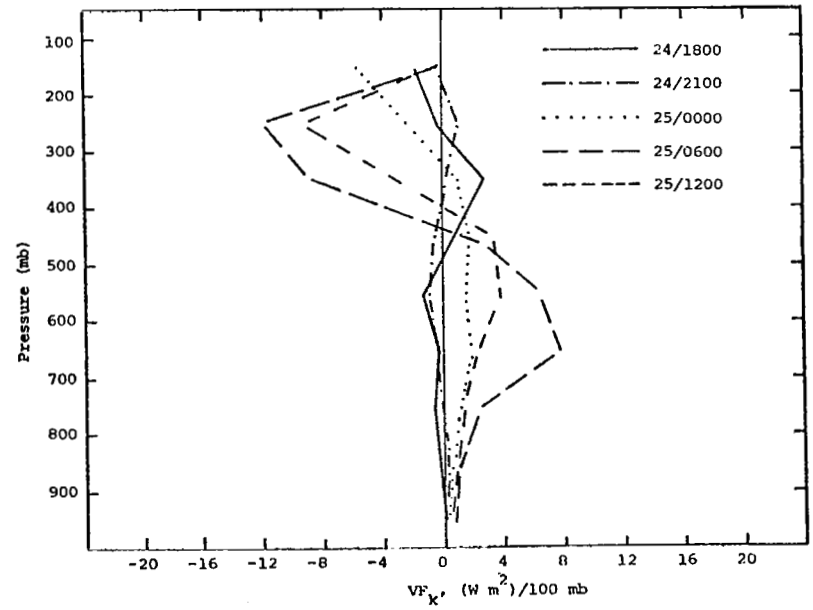

Fig. 17. Vertical profiles of term VF_K for the squall line of 25 April.

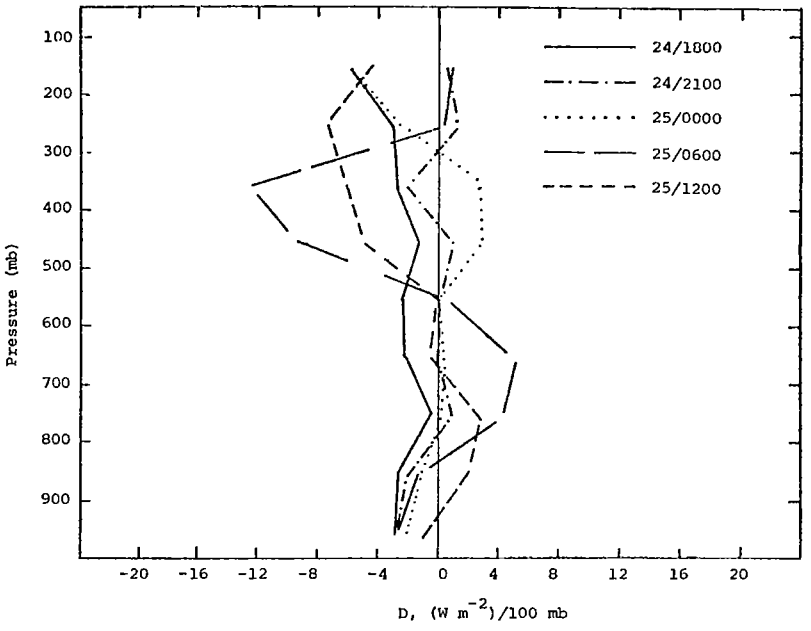

Fig. 18. Vertical profiles of term D for the squall line of 25 April.

most of the previous terms. Vertical totals of term D presented by McInnis and Kung (1972) also show considerable fluctuations. Since turbulence and other subgrid phenomena are large in thunderstorm areas, large values of term D of both signs should be expected. The diurnal tendency of term D (Kung, 1967) is small and is not thought to be important in explaining these results. Satellite pictures of this area reveal the presence of wave phenomena in the cloud patterns. Their presence could be important in explaining the observed values of D, but firm conclusions are not possible.

v. Time derivative of kinetic energy. The net effect of the various physical processes on kinetic energy within the limited volume is rather small because, for the most part, the processes cancel each other (Fig. 19). Values below 500 mb are only about ± 2 W m^{-2}/100 mb; above 500 mb they are ± 6 W m^{-2}/100 mb. Term $\frac{\partial K}{\partial t}$ appears slightly more negative as the convection intensifies, but the effect is small.

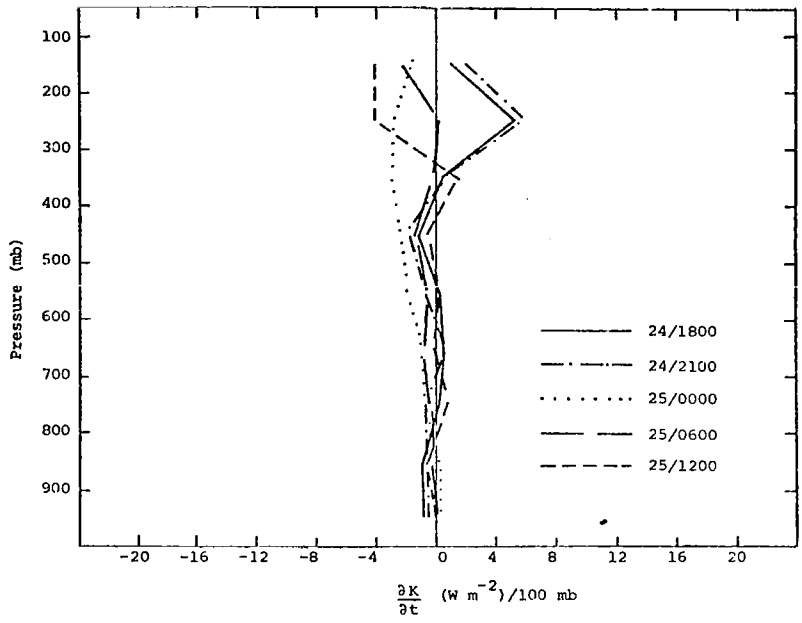

Fig. 19. Vertical profiles of term $\frac{\partial K}{\partial t}$ for the squall line of 25 April.

vi. Boundary fluxes of total potential energy. The vertical profile of term HF_{Π} at 1800 GMT indicates horizontal inflow of total potential energy in most levels of the atmosphere (Fig. 20). As the squall line develops the layer of inflow deepens while a region of outflow, apparent at 2100 GMT, decreases in depth and its maximum value increases in magnitude from about 2.0 x 10^3 W m^{-2}/100 mb at 2100 GMT to 7.5 x 10^3 W m^{-2}/100 mb at 0600 GMT. Magnitudes of the term decrease in value at 1200 GMT as the convection diminishes in intensity.

Profiles of term VF_{Π} also reveal a cyclic nature (Fig. 21). The top of the outflow layer near the surface rises from about 900 mb at 1800 GMT to near 500 mb at 0600 GMT. Correspondingly, the inflow layer aloft decreases in depth but peak values increase in magnitude during this period. Boundary flux terms indicate that potential energy in the lower atmosphere is transported horizontally

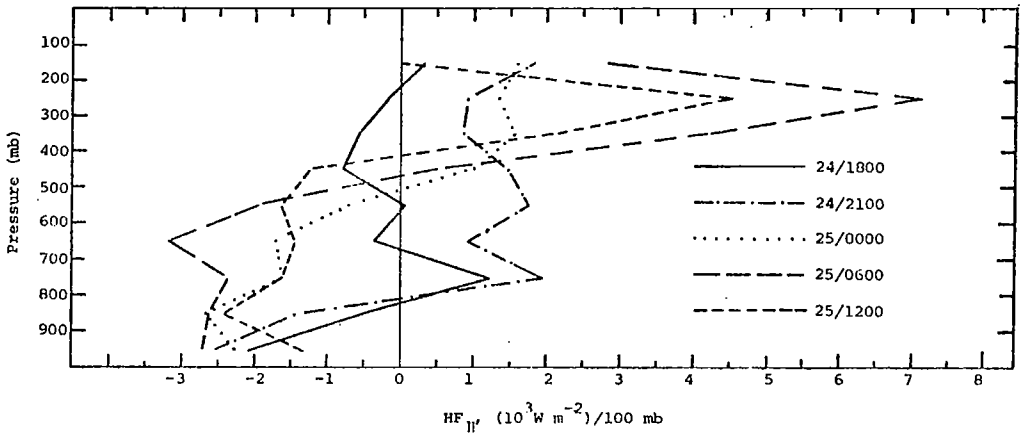

Fig. 20. Vertical profiles of term HF_{Π} for the squall line of 25 April.

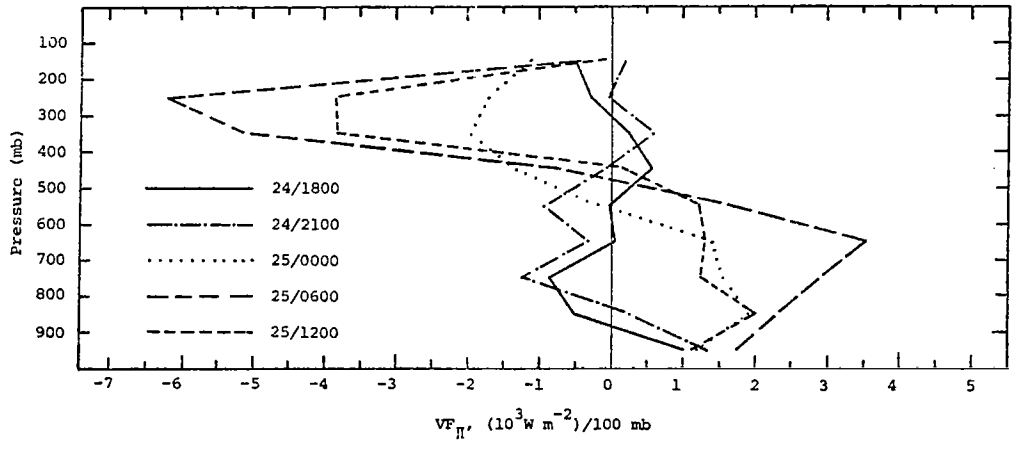

Fig. 21. Vertical profiles of term VF_{Π} for the squall line of 25 April.

into the convective area, transported vertically due to upward vertical motion, and then exported in the upper atmosphere.

3) Energy budget at peak intensity

i. Discussion. The synoptic-scale energy budget for the limited volume enclosing the squall line at peak intensity (0600 GMT) reveals very large conversion and transport processes. Table 6 gives this budget for a volume whose horizontal area is 12.2×10^{11} m^2 (Fig. 11, p. 52) about one-fourth the area of the total AVE IV experimental network. Diabatic heating, assumed to be the cause of the other energy changes, reaches a value of 569.0 W m^{-2} in the 800- to 200-mb layer. The maximum value in a 100-mb layer is 222.4 W m^{-2} which occurs between 500-400 mb. Krishnamurti and Moxim (1971) stated that convective heating should be largest in the upper troposphere in situations of deep convection with little entrainment. Assuming that all of the heating is due to latent heat of condensation, the value of 569.0 W m^{-2} corresponds to an average precipitation rate of 0.076 cm h^{-1} (0.03 in h^{-1}) over the area which seems reasonable since active convective cells cover only a small fraction of the total area. Fankhauser (1969) noted that if total heat production for a heating area is compared to the total latent heat production from all thunderstorms in that area, the orders of magnitude are comparable so that the net effect of storm presence is realized.

Values of terms C_A and $-C_K$ indicate large conversion from potential to kinetic energy while the small values of $|-C_K| / |C_A|$ indicate a great deal of interaction between the relatively small volumes enclosing convection and the surrounding volumes. Although the surface- to 100-mb value of K-conversion is 52.2 W m^{-2}, a corresponding increase in kinetic energy does not occur in the volume because of dissipation and boundary fluxes. In fact, the surface- to 100-mb layer sustains a net loss of kinetic energy of 6.2 W m^{-2} because 43.9 W m^{-2} of kinetic energy is transported horizontally out of the region while 14.5 W m^{-2} is transferred to subgrid scales of motion.

Table 6. Average energy budget for the limited area enclosing a squall line at 0600 GMT on April 25. The area is 12.2×10^{11} m^2 (Fig. 11, p. 52).

Pressure Layer mb	K 10^5 J m^{-2}	$\frac{\partial K}{\partial t}$ W m^{-2}	HF_K W m^{-2}	VF_K W m^{-2}	$-C_K$ W m^{-2}	D W m^{-2}	G W m^{-2}	C_K W m^{-2}	PW W m^{-2}	HF_Π W m^{-2}	VF_Π W m^{-2}	C_A W m^{-2}
200-100	4.8	-2.2	7.5	-0.1	4.3	0.9	-88.4	-4.3	676.9	2830.4	-461.5	65.4
300-200	6.0	0.2	28.8	-11.6	16.9	0.4	2.4	-16.9	474.8	7869.9	-6208.1	-318.1
400-300	4.4	-0.1	10.8	-8.8	14.3	-12.4	137.3	-14.3	-260.6	4183.9	-5096.1	-803.4
500-400	3.6	-1.4	1.3	1.8	11.0	-9.3	222.4	-11.0	-57.2	510.0	-701.5	-797.7
600-500	2.6	-0.9	-0.9	6.4	4.1	0.6	136.3	-4.1	-85.9	-1953.4	1652.8	-630.9
700-600	1.7	-1.0	-1.2	7.8	0.5	5.2	45.3	-0.5	94.7	-3184.5	3516.3	-406.7
800-700	1.0	-0.5	-0.3	2.6	-2.6	4.4	25.3	2.6	150.6	-2385.2	2913.3	-223.9
900-800	0.9	-0.3	-1.1	1.1	1.3	-1.5	-96.8	-1.3	-97.9	-2649.3	2306.1	-110.0
sfc-900	0.4	-0.1	-1.0	0.7	2.4	-2.7	-145.4	-2.4	-279.1	-2719.4	1740.1	-28.3
Vertical total	25.5	-6.2	43.9	-0.1	52.2	-14.5	238.4	-52.2	616.3	2502.4	-347.6	-3253.8

The vertical total of $-C_K$ is about twice the value given by Kung and Smith (1974) (Table 4, p. 41) for the vicinity of mature cyclones and suggests that large areas of intense convection may affect the general circulation as much as or more than mature cyclones. A striking difference between results of this study and those involving mature cyclones (Table 4) is found in the horizontal boundary flux term of kinetic energy. Net outflow in the surface- to 100-mb layer is seen in this study while large net inflow is observed in most mature cyclones; Petterssen and Smebye (1971) have found export associated with a mature cyclone, however. While net vertical flux of kinetic energy is near zero for the average mature cyclone, Smith (1973b) and West (1973) obtained vertical outflow near the ground and inflow in the upper atmosphere, as observed in this case. Petterssen and Smebye (1971), however, found vertical export aloft, and import into the middle troposphere. The vertical total of term D is larger in the vicinity of mature cyclones than near the squall line case at peak intensity. Vertical profiles of term D appear similar in mature cyclones and in this squall line case with transfer to subgrid scales of motion occurring near the ground and near the jet stream, while slight transfer of energy to larger scales of motion occurs in the middle troposphere (Smith, 1973a and b).

The budget of total potential energy is dominated by the boundary flux terms, HF_Π and VF_Π. As stated previously, sample calculations indicated that term $\frac{\partial \Pi}{\partial t}$ was several orders of magnitude smaller that terms HF_Π and VF_Π. Values of HF_Π and VF_Π given by West (1973) for individual layers of a mature cyclone are similar in both magnitude and sign to the present results.

Many of the processes observed near the squall line are reflected in the energy budget for the entire AVE area at 0600 GMT (Table 7). Vertical totals of all terms except G have the same sign for both areas, and values at individual layers indicate that maxima and minima for individual terms often occur near the same pressure level. Since values for the limited volume are often an order of magnitude greater than corresponding values for the large

Table 7. Average budget for the AVE IV experiment area at 0600 GMT on 25 April. The area is 49.0 x 10^{11} m^2.

Pressure Layer	K	$\frac{\partial K}{\partial t}$	HF_K	VF_K	$-C_K$	D	G	C_K	PW	HF_{Π}	VF_{Π}	C_A
mb	10^5 J m^{-2}	W m^{-2}	W m^{-2}	W m^{-2}	W m^{-2}	W m^{-2}	W m^{-2}	W m^{-2}	W m^{-2}	W m^{-2}	W m^{-2}	W m^{-2}
200-100	4.2	-0.7	0.7	-0.1	-1.1	1.1	-20.2	1.1	216.4	776.4	-18.7	22.6
300-200	5.6	0.9	1.6	-1.7	3.5	-2.7	1.3	-3.5	72.5	920.6	-666.7	-45.2
400-300	3.4	0.1	0.8	-1.2	0.3	-0.7	16.0	-0.3	88.3	655.6	-346.6	-73.7
500-400	2.1	-0.9	0.5	-0.3	-0.5	-0.2	35.2	0.5	59.3	349.4	-139.9	-75.4
600-500	1.3	-0.9	0.3	1.0	-0.7	1.2	6.5	0.7	59.6	-7.4	216.2	-58.6
700-600	0.9	-0.7	0.5	1.4	-0.6	1.7	-13.8	0.6	65.0	125.7	101.8	-40.5
800-700	0.6	-0.3	0.3	0.5	-0.7	1.2	-12.0	0.7	7.3	-288.6	314.2	-30.2
900-800	0.5	-0.1	0.1	0.3	0.9	-0.6	-81.6	-0.9	-6.9	-329.9	305.6	-12.7
sfc-900	0.3	-0.0	0.1	0.1	1.6	-1.4	-109.4	-1.6	-72.9	-288.8	33.0	-4.0
Vertical total	18.9	-2.5	4.7	-0.0	2.7	-0.6	-178.1	-2.7	489.3	1913.1	-201.1	-317.7

volume, this suggests further the great impact that relatively small volumes enclosing convection have on surrounding larger volumes.

The importance of convection also can be seen by comparing the budget of the limited volume enclosing the squall line (Table 6) with the budget obtained by averaging over the entire AVE IV area and over all nine time periods (Table 4, p. 41). Differences in sign of vertical totals of K-conversion and dissipation are especially noticeable; vertical profiles of these two terms are quite different for the two averages as well. Although the large area is characterized by K-conversion to potential energy and transfer of kinetic energy to grid scales of motion, significant areas of the opposite processes are occurring. The remaining terms often exhibit similar shaped vertical profiles, but the magnitudes of the terms for the individual squall line are generally much larger than those obtained by averaging over the entire experiment.

These results indicate that imbedded within the tranquil-looking energy budget of the entire AVE IV experiment is a squall line whose energy processes are larger than those reported for mature cyclones.

ii. Energy balance of the total potential energy equation. When the total potential energy budget is computed for such a limited volume and for only one time period, the question of a balanced budget naturally arises. Good balance is found for this study, however. A residual was computed from the potential energy equation, (21); term $\frac{\partial \Pi}{\partial t}$ was neglected because of its small size. The residual represents errors due to the input data, the assumptions made, and limitations of the computational procedures, and also reflects an inability to resolve relatively small-scale features in both time and space with the available data. To some extent then, it indicates a transfer of total potential energy between subgrid scales and larger scales. The value of the residual always is smaller than the values of the more important budget terms in the nine 100-mb layers and frequently is an order of magnitude smaller at 0600 GMT on 25 April. The ratio of the residual to the sum of the absolute values of the other individual terms

in (21) is less than 0.15 in most layers. Balance is generally poorest in the 200- to 100-mb layer. A ratio of about 0.12 was obtained in 250-mb layers for an available potential energy study of North America during an entire month (Smith and Horn, 1969). Balance for some time periods and volumes of this study is better than at 0600 GMT, and worse than at 0600 GMT for others, but it is felt that the trends of the results and the nature of the inferred processes can be considered with great confidence.

d. The energy budget of a decaying squall line

A second squall line case is examined in this section to determine if results of the previous case are an isolated phenomenon. This squall line began prior to the start of the AVE IV experiment and was already well developed, but not at peak intensity, when the experiment began at 0000 GMT on 24 April. The dissipation stage of the life cycle of convection can be examined in greater detail with this case. The same investigative approach as before was used for this squall line; Table 8 gives horizontal areas of the limited volumes used to enclose the squall line at four sampling times.

Table 8. Areas for which average energy budgets were computed for the squall line forming at 0000 GMT on 24 April.

Time	Number of points	Area (m^2)
0000 GMT, 24 April	22	8.2×10^{11}
0600 GMT, 24 April	28	10.0×10^{11}
1200 GMT, 24 April	25	9.1×10^{11}
1500 GMT, 24 April	20	7.6×10^{11}

1) Average energetics in the vicinity of the squall line

i. Diabatic processes. Heating in the middle and upper troposphere is the dominant feature in the vertical profile of

diabatic processes (Fig. 22). The maximum value of 285 W m^{-2}/100 mb occurs at 0600 GMT at 450 mb, near the time of peak convective activity. Values of heating decrease after 0600 GMT. Radiation effects dominate near the ground and near 150 mb in a similar manner to that observed for the previous squall line case.

ii. Energy conversion terms. The value of term C_A in the surface- to 100-mb layer is near zero at the beginning of the experiment although some conversion to kinetic energy is evident below 600 mb and above 300 mb (Fig. 23). Conversion to kinetic energy increases at all levels at 0600 GMT then steadily decreases so that the range of values observed near the time of dissipation (1500 GMT) is similar to that observed in the formation stage. The maximum value, occurring at about 450 mb, is somewhat larger for this case than for the previous case; the same is true for the maximum value of term G.

Conversion from potential to kinetic energy due to cross-contour flow (term $-C_K$) is occurring at all levels at 0000 GMT (Fig. 24). The conversion to kinetic energy increases in magnitude by the time of peak convective activity, then decreases by 1200 GMT so that conversion to potential energy occurs above 300 mb. At the last time period (1500 GMT) conversion to kinetic energy exists below 400 mb with conversion to potential energy occurring above that level. The cyclic nature of changes in term $-C_K$ is similar to that observed for the previous case above approximately 600 mb, but the tendency for enhanced conversion to potential energy in the 800- to 600-mb layer associated with peak convective activity is not as evident, however.

The ratio $|-C_K|/|C_A|$ in the surface- to 100-mb layer is near 0.35 at 0000 GMT but is less than 0.06 at the remaining times, and vertical profiles of $-C_K$ and C_A are generally quite dissimilar which indicates major interaction between the limited volume and the surrounding volume.

iii. Boundary fluxes of kinetic energy. Values of term HF_K (Fig. 25) are cyclic in nature and appear very similar to those of the previous squall line. Outflow of kinetic energy in the

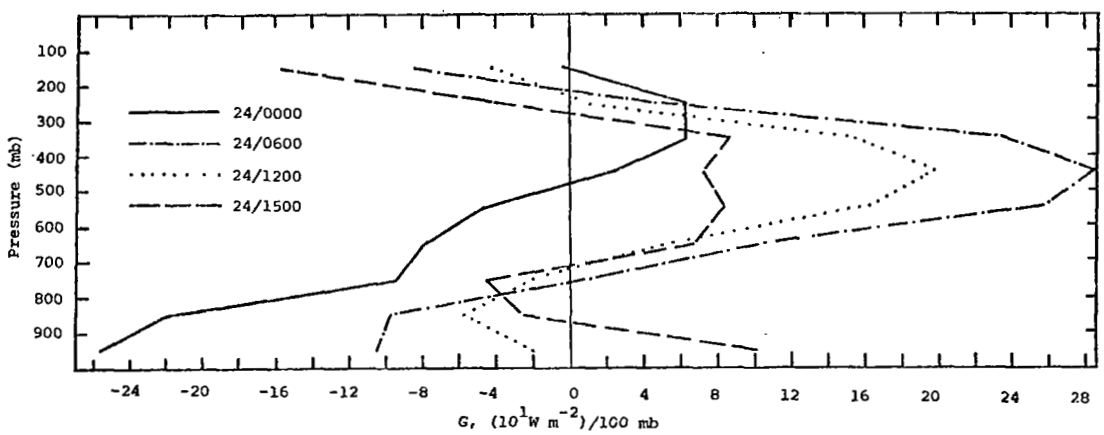

Fig. 22. Vertical profiles of term G for the squall line of 24 April.

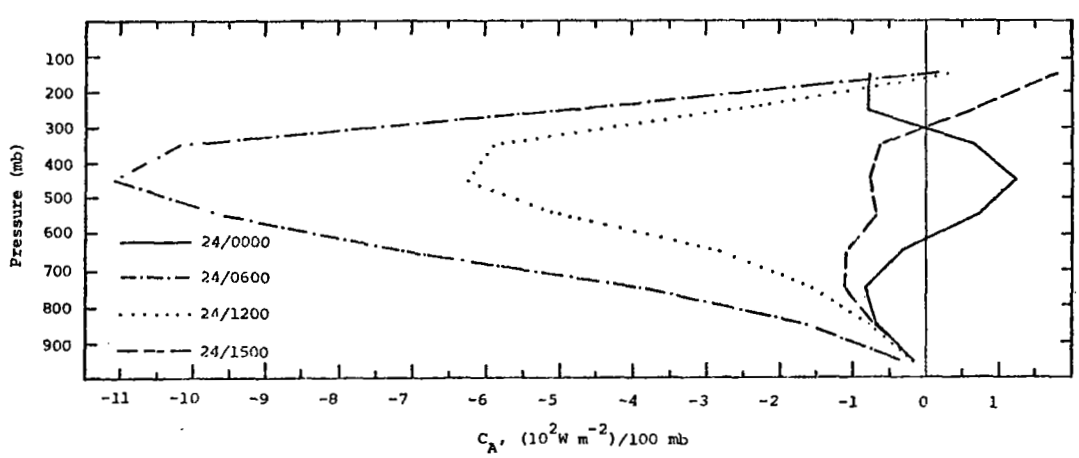

Fig. 23. Vertical profiles of term C_A for the squall line of 24 April.

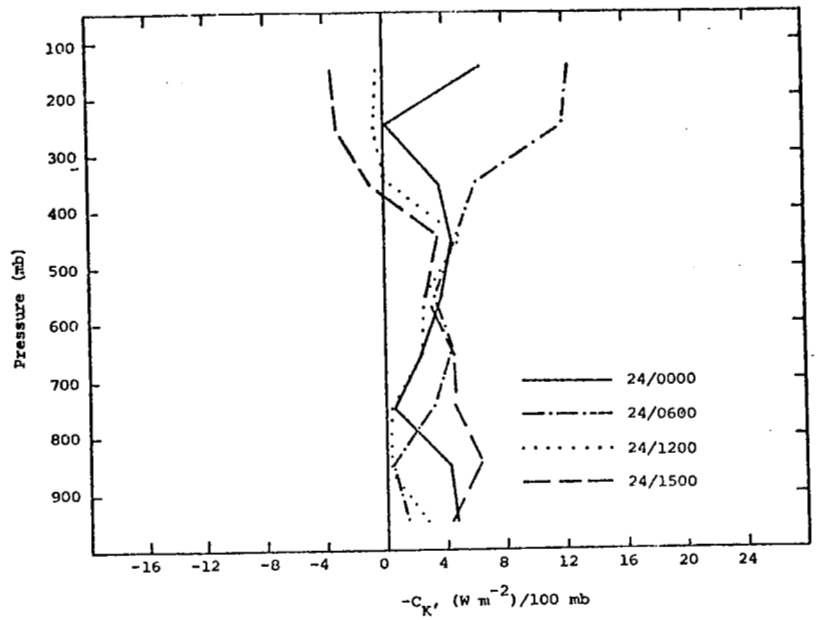

Fig. 24. Vertical profiles of term $-C_K$ for the squall line of 24 April.

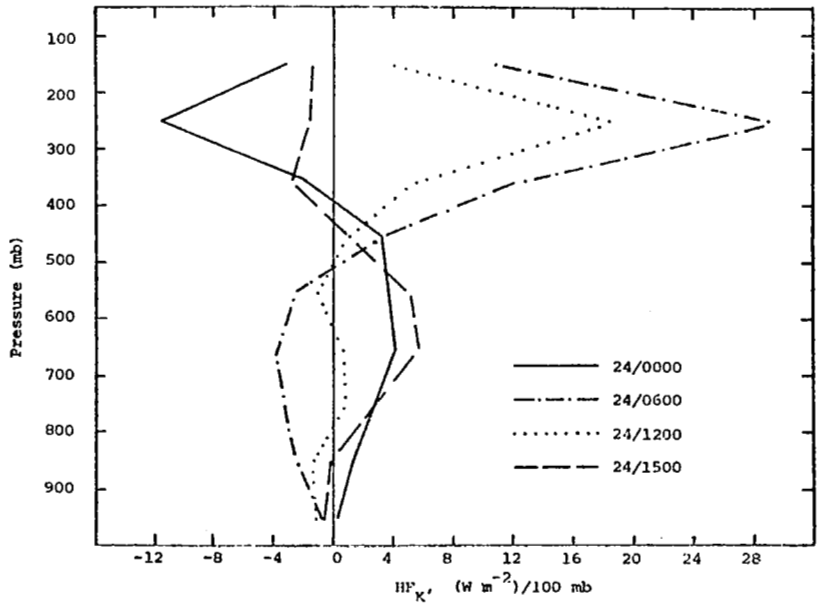

Fig. 25. Vertical profiles of term HF_K for the squall line of 24 April.

lower half of the atmosphere and inflow in the upper half at 0000 GMT change to inflow in the lower half and outflow aloft by 0600 GMT, then return to the original configuration by 1500 GMT. Low-level horizontal inflow at peak intensity is more pronounced for this case than for the previous squall line. The value of horizontal transport near 300 mb is influenced by the proximity of the convection to the jet stream. Kinetic energy is advected into the volume enclosing convective activity during the formation stage and advected out of the volume afterwards.

Values of VF_K (Fig. 26) also are similar to those observed previously. Minimal vertical flux at 0000 GMT changes to strong export of kinetic energy in the lower half of the atmosphere and strong import of kinetic energy aloft at the time of peak convective activity (0600 GMT). Values then decrease to near zero by 1500 GMT. Since upward vertical motion occurs in the area, values of HF_K and VF_K indicate that low-level kinetic energy is imported horizontally, carried aloft, and then exported horizontally near the jet stream.

iv. Dissipation of kinetic energy. Vertical profiles of D (Fig. 27) are considerably different for this case than for the previous one. Instead of enhanced transfer of kinetic energy from subgrid scales of motion to larger scales near 700 mb, values at this level remain nearly constant with no systematic changes occurring. Above 500 mb, transfer of energy to subgrid scales of motion at 0000 GMT gradually changes to transfer of energy to larger scales by 1200 GMT, then becomes near zero by 1500 GMT. Physical processes that are unresolvable in space and time produce a different result for this squall line, but their nature is unknown.

v. Time derivative of kinetic energy. Values of term $\frac{\partial K}{\partial t}$ range between ± 3 W m^{-2}/100 mb in the lower half of the atmosphere and are between 3 W m^{-2}/100 mb and -12 W m^{-2}/100 mb above 500 mb (Fig. 28). In this squall line case, term $\frac{\partial K}{\partial t}$ appears less negative when the enclosed convection is intense. The effect is small and differs from the result of the previous case indicating that

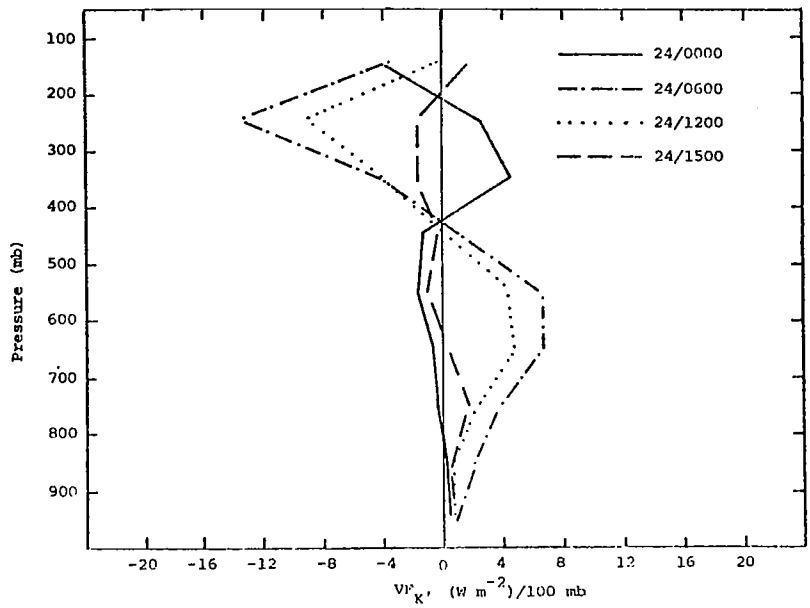

Fig. 26. Vertical profiles of term VF_K for the squall line of 24 April.

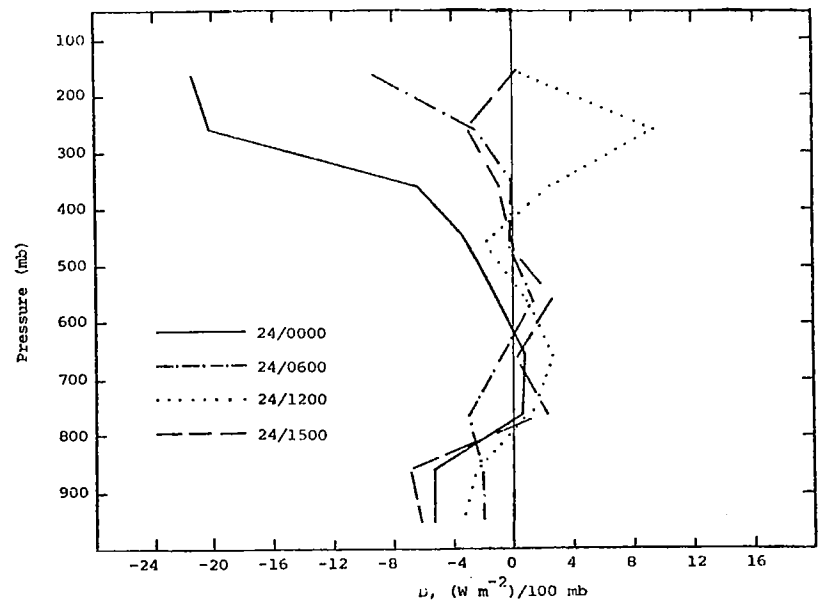

Fig. 27. Vertical profiles of term D for the squall line of 24 April.

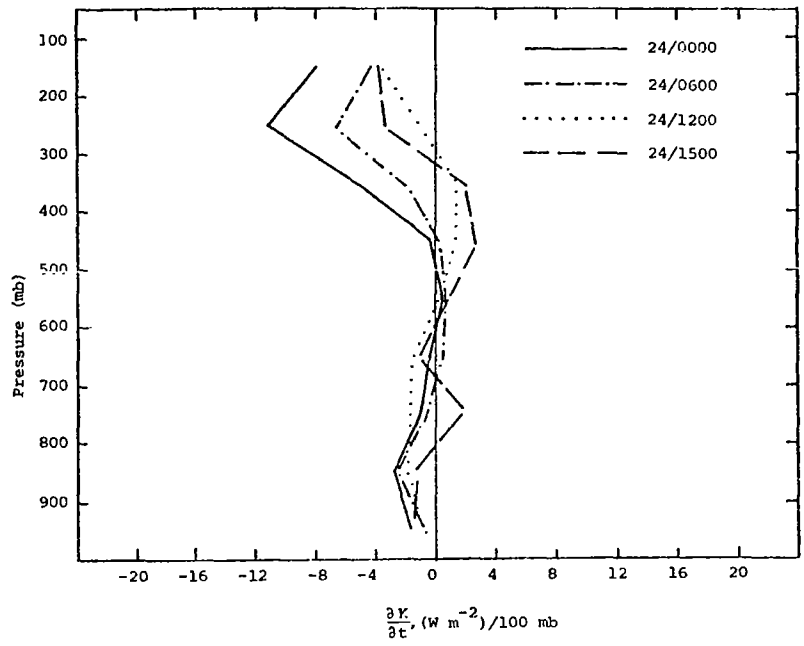

Fig. 28. Vertical profiles of term $\frac{\partial K}{\partial t}$ for the squall line of 24 April.

the net balance between the component processes affecting kinetic energy is somewhat different.

vi. Boundary fluxes of total potential energy. Values of terms HF_{Π} (Fig. 29) and VF_{Π} (Fig. 30) indicate that total potential energy is imported horizontally in the lower half of the atmosphere, transported aloft, and then exported horizontally when convection enclosed by the volume is at peak intensity (0600 GMT). Values of the two terms decrease systematically in magnitude after that time. The boundary flux processes are similar to those observed during the previous squall line.

2) Energy budget at peak intensity

Table 9 gives a composite energy picture of this squall line case at peak intensity, 0600 GMT on 24 April, for an area of 10.0×10^{11} m^2 shown in Fig. 12 (p. 53). The magnitudes and types of energy processes occurring at this time are similar to those

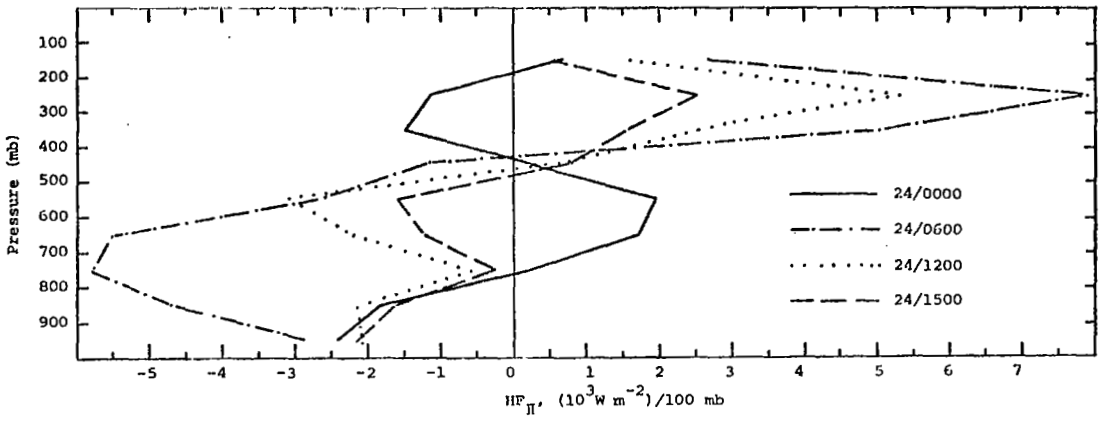

Fig. 29. Vertical profiles of term HF_{II} for the squall line of 24 April.

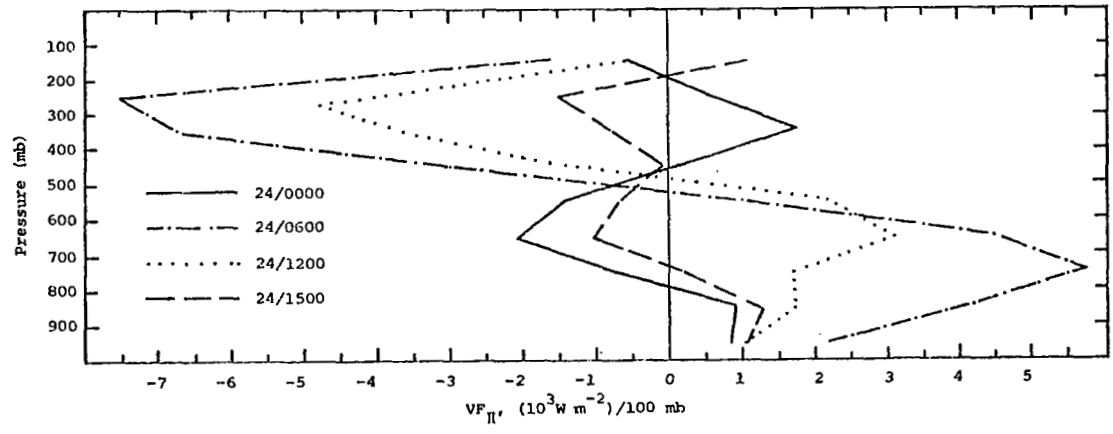

Fig. 30. Vertical profiles of term VF_{II} for the squall line of 24 April.

Table 9. Average energy budget for the limited area enclosing a squall line at 0600 GMT on 24 April. The area is 10.0×10^{11} m^2 (Fig. 12, p. 53).

Pressure Layer mb	K 10^5 J m^{-2}	$\frac{\partial K}{\partial t}$ W m^{-2}	HF_K W m^{-2}	VF_K W m^{-2}	$-C_K$ W m^{-2}	D W m^{-2}	G W m^{-2}	C_K W m^{-2}	PW W m^{-2}	HF_Π W m^{-2}	VF_Π W m^{-2}	C_A W m^{-2}
200-100	5.2	-4.3	10.9	-3.7	12.2	-9.3	-84.7	-12.2	303.9	2673.0	-1609.5	20.4
300-200	5.4	-6.5	29.5	-13.7	11.8	-2.4	50.2	-11.8	111.3	7914.1	-7524.6	-469.7
400-300	3.7	-2.1	12.8	-4.5	6.2	0.1	234.1	-6.2	-496.1	4967.5	-6710.7	-1015.3
500-400	3.0	0.2	3.7	0.8	4.8	-0.1	285.0	-4.8	-501.2	1187.0	-2941.4	-1109.4
600-500	2.4	0.5	-2.4	6.5	3.3	1.5	257.3	-3.3	-442.6	-2683.8	1134.3	-957.9
700-600	1.7	0.4	-3.6	6.8	4.4	-0.6	102.8	-4.4	-308.2	-5536.9	4457.7	-683.6
800-700	1.3	-0.6	-3.2	3.8	2.9	-2.9	7.6	-2.9	-18.3	-5797.0	5732.9	-383.0
900-800	1.0	-1.4	-2.3	2.2	0.5	-2.1	-97.8	-0.5	-161.2	-4697.5	4131.1	-163.0
sfc-900	0.4	-0.7	-0.9	1.0	1.5	-2.1	-105.2	-1.5	-192.8	-2871.6	2195.4	-34.1
Vertical total	24.1	-14.4	44.6	-0.8	47.5	-18.0	649.4	-47.5	-1707.0	-4845.3	-1134.8	-4795.7

observed for the previous case at peak intensity (Table 6, p. 64). Heating in the 800- to 200-mb layer totals 937.0 W m^{-2}, corresponding to a rainfall rate of 0.13 cm h^{-1} (0.05 in h^{-1}) if all of the heating is due to latent heat of condensation, and is somewhat larger than the previous case. Maximum heating for both cases occurs near 450 mb.

A-conversion to kinetic energy (term C_A) is also greater for this case than the previous one although the vertical profiles are similar in shape. Only about 1.0% of term C_A is realized in cross-contour conversion to kinetic energy (term $-C_K$). The vertical total of 47.5 W m^2 for term $-C_K$ is much larger than observed in the vicinity of mature cyclones (Kung and Smith, 1974). Vertical totals of terms HF_K and VF_K are similar for the two cases. Boundary flux and dissipation processes are large enough in both cases to overcome the large generation of kinetic energy and produce negative values of term $\frac{\partial K}{\partial t}$ in most layers of the atmosphere. Boundary fluxes of total potential energy are somewhat larger for this case than for the previous one and dominate the budget.

Some of the processes observed in the relatively small volume enclosing the squall line at peak intensity are reflected, to a lesser degree, in the budget of the entire AVE area at 0600 GMT (Table 10), but there are some notable exceptions. The large volume is characterized by K-conversion to potential energy and transfer of kinetic energy from subgrid to grid scales of motion while the opposite processes occur near the area of intense convection. Diabatic cooling near the surface and above 300 mb is large enough to cancel the weak heating occurring in the middle troposphere for the larger volume, but heating is indicated in the vertical total of the small volume.

Values of all terms are smaller for the large volume than for the more limited volume and like the previous squall line case, some terms are an order of magnitude smaller. Vertical profiles of the various boundary flux terms and time derivative term are generally similar in shape for both volume sizes.

In summary, most of the systematic changes observed for the

Table 10. Average energy budget for the AVE IV experiment area at 0600 GMT on 24 April. The area is 49.0×10^{11} m^2.

Pressure Layer mb	K 10^5 J m^{-2}	$\frac{\partial K}{\partial t}$ W m^{-2}	HF_K W m^{-2}	VF_K W m^{-2}	$-C_K$ W m^{-2}	D W m^{-2}	G W m^{-2}	C_K W m^{-2}	PW W m^{-2}	HF_Π W m^{-2}	VF_Π W m^{-2}	C_A W m^{-2}
200-100	4.6	-1.7	2.7	0.4	-4.5	5.9	-66.2	4.5	269.4	943.9	-1.1	50.4
300-200	5.3	-1.3	4.6	-2.6	-2.9	3.6	-13.9	2.9	117.4	1435.9	-1025.3	-45.0
400-300	3.3	-0.1	0.6	-0.7	-1.1	0.8	22.4	1.1	110.5	1063.6	-677.0	-104.6
500-400	2.1	-0.3	0.2	-0.1	-1.6	1.5	20.5	1.6	54.3	570.1	-380.2	-120.3
600-500	1.5	-0.4	-0.1	0.9	-2.1	2.5	16.0	2.1	53.7	-21.6	209.5	-102.0
700-600	1.2	-0.5	0.0	0.7	-1.4	1.6	-13.9	1.4	51.7	-259.8	440.9	-70.4
800-700	1.0	-0.6	0.1	0.3	-0.9	0.8	-39.6	0.9	19.2	-505.7	572.8	-42.2
900-800	1.1	-0.3	0.2	0.6	1.2	-0.7	-98.6	-1.2	-28.5	-591.5	491.5	-16.4
sfc-900	0.5	-0.1	0.2	0.3	2.9	-2.5	-100.7	-2.9	-82.0	-203.6	-84.2	-2.9
Vertical total	20.5	-5.4	8.7	-0.2	-10.5	13.5	-274.0	10.5	565.6	2431.2	-453.0	-453.3

first squall line case are observed in the second case as well. Although there are considerable differences in terms $\frac{\partial K}{\partial t}$ and D between the two cases, vertical profiles and magnitudes of the remaining terms are generally similar. The two sets of results suggest that observed energy changes associated with intense convection are not isolated phenomena.

e. Spatial maps of energy budget terms

The final step of "telescoping in" on energy processes associated with convection is a discussion of spatial maps of energy budget terms. These maps provide a means of directly relating energetics to observed areas of convection without averaging over particular volumes. Since the limited volumes of the previous sections were defined solely on the basis of MDR data, average values for such volumes do not describe adequately energy processes that are not centered over the area of convection. Fields of terms G, C_A, $-C_K$, HF_K, VF_K, $\frac{\partial K}{\partial t}$, and D are shown at three time periods on 25 April at 0000 GMT, 0600 GMT, and 1200 GMT, so that energetics of the squall line can be examined before, during, and after peak intensity. It is not possible to present spatial fields of all terms in the energy budget equations at all nine time periods because of the large number of maps involved, but those presented describe some of the more important energy processes and establish time continuity and vertical consistency of the fields. In the discussion that follows, layer 1 will be used to refer to the surface- to 700-mb layer, layer 2 to the 700- to 400-mb layer, and layer 3 to the 400- to 100-mb layer. Positive values of terms are shown by solid lines, and negative values by dashed lines; all values represent integrated quantities through the given layer expressed in W m^{-2}. Convection with MDR values greater than or equal to 4 is indicated by scalloping.

1) Spatial fields at 0000 GMT on April 25

i. Diabatic processes. Areas of generation of total potential energy due to diabatic heating in layer 2 relate well to the precipitation occurring over South Dakota, the Appalachians, and

the Midwest States (Fig. 31a). The convection occurring near Oklahoma had formed during the previous hour, and no heating is indicated in that area. Maximum diabatic heating over the squall line is about 600 W m^{-2} in layer 2 over Missouri.

ii. Energy conversion terms. A-conversion to kinetic energy occurs over many of the precipitation areas in layer 1 (Fig. 31b) with maxima located over Missouri and West Virginia. Conversion to kinetic energy due to cross-contour flow (term $-C_K$) occurs over almost the entire AVE IV area (Fig. 31c) which is expected since frictional effects aid in this conversion near the ground. Maximum values of term $-C_K$ are over North Carolina, slightly east of the shower activity and southeast of the maximum value of term C_A. No closed centers of K-conversion are seen at this time over the Midwest States associated with the developing squall line.

Negative values of term C_A, indicating conversion to kinetic energy, occur in layer 3 along the squall line in the Midwest with magnitudes reaching -2.5×10^3 W m^{-2} over southeastern Oklahoma (Fig. 31d). Areas of maximum K-conversion in layer 3 (Fig. 31e) occur near the areas of maximum A-conversion. Conversion to kinetic energy is seen along and slightly west of the squall line while conversion to potential energy is occurring over the southern Mississippi Valley.

iii. Horizontal boundary flux of kinetic energy. Weak low-level inflow of kinetic energy, less than -10 W m^{-2}, occurs along and just east of the squall line in the Midwest (Fig. 31f). Areas of horizontal inflow and outflow are associated with the older precipitation area occurring along the Appalachians. Similar areas will be seen along the squall line at later time periods. The conditions seen in layer 1 generally reverse in layer 3 (Fig. 31g) as seen previously in budgets for limited areas. Maximum magnitudes of term HF_K in layer 3 generally are less than 75 W m^{-2}.

iv. Vertical boundary flux of kinetic energy. Fields of VF_K in layers 1 and 3 (Figs. 31h-i) and vertical motion (Fig. 10, p. 45) indicate that kinetic energy is transported aloft near the squall line and near the Appalachians. Magnitudes of VF_K are rather

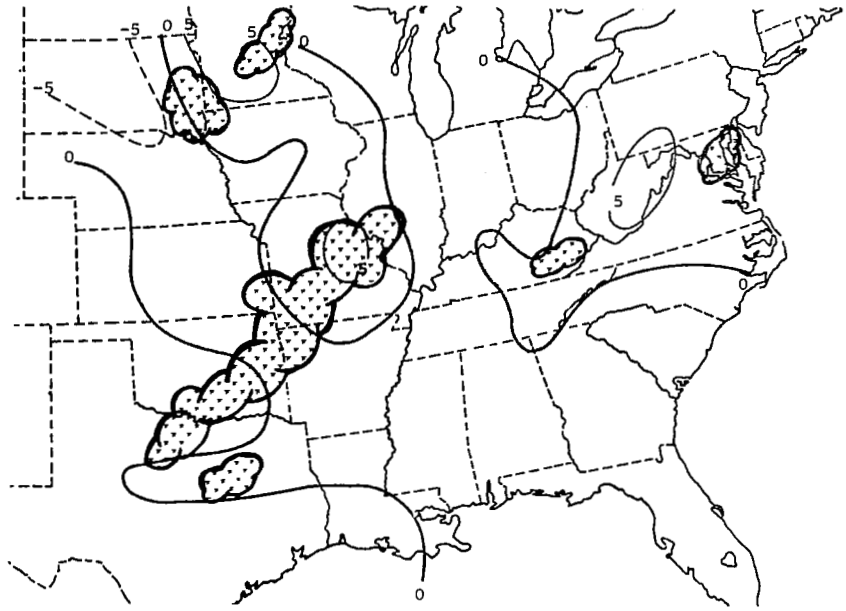

(a) Term G, 10^2 W m^{-2}, layer 2

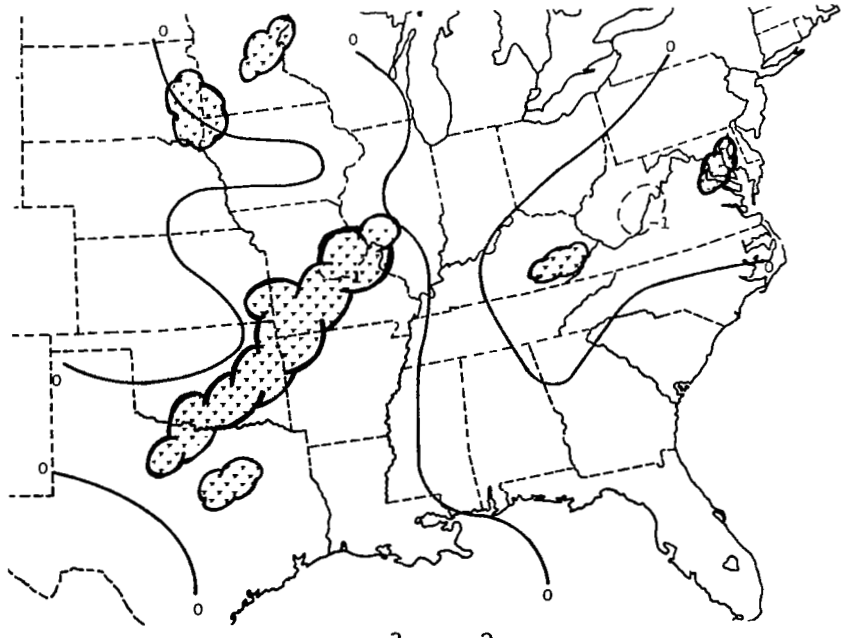

(b) Term C_A, 10^3 W m^{-2}, layer 1

Fig. 31. Spatial fields of energy budget terms at 0000 GMT on 25 April. Superimposed are areas of MDR values ≥ 4.

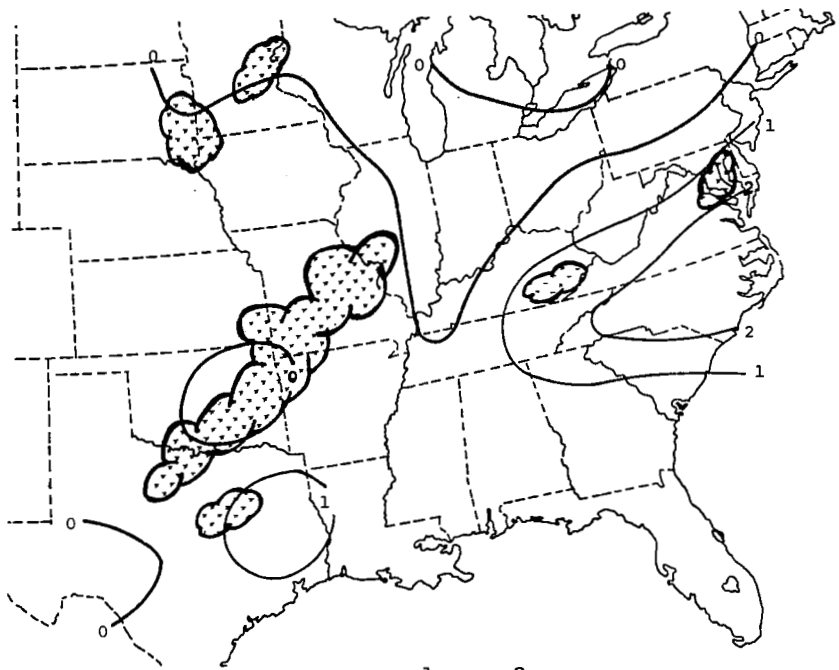

(c) Term $-C_K$, 10^1 W m^{-2}, layer 1

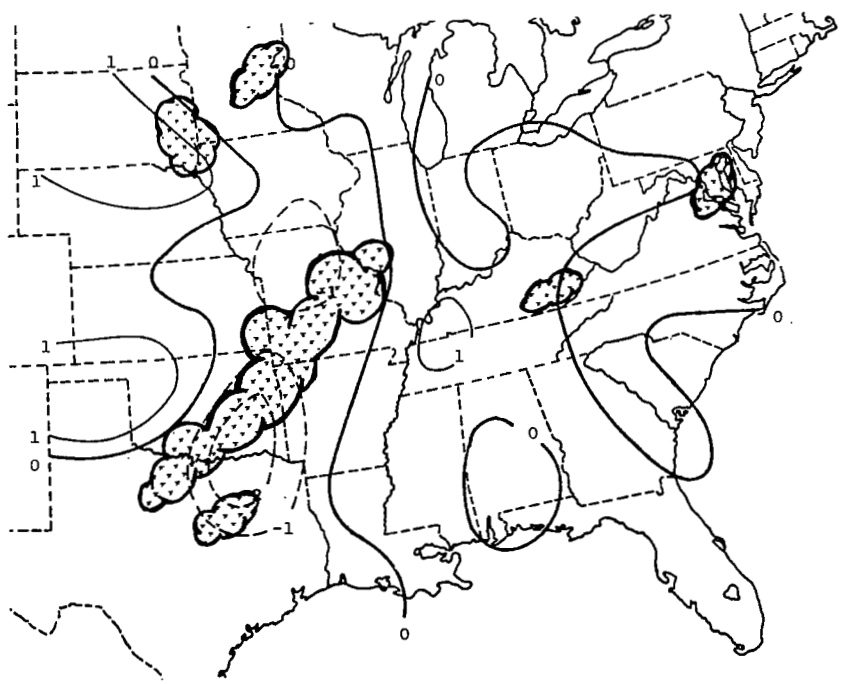

(d) Term C_A, 10^3 W m^{-2}, layer 3

Fig. 31. (Continued)

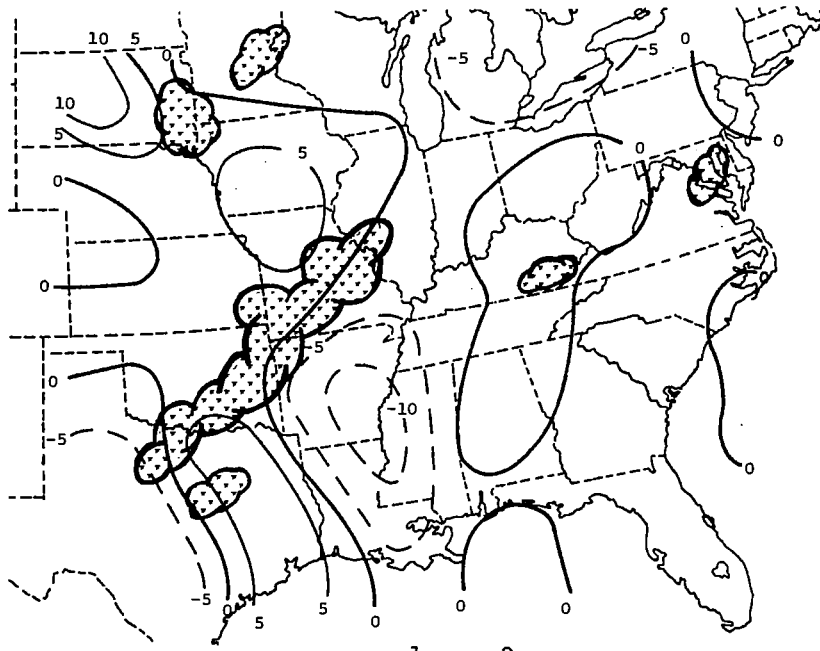

(e) Term $-C_K$, 10^1 W m^{-2}, layer 3

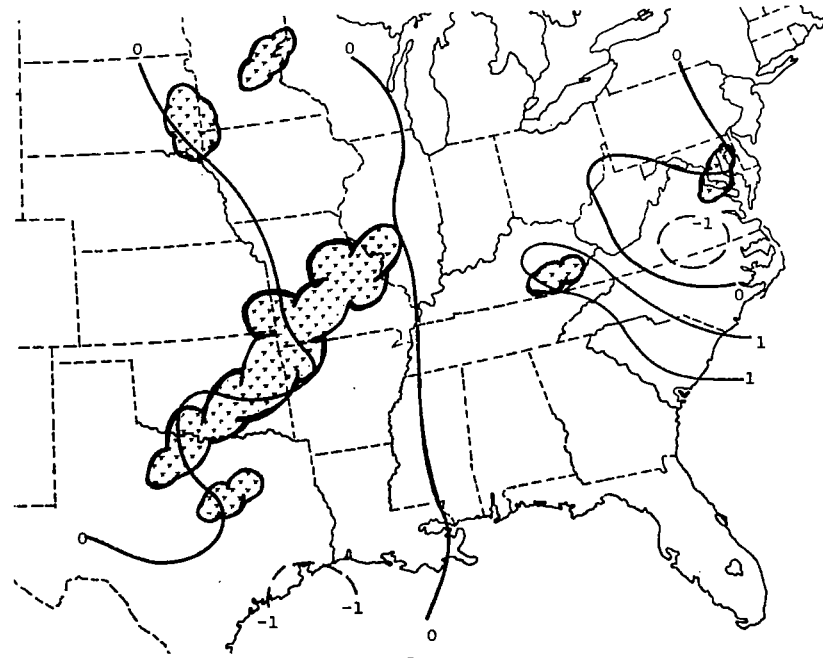

(f) Term HF_K, 10^1 W m^{-2}, layer 1

Fig. 31. (Continued)

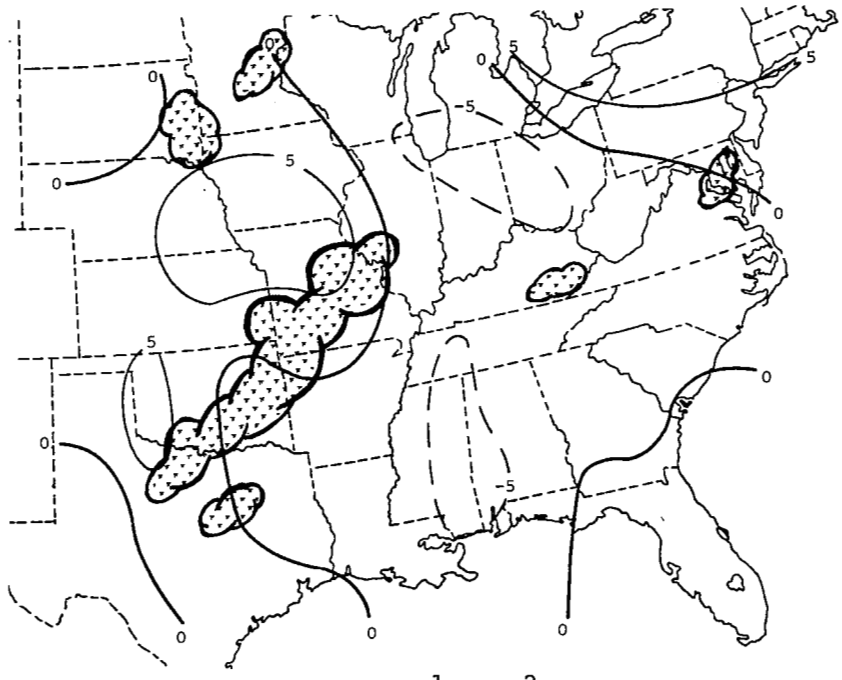

(g) Term HF_K, 10^1 W m^{-2}, layer 3

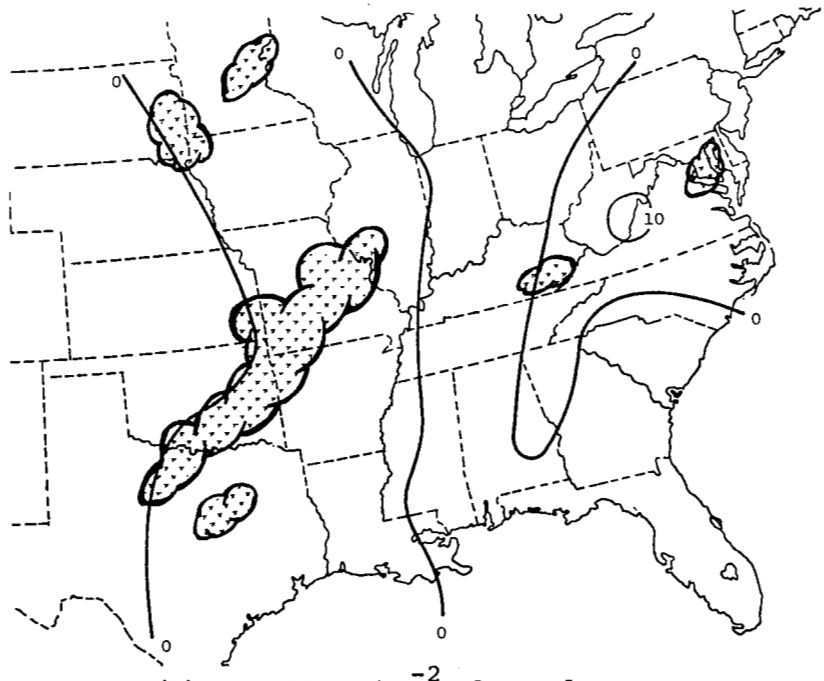

(h) Term VF_K, W m^{-2}, layer 1

Fig. 31. (Continued)

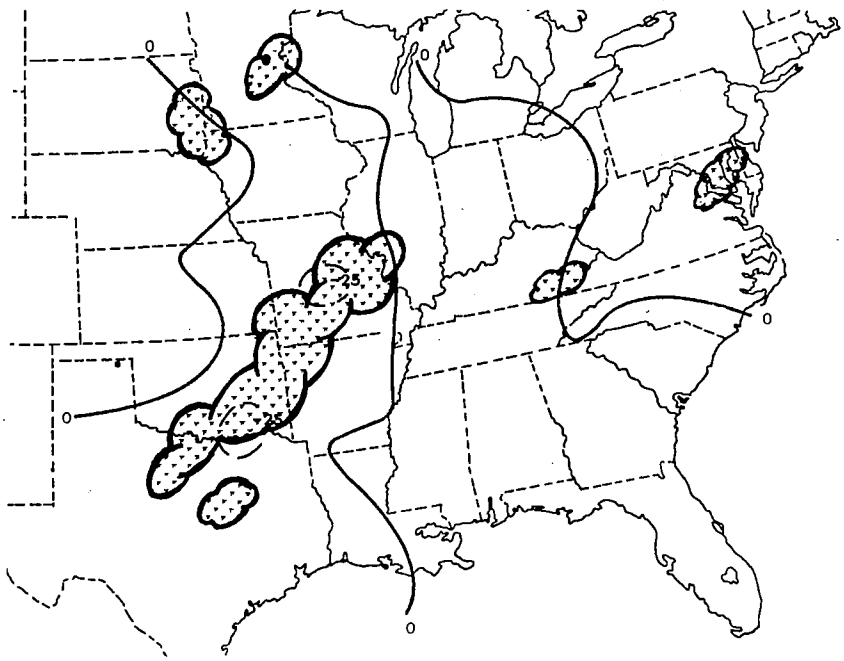

(i) Term VF_K, W m^{-2}, layer 3

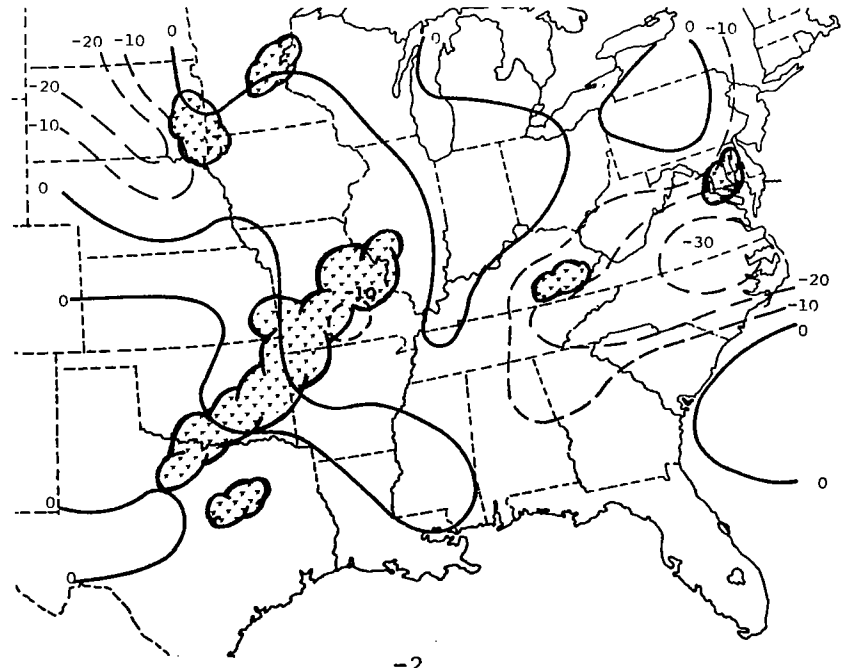

(j) Term D, W m^{-2}, layer 1

Fig. 31. (Continued)

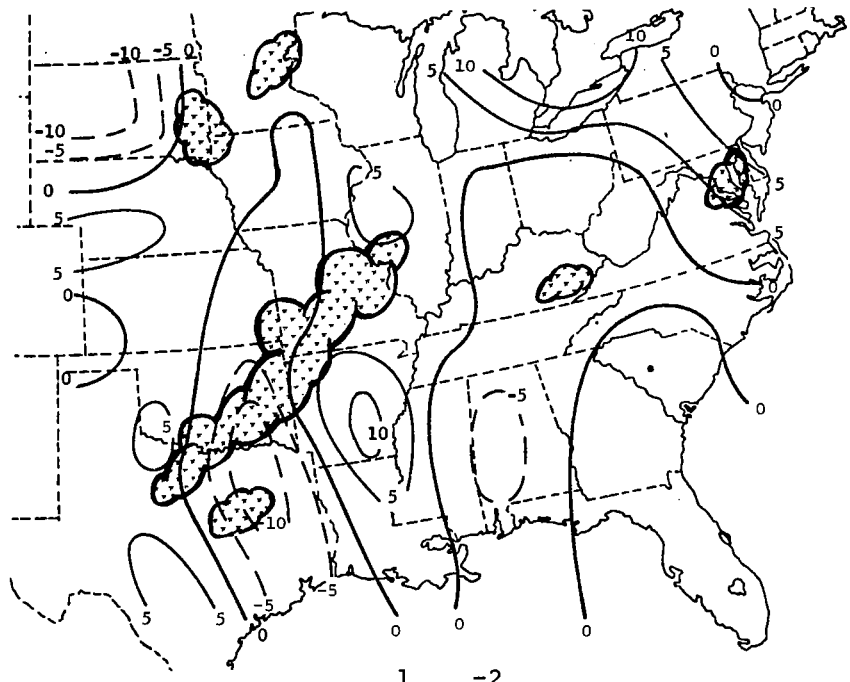

(k) Term D, 10^1 W m^{-2}, layer 3

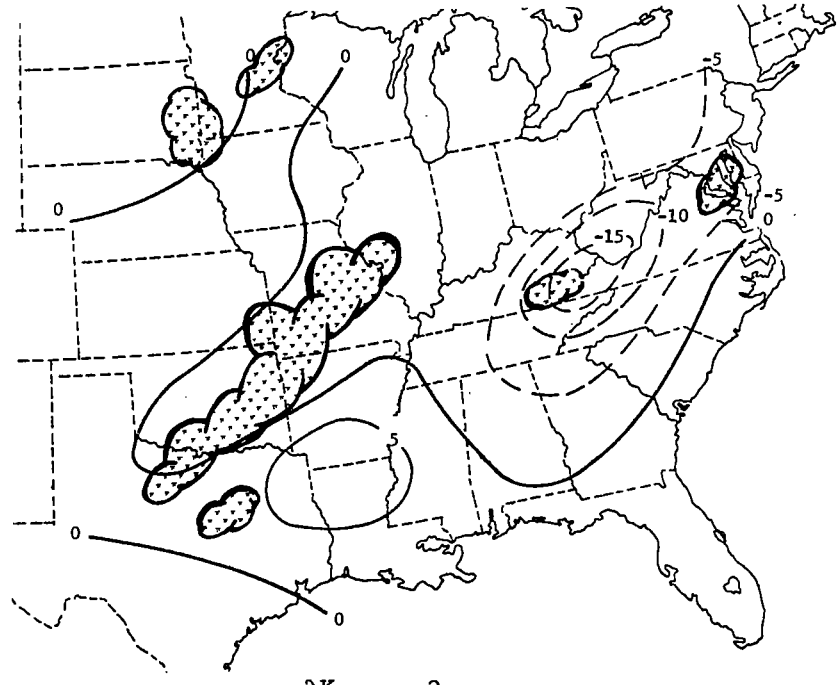

(l) Term $\frac{\partial K}{\partial t}$, W m^{-2}, layer 1

Fig. 31. (Continued)

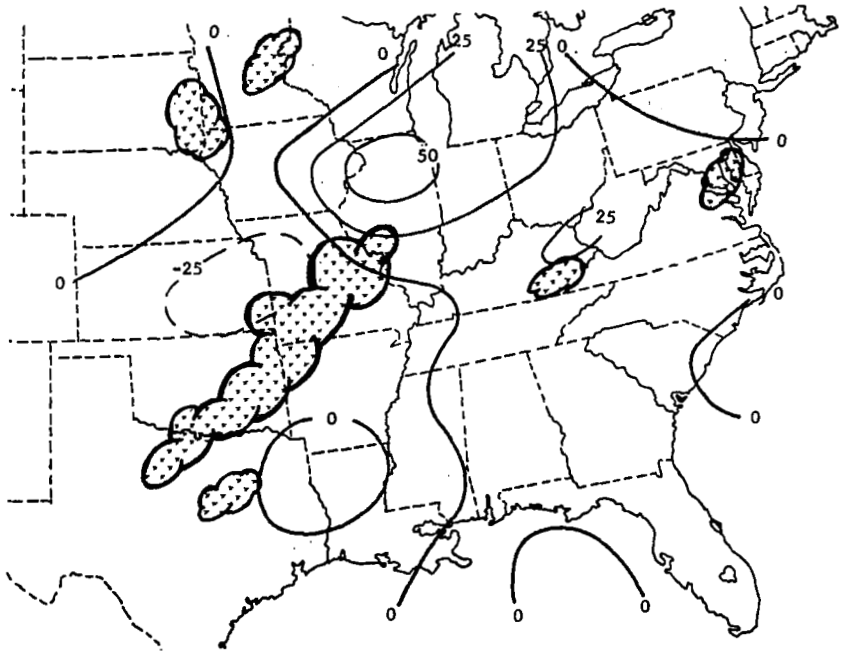

(m) Term $\frac{\partial K}{\partial t}$, W m^{-2}, layer 3

Fig. 31 (Continued)

weak at this time, less than 6 W m^{-2} in layer 1 and less than 30.0 W m^{-2} in layer 3.

v. Dissipation of kinetic energy. Most of the area in layer 1 is experiencing negative dissipation which is expected since layer 1 includes the surface (Fig. 31j). Positive values are much smaller than the negative values and do not show much relation to the convection. Centers of positive and negative dissipation are seen in layer 3 (Fig. 31k). Transfer of kinetic energy from subgrid to grid scales occurs in the northeastern portion of the squall line while the reverse occurs in the central and southwestern portions.

vi. Time derivative of kinetic energy. Relatively small values of $\frac{\partial K}{\partial t}$ are seen in layer 1; negative values are largest in the Appalachians and are associated with a low-level wind maximum (Fig. 31l). Maximum increases in kinetic energy in layer 3 are found in northern Illinois just east of an advancing short wave and north of the squall line (Fig. 31m), but values are relatively small when compared to the component energy processes.

2) Spatial fields at 0600 GMT on April 25

Although the vertical profiles of energy budget terms shown previously indicate considerable changes between 0000 GMT and 0600 GMT, the changes in spatial fields are even more dramatic. Figure 32 contains maps for 0600 GMT.

i. Diabatic processes. The area of diabatic heating in layer 2 grows in area and intensity as the squall line intensifies (Fig. 32a). The maximum value of 2.3 x 10^{3} W m^{-2} is nearly four times larger than the maximum value observed 6 h earlier while the area of heating corresponds almost perfectly to the area of convection. The maximum value corresponds to a rainfall rate of 0.32 cm h^{-1} (0.13 in h^{-1}) which is well below the maximum observed rainfall rate of 5.1 cm h^{-1} (2.0 in h^{-1}), but as Fankhauser (1969) pointed out, such differences are reasonable when area coverage is considered. Weak diabatic cooling is occurring over most of the remainder of the AVE IV area.

ii. Energy conversion terms. Maximum A-conversion to kinetic energy in layer 1 occurs along and slightly east of the squall line

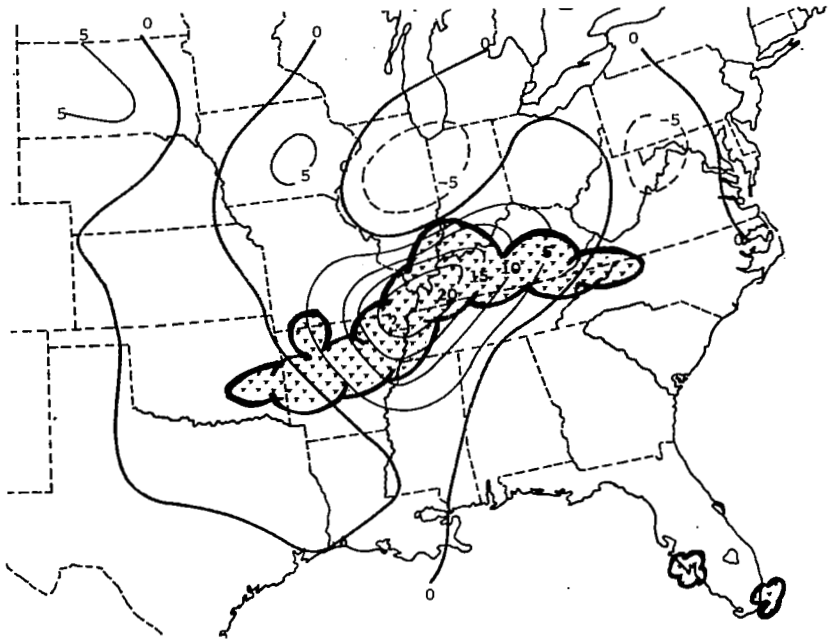

(a) Term G, 10^2 W m^{-2}, layer 2

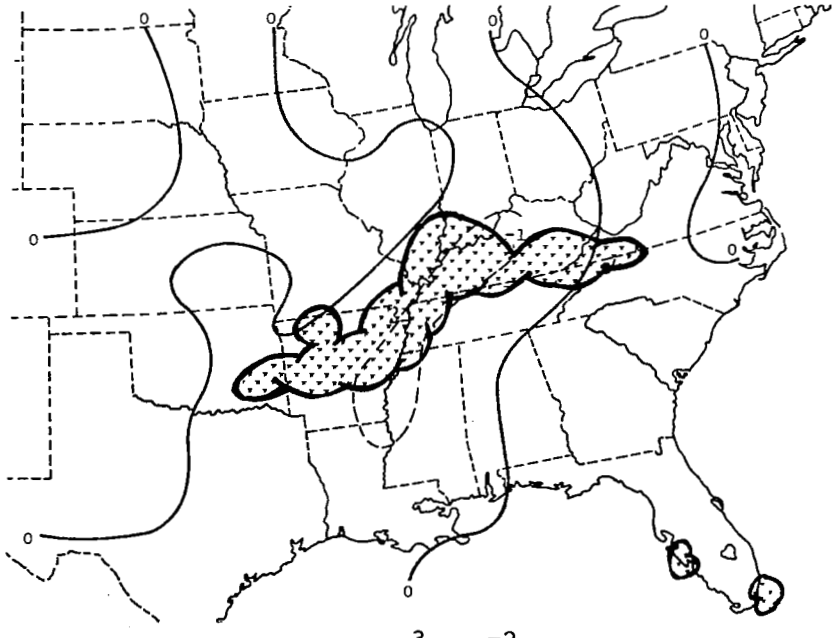

(b) Term C_A, 10^3 W m^{-2}, layer 1

Fig. 32. Spatial fields of energy budget terms at 0600 GMT on 25 April. Superimposed are areas of MDR values ≥ 4.

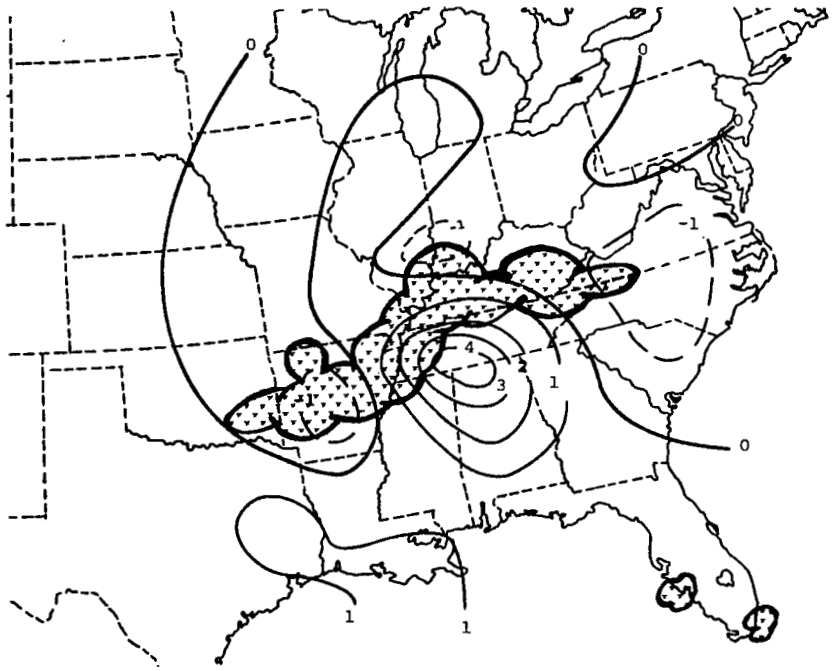

(c) Term-C_K, 10^1 W m^{-2}, layer 1

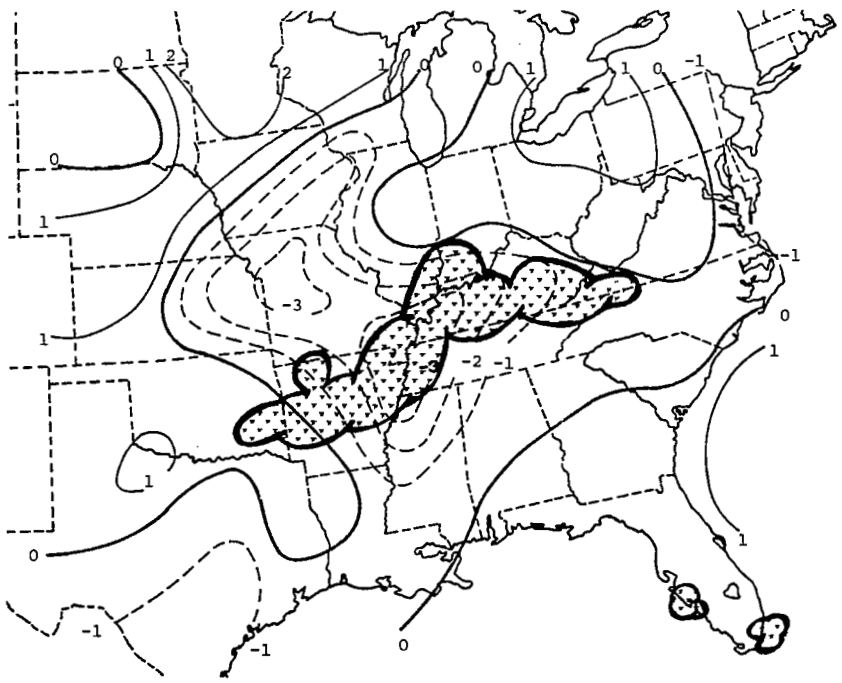

(d) Term C_A, 10^3 W m^{-2}, layer 3

Fig. 32. (Continued)

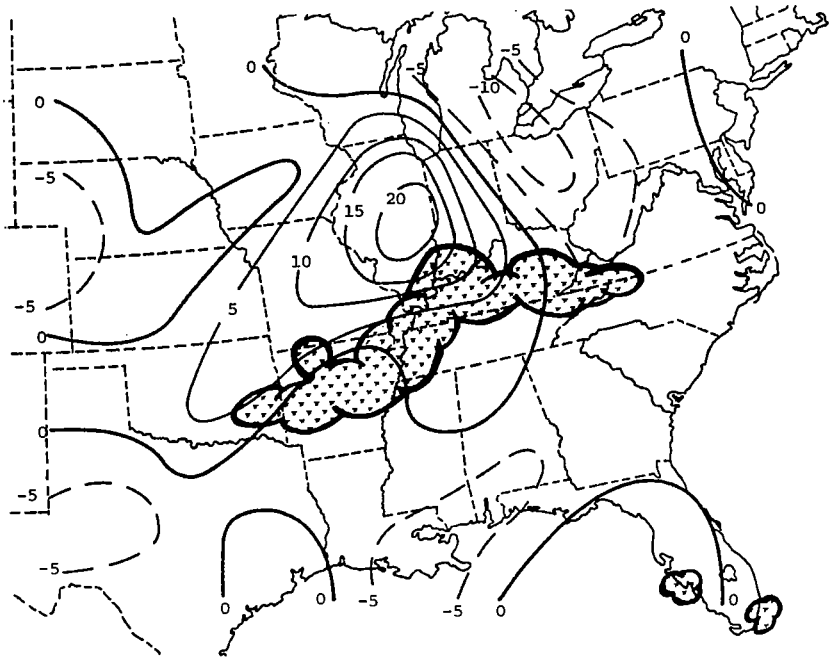

(e) Term $-C_K$, 10^1 W m^{-2}, layer 3

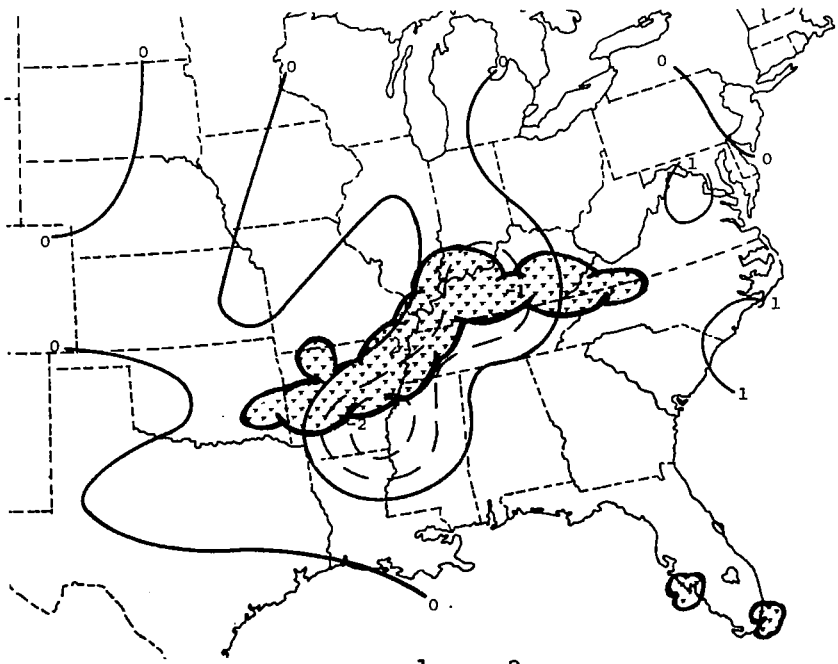

(f) Term HF_K, 10^1 W m^{-2}, layer 1

Fig. 32. (Continued)

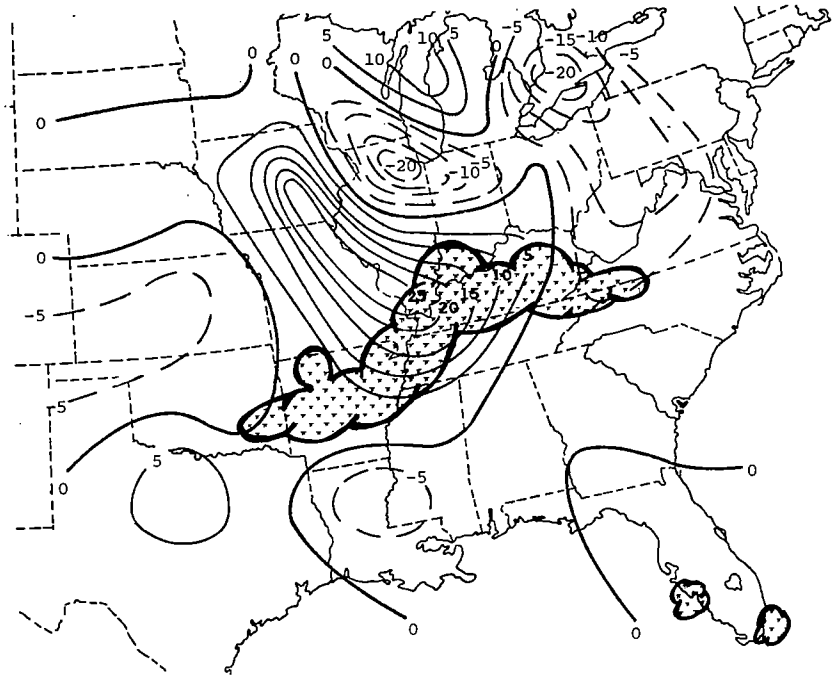

(g) Term HF_K, 10^1 W m^{-2}, layer 3

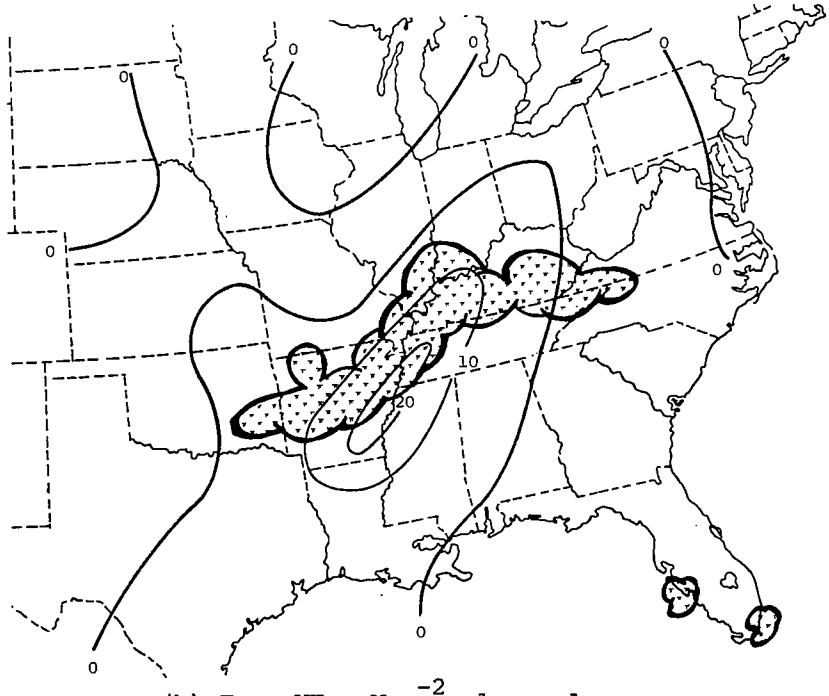

(h) Term VF_K, W m^{-2}, layer 1

Fig. 32. (Continued)

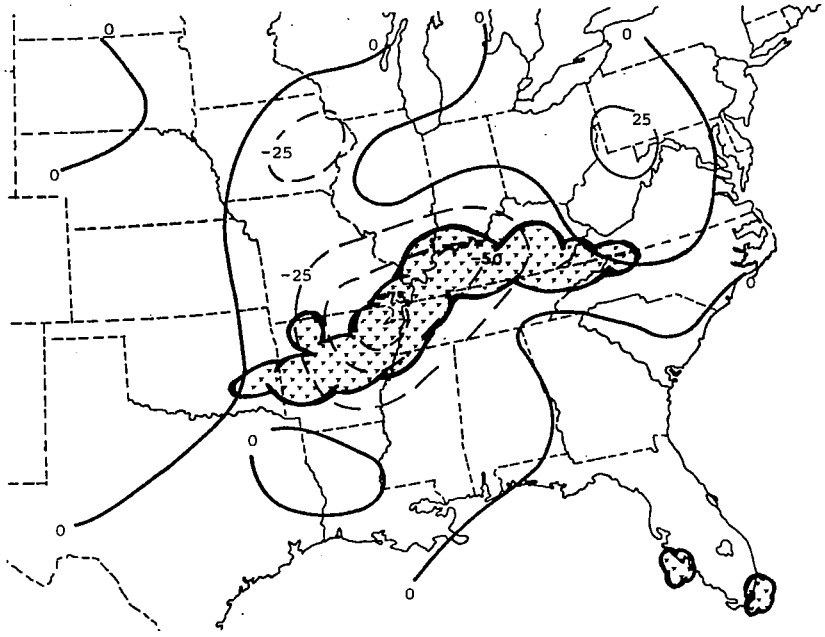

(i) Term VF_K, W m^{-2}, layer 3

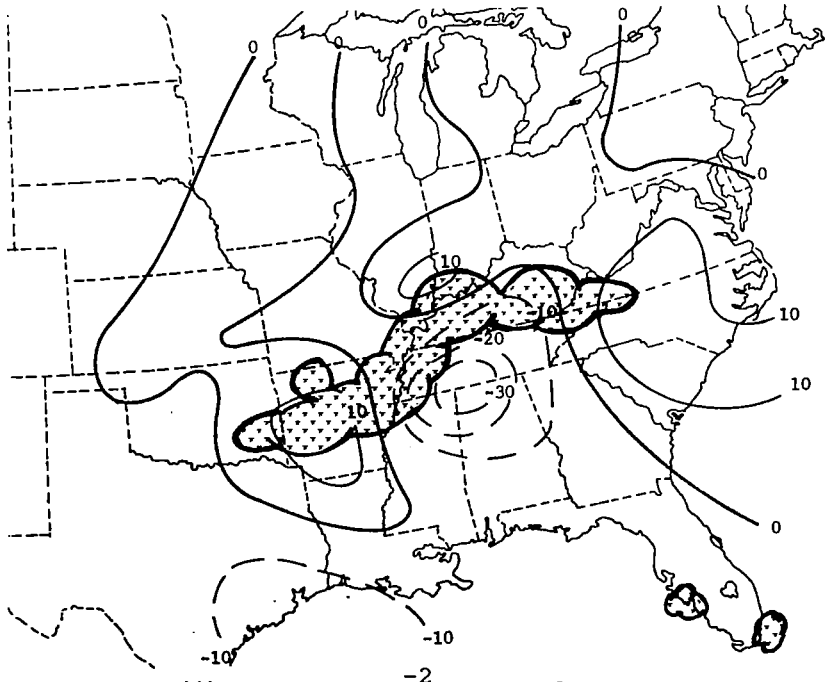

(j) Term D, W m^{-2}, layer 1

Fig. 32. (Continued)

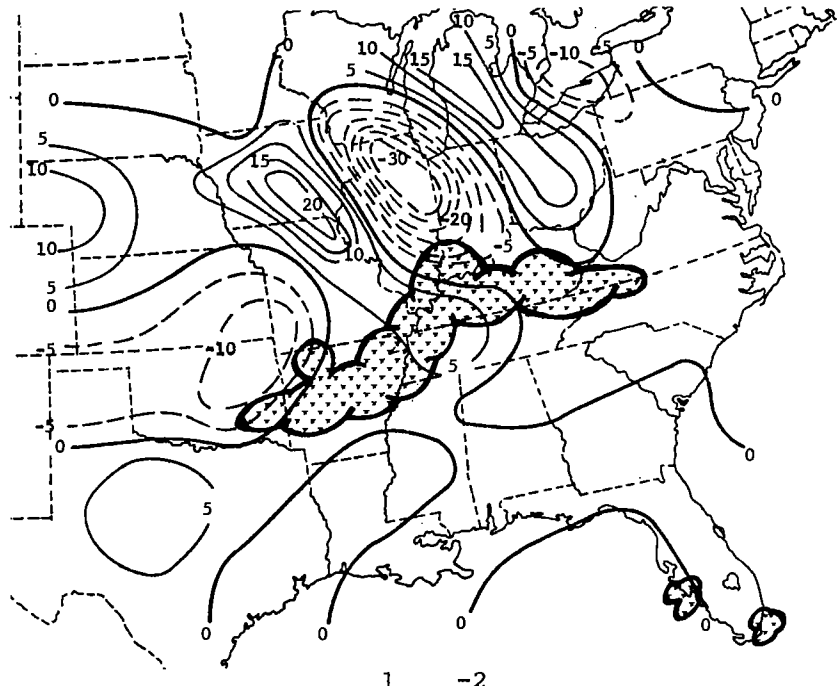

(k) Term D, 10^1 W m^{-2}, layer 3

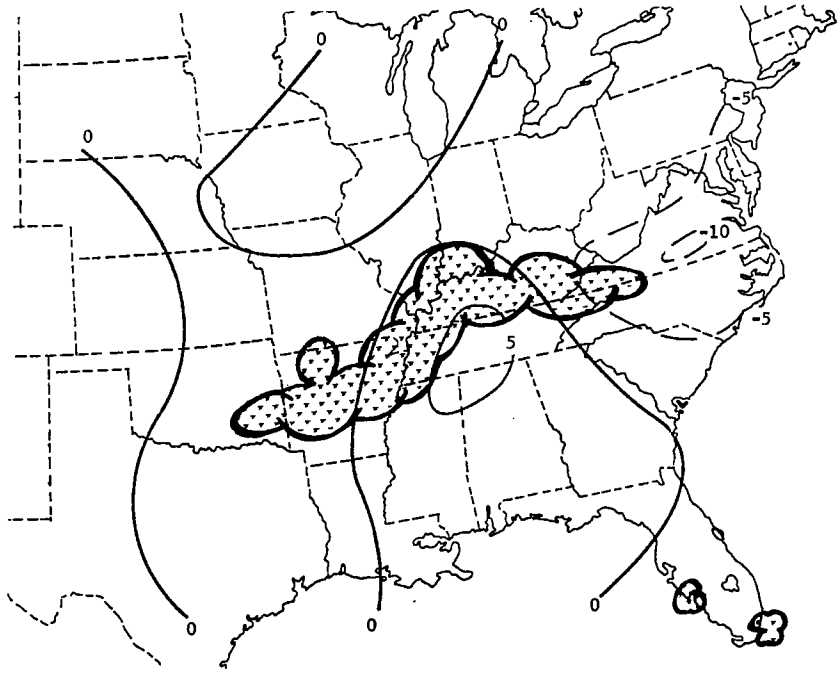

(l) Term $\frac{\partial K}{\partial t}$, W m^{-2}, layer 1

Fig. 32. (Continued)

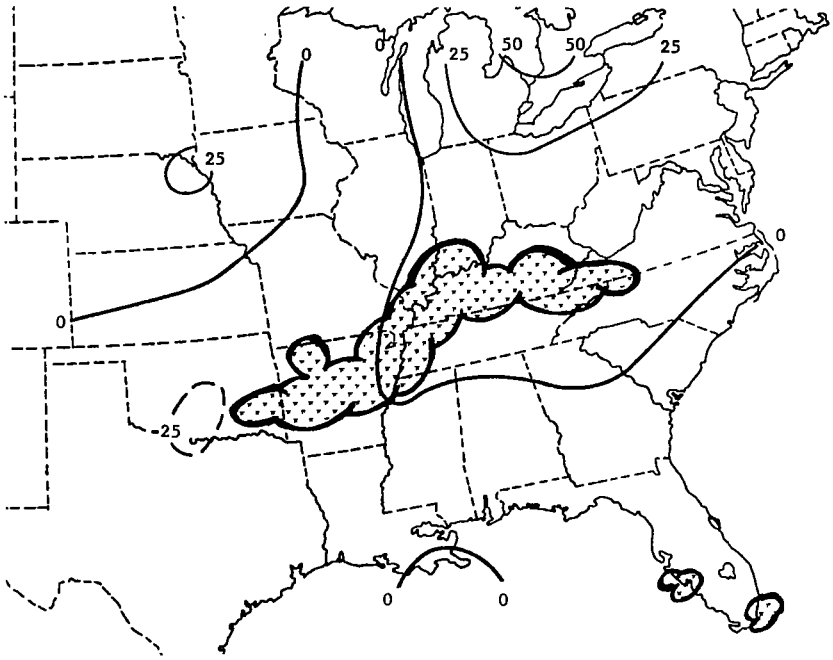

(m) Term $\frac{\partial K}{\partial t}$, W m^{-2}, layer 3

Fig. 32. (Continued)

(Fig. 32b). The area has expanded since 0600 GMT, and maximum values have nearly doubled to near -1.8×10^3 W m^{-2}.

A well defined area of K-conversion to kinetic energy (Fig. 32c) has formed over western Tennessee, just east of the squall line and near the location of maximum A-conversion to kinetic energy. The maximum value of $-C_K$ is 44 W m^{-2} or about 2.5% of the maximum value of C_A. Relatively weak K-conversion to potential energy occurs over much of the area covered by the squall line; centers are located to the northeast and southwest of the strong area of conversion to kinetic energy. The spatial fields provide valuable information in this situation since the maximum value of term $-C_K$ is located barely inside the limited area over which averages were computed (Fig. 11, p. 52).

The area of A-conversion to kinetic energy in layer 3 is much larger at 0600 GMT than at 0000 GMT; and maximum values have increased to -3.8×10^3 W m^2 over southwestern Missouri (Fig. 32d). Dual centers are located near the area of most intense convection while much weaker conversion to potential energy occurs over most of the remainder of the AVE IV area.

K-conversion to kinetic energy occurs over nearly all of the squall line in layer 3 (Fig. 32e). The maximum value of 225 W m^{-2} is found over central Illinois, along the northern edge of the squall line. While this value is very large compared to results of previous investigators, most previous work has been presented in terms of averages only. West (1973), who has presented spatial fields, reported a maximum value of about 200 W m^{-2} associated with cyclogenesis, however. Synoptic maps for the current study reveal wind speeds of $\sim$50 m s^{-1} associated with the jet stream near Illinois with marked cross-contour flow; this suggests that the large value is indeed valid.

iii. Horizontal boundary flux of kinetic energy. Low-level horizontal inflow of kinetic energy continues to occur just east of the squall line, and maximum values have more than doubled since the last time period and are now -25 W m^{-2} (Fig. 32f). An area of much weaker horizontal outflow occurs along the western portion of the

squall line. Outside the squall line area, values of HF_K are relatively small.

Very large values of HF_K occur in layer 3 along and northwest of the squall line (Fig. 32g). Maximum values of outflow are near 300 W m^{-2} or about four times the maximum value observed at the previous time period. The large magnitude of HF_K is quite remarkable, and values of horizontal velocity divergence, which reach 1.4 x 10^{-4} s^{-1} at 200 mb over southern Illinois, are equally remarkable, Ninomiya (1971a) reported divergence values of $\sim 10^{-4}$ s^{-1} in the vicinity of intense convection and found dramatic changes occurring in the value as the convection developed. Changes in vertical motion associated with the convection have been shown in Fig. 10 (p. 45). Figure 32g indicates areas of horizontal inflow of kinetic energy to the northeast and southwest of the squall line in layer 3. The presence of a jet maximum over northern Illinois helps explain this particular configuration of areas.

iv. Vertical boundary flux of kinetic energy. Vertical export of kinetic energy near the ground (Fig. 32h) and vertical import of kinetic energy in the upper atmosphere (Fig. 32i) occur at 0600 GMT near the squall line. Maximum values in both layers have increased greatly in magnitude while the locations of maximum values coincide well with the squall line. Much weaker values occur over the remainder of the AVE IV area.

v. Dissipation of kinetic energy. A pronounced center of negative dissipation is present in layer 1 over southcentral Tennessee, just east of the squall line, while centers of positive dissipation occur along the northern and southern portions of the squall line (Fig. 32j). These areas are most likely related to the convection (Kornegay and Vincent, 1976), but an exact explanation is difficult, if not impossible, to determine. Ward and Smith (1976) stated that downdrafts should add momentum to the grid-scale motions near the ground and thus produce positive dissipation, but to conclude in this study that positive areas are associated with downdrafts and the negative areas with updrafts does not seem warranted. The fields of HF_K and VF_K in layer 1 (Figs. 32f, h) are not very help-

ful in resolving the question of drafts, which is not surprising because of the scales of motion that can be resolved. Since fields of D are quite similar to those of $-C_K$ (Fig. 32e), non-representative fields of term $-C_K$ could be factors in producing the observed fields of D.

Spatial fields of the residual in the vorticity equation have been presented by Read (1976) for the AVE IV period. Fields of values of his residual are often quite similar to those of term D, which also was computed as a residual. The similarity suggests that fields of both terms are not caused primarily by computational uncertainties, but instead are due mostly to subgrid processes which are not resolved in either study since the same data were used in each.

Maximum transfer to subgrid scales occurs over Illinois in layer 3 (Fig. 32k). This area lies to the north of the squall line and is flanked by areas of positive dissipation to the east and west. Maximum values in these centers are up to three times as large as those observed 6 h earlier. The convection undoubtedly is related to these areas as well, but again the processes only can be speculated. Ward and Smith (1976) suggested that either cumulus cells acting as barriers to the flow or nearby jet stream activity may cause the observed patterns.

vi. Time derivative of kinetic energy. Values of $\frac{\partial K}{\partial t}$ in layer 1 (Fig. 321) and layer 3 (Fig. 32m) are small. Increases in kinetic energy generally are found east of the squall line while decreases are found to the west, but values of the term are often an order of magnitude smaller than those of component terms. Although small values at 0600 GMT are due partly to use of a 12-h centered time difference, trial use of a 6-h uncentered time difference did not produce greatly different results. While data are too coarse in space to resolve many important features, the problem of temporal resolution also should be stressed, even when data at 3- and 6-h intervals are used.

Maximum values of nearly all the terms presented occur near the squall line. Clearly, the squall line is the center of major

energetic activity in the AVE IV area.

3) Spatial fields at 1200 GMT on April 25

The very large values of energy terms observed when the squall line was at peak intensity become smaller at 1200 GMT (Fig. 33) as the convection decreases in strength. The strongest convection is now occurring in southeast Arkansas.

i. Diabatic processes. Although maximum values of heating are approximately half the maximum magnitude observed at 0600 GMT, areas of heating relate well to the location of the squall line (Fig. 33a). Areas of cooling are located to the northeast and west of the convective activity.

ii. Energy conversion terms. Maximum A-conversion to kinetic energy continues along and slightly east of the squall line in layer 1 (Fig. 33b) while the area of largest values has decreased somewhat. An area of conversion to potential energy is located to the west of the convective area and has become stronger since 0600 GMT.

Maximum K-conversion to kinetic energy in layer 1 is located over northern Alabama with conversion to potential energy occurring over eastern Tennessee and along the border of Arkansas and Louisiana (Fig. 33c). The area over Alabama is smaller and less intense, but the areas of conversion to potential energy are defined better at this time period.

The area of maximum A-conversion in layer 3 occurs along the Ohio River Valley and over southeast Arkansas (Fig. 33d). The area is not as pronounced at this time period, and maximum values are about 25×10^{3} W m^{-2}, about half those observed at 0600 GMT. The area of conversion to potential energy continues near Ohio while an additional area has developed over Missouri.

An area of K-conversion to kinetic energy in layer 3 is located along the border of Tennessee and Missouri (Fig. 33e). The area has remained nearly stationary and is located to the northwest of the squall line; maximum values have decreased somewhat to 170 W m^{-2}. A short-wave ridge over eastern Texas is related to the area of conversion to potential energy located over that area.

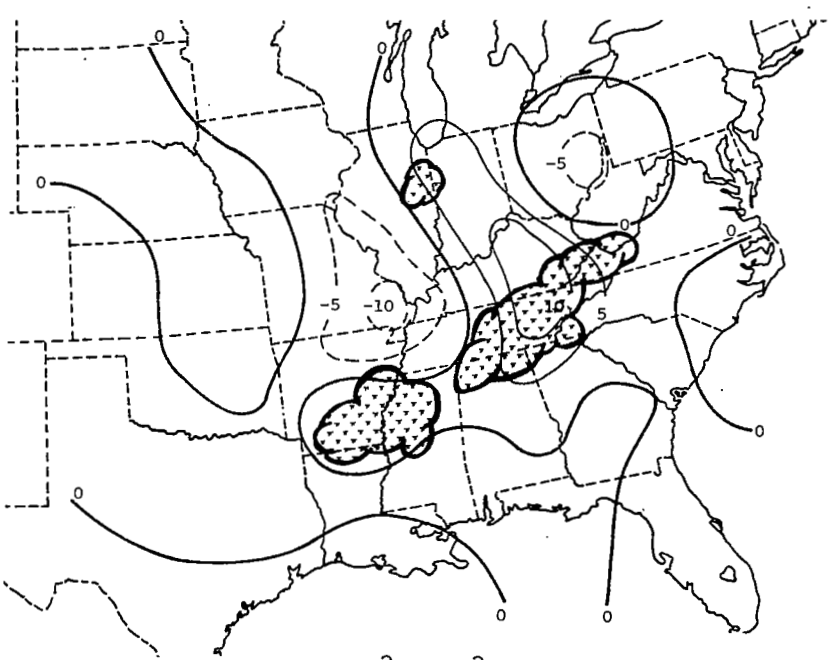

(a) Term G, 10^2 W m^{-2}, layer 2

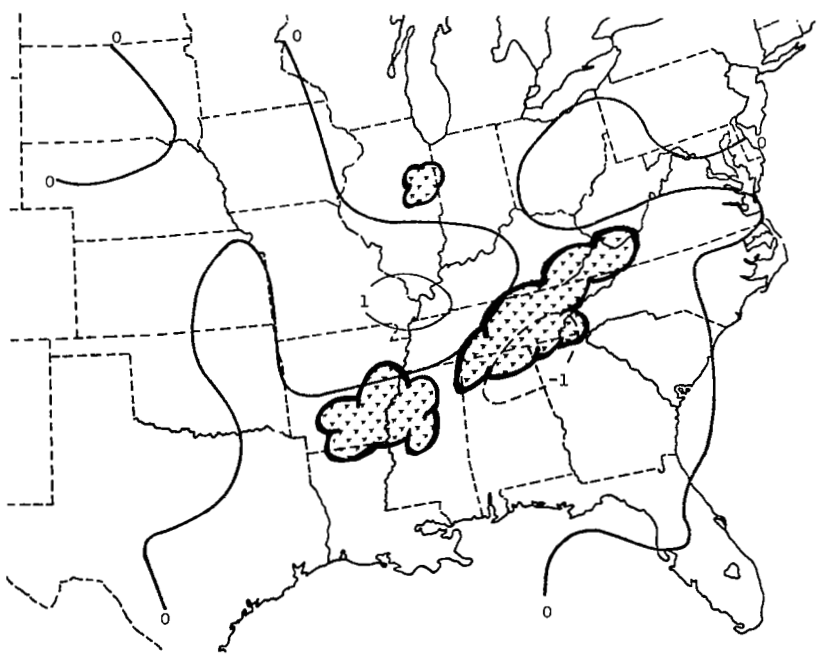

(b) Term C_A, 10^3 W m^{-2}, layer 1

Fig. 33. Spatial fields of energy budget terms at 1200 GMT on 25 April. Superimposed are areas of MDR values ≥ 4.

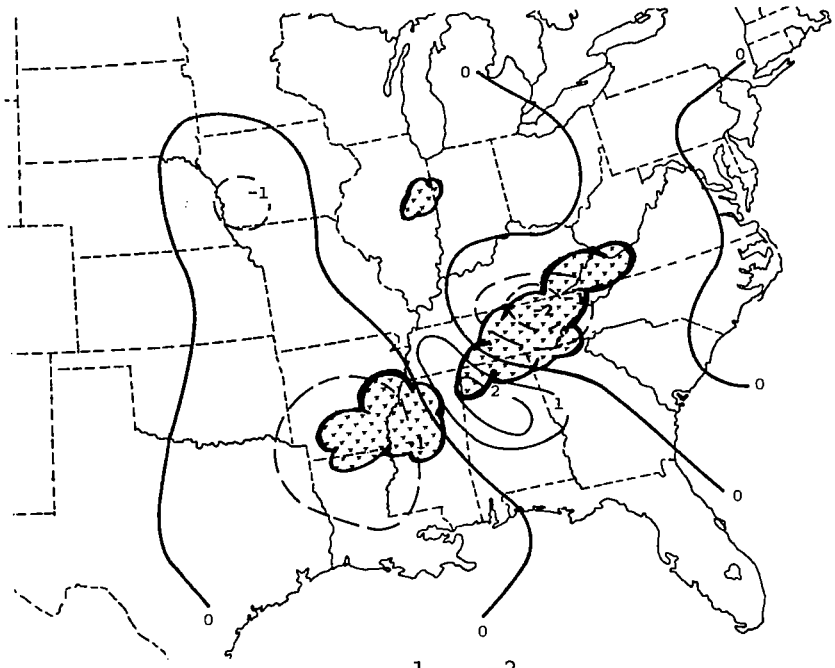

(c) Term $-C_K$, 10^1 W m^{-2}, layer 1

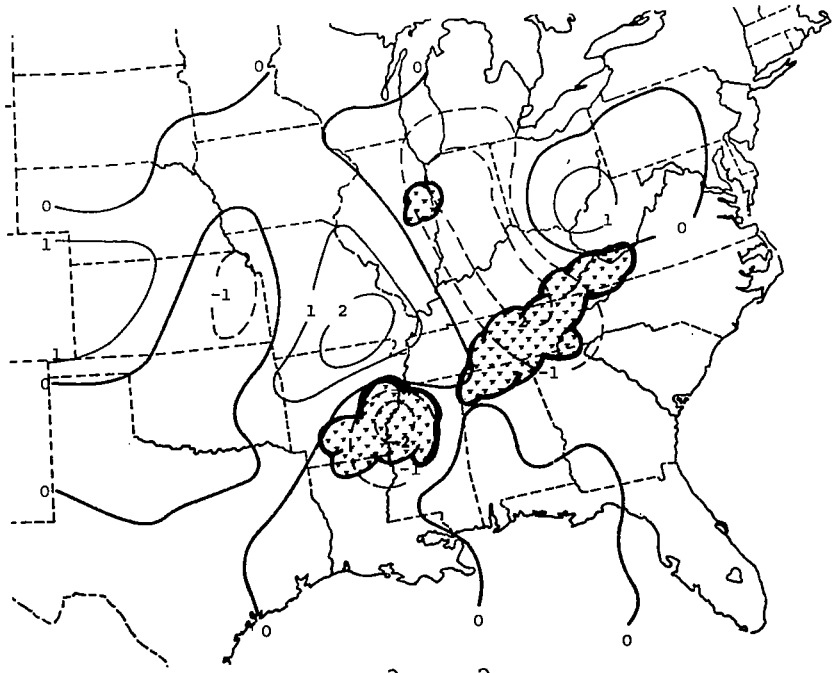

(d) Term C_A, 10^3 W m^{-2}, layer 3

Fig. 33. (Continued)

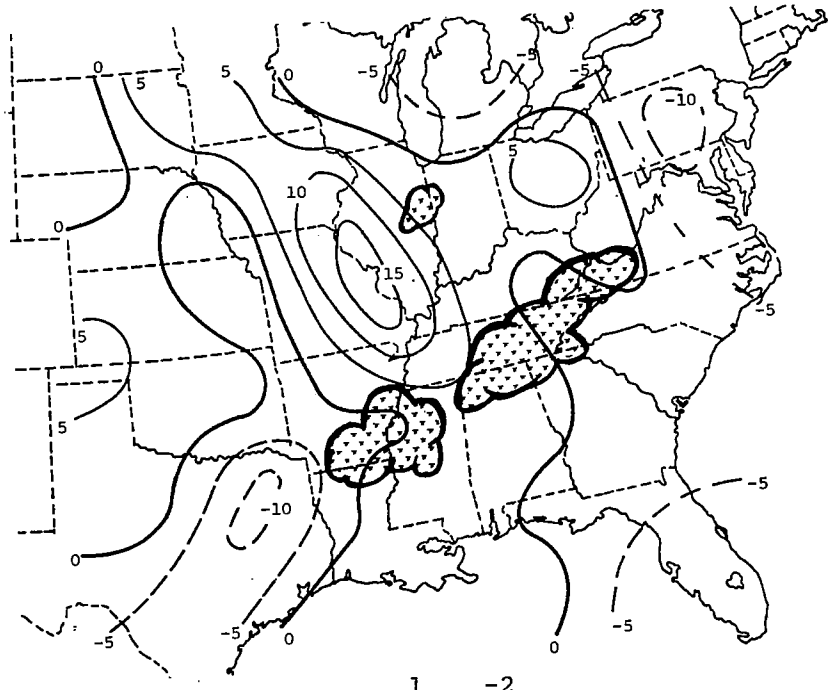

(e) Term $-C_K$, 10^1 W m^{-2}, layer 3

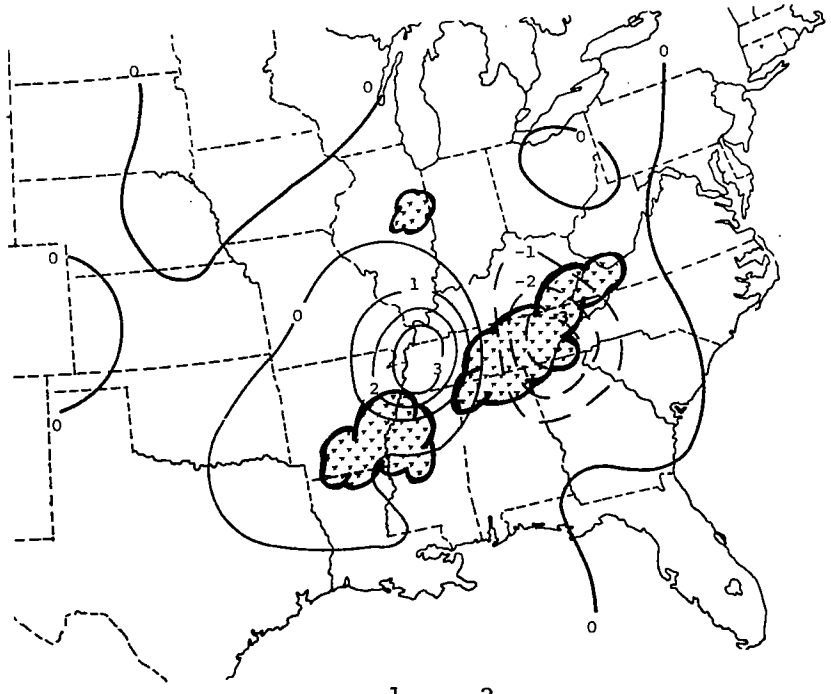

(f) Term HF_K, 10^1 W m^{-2}, layer 1

Fig. 33. (Continued)

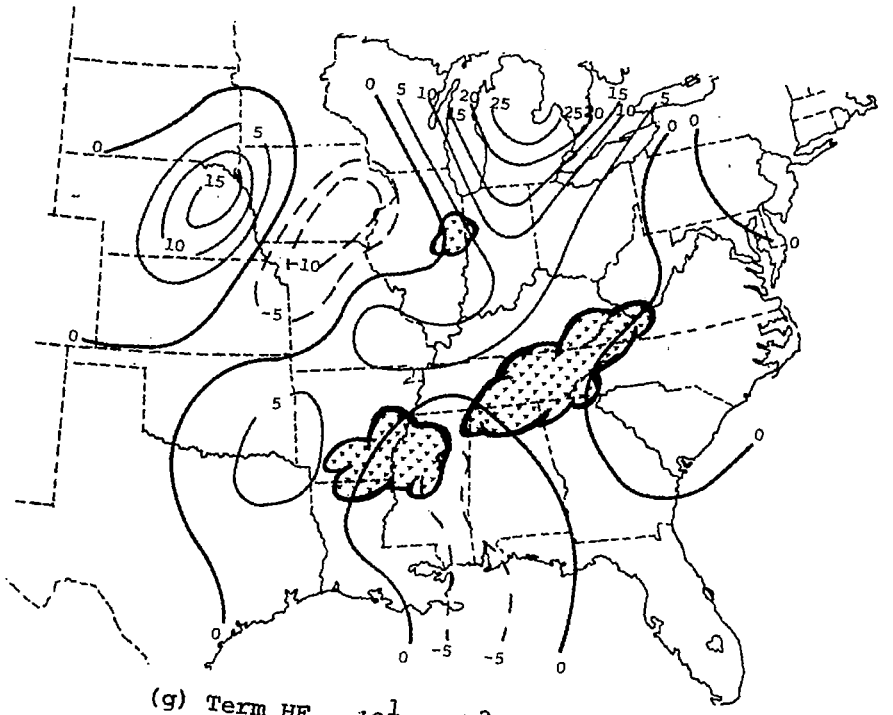

(g) Term $HF_{K'}$, 10^1 W m^{-2}, layer 3

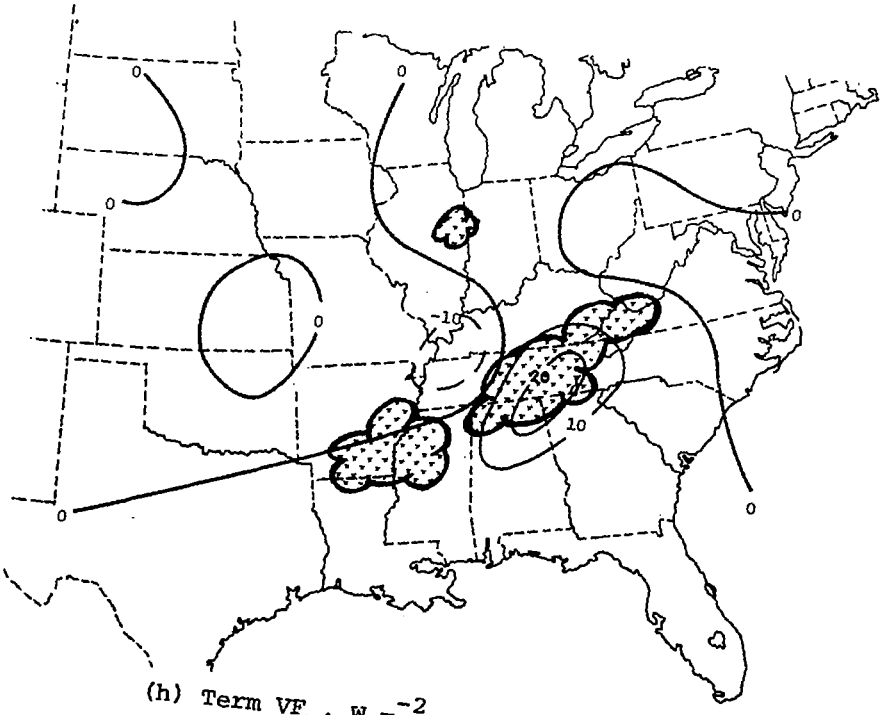

(h) Term $VF_{K'}$, W m^{-2}, layer 1

Fig. 33. (Continued)

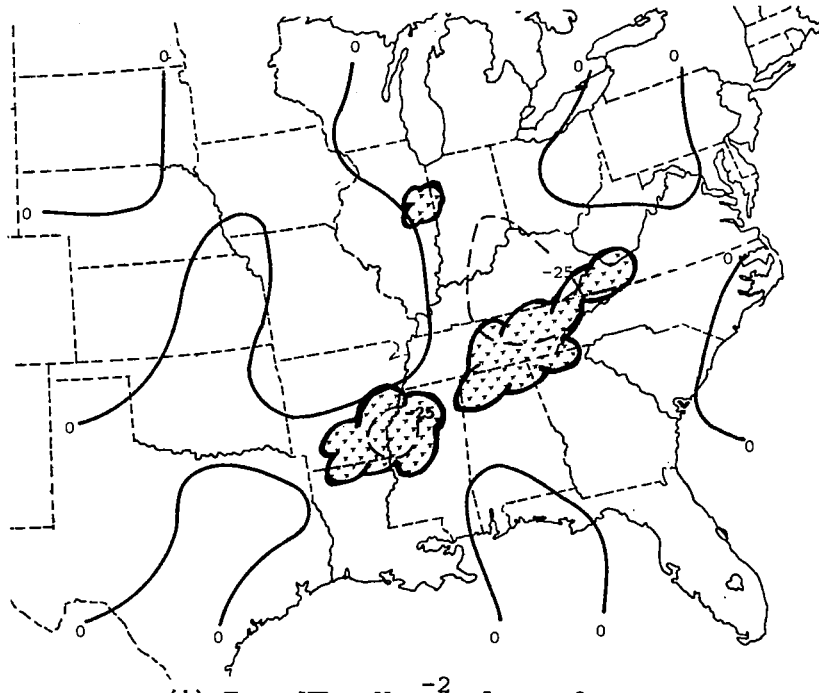

(i) Term VF_K, W m^{-2}, layer 3

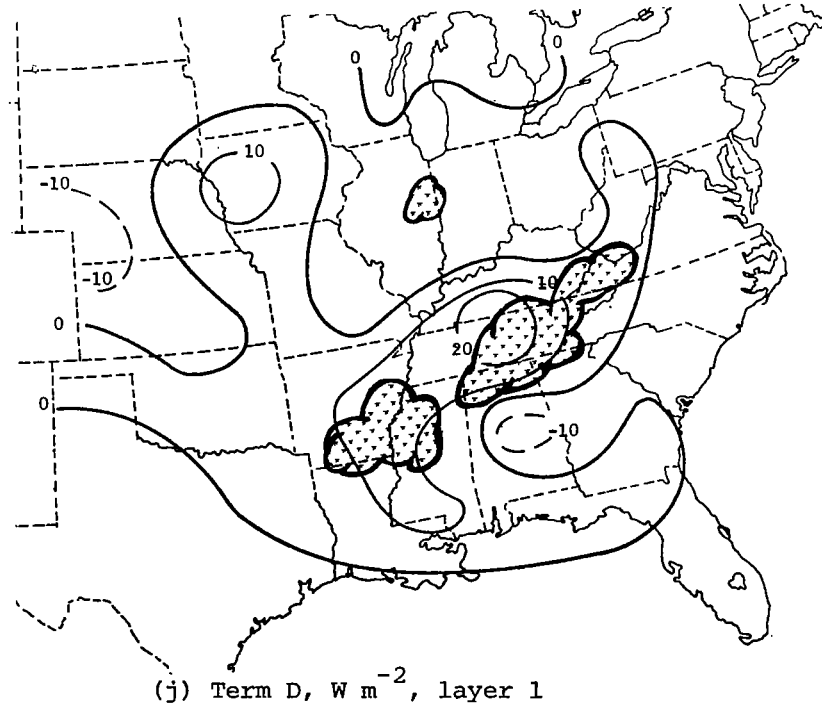

(j) Term D, W m^{-2}, layer 1

Fig. 33. (Continued)

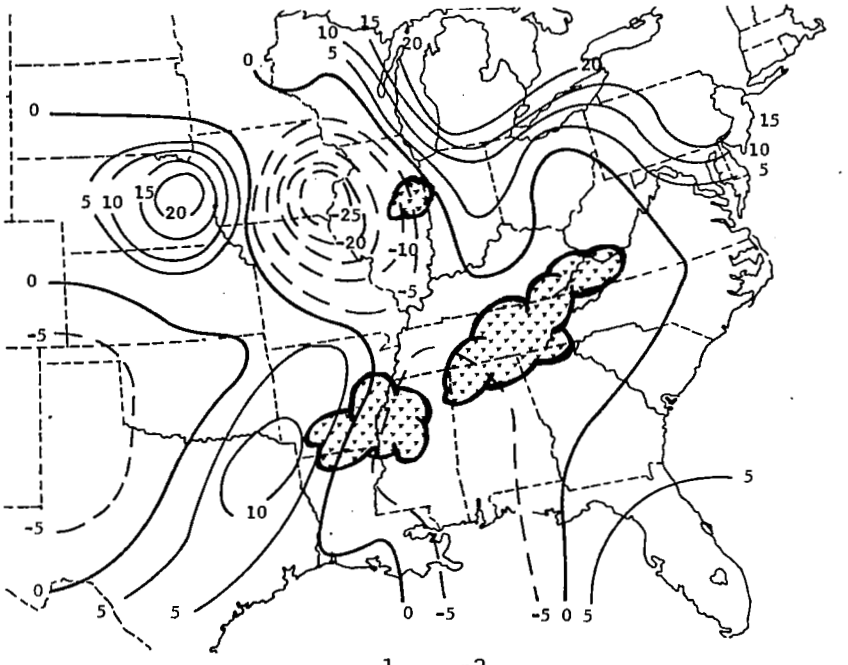

(k) Term D, 10^1 W m^{-2}, layer 3

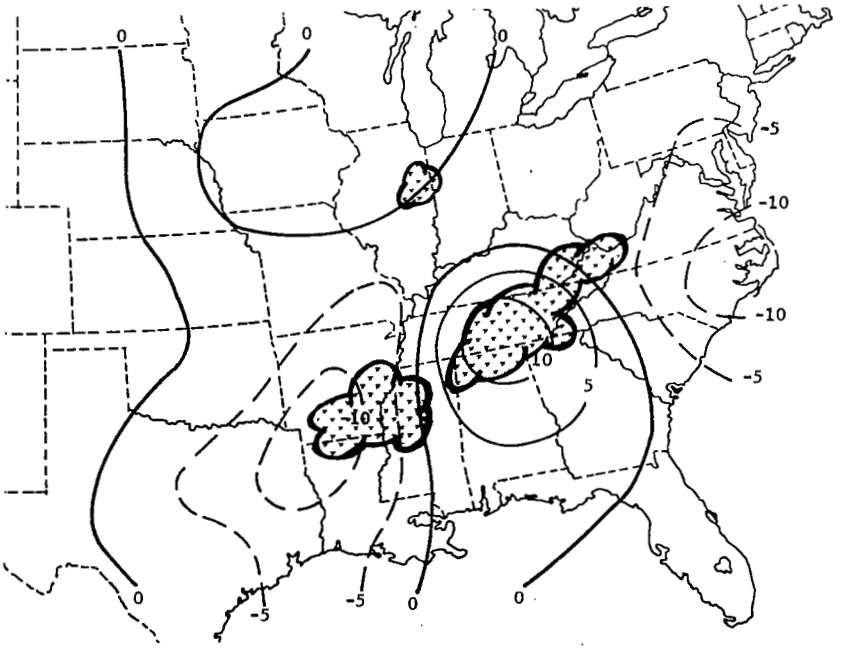

(l) Term $\frac{\partial K}{\partial t}$, W m^{-2}, layer 1

Fig. 33. (Continued)

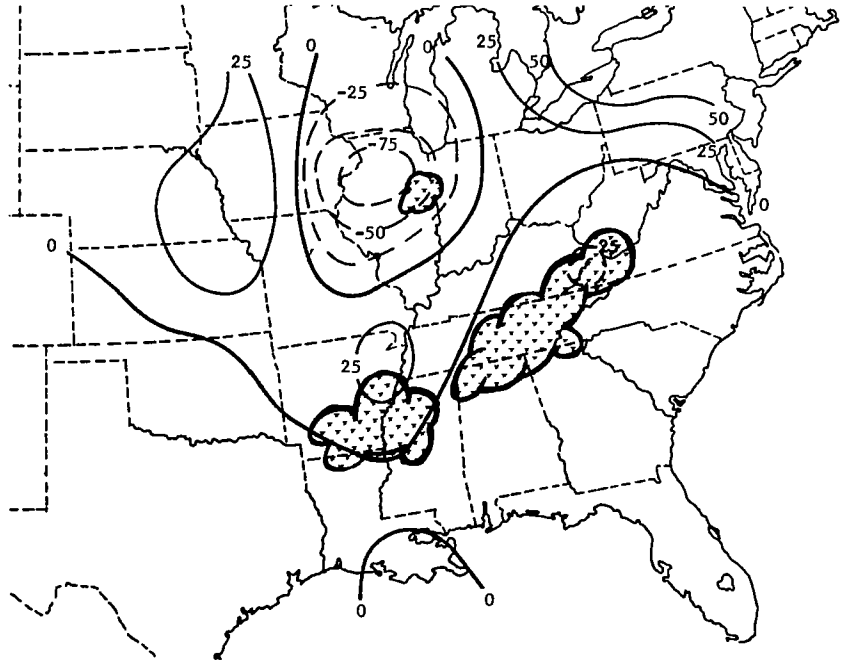

(m) Term $\frac{\partial K}{\partial t}$, W m^{-2}, layer 3

Fig. 33. (Continued)

iii. Horizontal boundary flux of kinetic energy. Low-level horizontal inflow of kinetic energy continues along the eastern portion of the squall line (Fig. 33f). The area of largest values has decreased while the greatest observed value has increased. The area of weak horizontal outflow to the west of the squall line at 0600 GMT has increased in intensity and is defined better at 1200 GMT than at 0600 GMT.

Values of HF_K in layer 3 have decreased dramatically (Fig. 33g). Maximum values of outflow are reduced to near 200 W m^{-2} near the Great Lakes and reduced to near 75 W m^{-2} over southern Illinois. Horizontal outflow occurs generally over the decaying squall line.

iv. Vertical boundary flux of kinetic energy. Maximum vertical outflow of kinetic energy in layer 1 is confined to a relatively small area along the Appalachians while an area of vertical inflow is located over the central Mississippi River Valley (Fig. 33h). The area of inflow formed during the past 6 h. Opposite conditions are found in layer 3 (Fig. 33i) where vertical inflow is located near the Appalachians and vertical outflow near Missouri. Vertical motion fields (Fig. 10., p. 45) indicate that kinetic energy is transported aloft over the Appalachians and downward over Missouri.

v. Dissipation of kinetic energy. A complex pattern of dissipation areas is seen in layer 1 (Fig. 33j). The pattern is somewhat similar to the previous time period since negative values occur ahead of the squall line while positive values are seen along the line itself. Positive values have doubled since 0600 GMT so that subgrid processes are now a significant source of kinetic energy. The patterns and magnitudes of layer 3 near the squall line (Fig. 33k) are similar to those observed at 0600 GMT; while the squall line has moved to the southeast, the centers of term D generally have moved east or northeast.

vi. Time derivative of kinetic energy. Fields of term $\frac{\partial K}{\partial t}$ also are similar to those observed at 0600 GMT in layers 1 and 3, but magnitudes have increased (Fig. 331-m). The areas in layer 1 have moved little although the squall line has advanced southeast; in layer 3, the maximum area over Illinois appears to have moved

westward. The shift from a centered to a backward time difference is a factor in these motions.

The decrease in magnitude of most of the energy terms at 1200 GMT is the most noticeable feature of the previous maps. The formation of areas near the squall line where kinetic energy is transported downward instead of upward and other areas where conversion to potential energy occurs is an interesting phenomenon. Perhaps, the atmosphere is undergoing some type of energy readjustment process following the violent processes associated with the intense squall line.

The continuity and vertical consistency of the spatial maps are further evidence of the reliability of the computations performed in this study. The maps reveal many interesting processes which are lost when averages are obtained, but only partial explanations are possible for many processes.

f. Energy budgets versus MDR values

1) Procedure

The limited volumes used previously to describe systematic energy changes associated with convection contained at least twenty grid points where precipitation intensity could vary from MDR 1 to 9. The relative intensity of convection within each limited area was subjectively determined from MDR data within those areas. The purpose of this section is to relate energetics objectively to the intensity of convection by averaging energy parameters over grid points that have equal MDR values. This is not a traditional spatial average since grid points comprising the average for a particular intensity are not necessarily adjacent. MDR values were assigned to each numerical grid point (Fig. 5, p. 20) at the nine time petiods by taking the maximum value within 1/2 grid distance (∿80 km). Averages were then computed over five MDR categories, combining all time periods, where MDR 0-9 included all 1512 grid points as described previously, MDR 0-1 included 1114 grid points associated with nonconvection, MDR 2-9 consisted of 398 grid points associated with all categories of convection, MDR 4-9 consisted of 193 points

associated with thunderstorm and severe thunderstorm activity, and MDR 8-9 consisted of 65 grid points associated with severe thunderstorm activity. The overlapping classification scheme was used so that averages were based on a large number of individual grid points.

2) Terms of the budget equations

Results of this section will demonstrate that magnitudes of energy processes are related to intensity of convection determined from individual grid points.

i. Diabatic processes. Diabatic processes associated with the average of all grid points and grid points of nonconvective areas are much smaller at all levels than those observed for grid points of convective areas (Fig. 34). Heating in the middle and upper troposphere is pronounced and increases with the intensity of convection reaching a maximum of 140 W m^{-2} in the 500- to 400-mb layer. Since more intense convection occurs in the late afternoon and evening, radiative cooling is very large near the surface for these categories. Radiative cooling from the tops of cirroform clouds occurs in the 200- to 100-mb layer.

ii. Energy conversion terms. Net A-conversion of energy is near zero in the layer from the surface to 100 mb for grid points in nonconvective regions, but conversion to kinetic energy steadily increases as averages focus in on more intense convection (Fig. 35). The profile of term $-C_K$ indicates conversion to kinetic energy near the ground and a near zero value in the 800- to 700-mb layer for all categories (Fig. 36). Conversion to potential energy becomes greater with altitude above 700 mb for the total area and the points associated with nonconvective regions, but conversion to kinetic energy increases above 700 mb for the grid points associated with convection. Maximum values of $-C_K$ occur near the jet stream in the case of MDR values 2 to 9, but reach a maximum near 450 mb for MDR values 4 to 9. A double maximum, occurring at 450 mb and 150 mb, is evident for the category of most intense convection and was not observed in previous results. Conversion to potential energy near 700 mb that was observed in the limited volume enclosing the squall

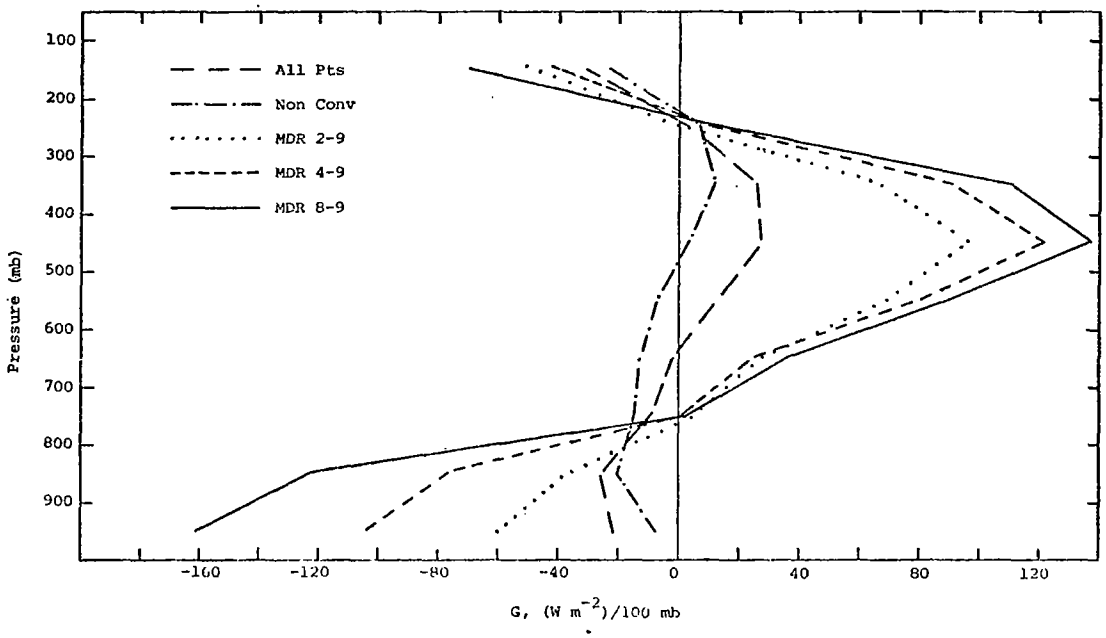

Fig. 34. Vertical profiles of term G for various ranges of MDR values.

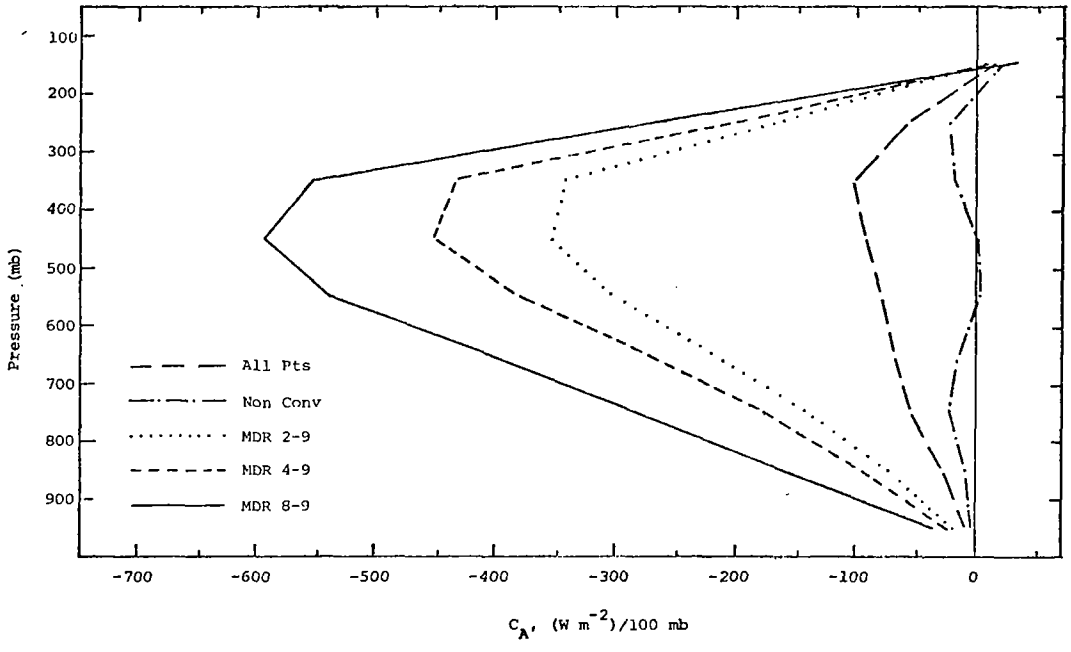

Fig. 35. Vertical profiles of term C_A for various ranges of MDR values.

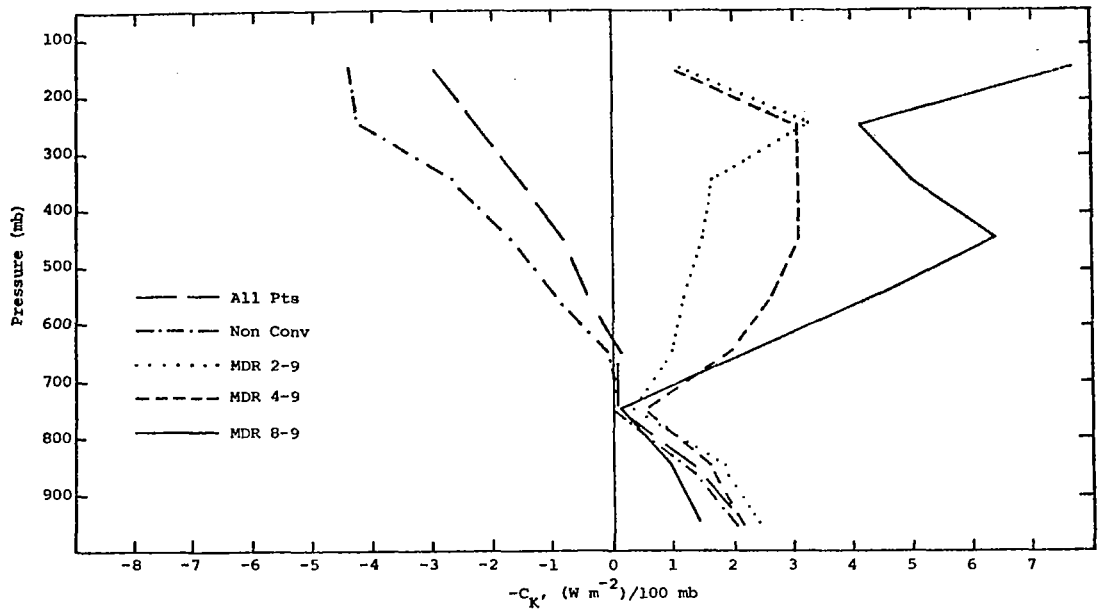

Fig. 36. Vertical profiles of term $-C_K$ for various ranges of MDR values.

line of 25 April at peak intensity (Fig. 15, p. 57) is not as pronounced in this averaging procedure.

iii. Boundary fluxes of kinetic energy. Values of term HF_K show relatively little variation among the five categories below 700 mb although the category of most intense convection is associated with slightly larger inflow (Fig. 37). Values in the 300- to 200-mb layer indicate a systematic increase in horizontal outflow with an increase in the intensity of convection. The level separating inflow from outflow is lower for the strongest convection than for the average of points having MDR values 2 to 9. This feature is not evident in the averages for particular volumes that were presented earlier.

Only small vertical flux is evident in the average of the entire AVE IV area and for grid points associated with nonconvective regions (Fig. 38). Low-level vertical outflow and upper-level inflow increase in magnitude for categories of more intense convection.

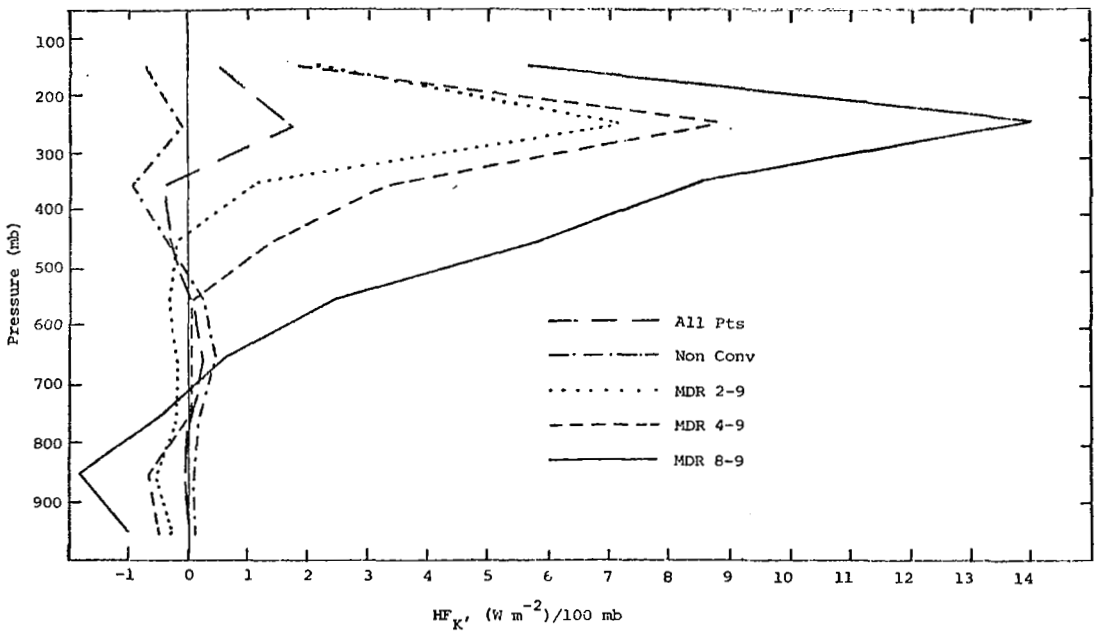

Fig. 37. Vertical profiles of term HF_K for various ranges of MDR values.

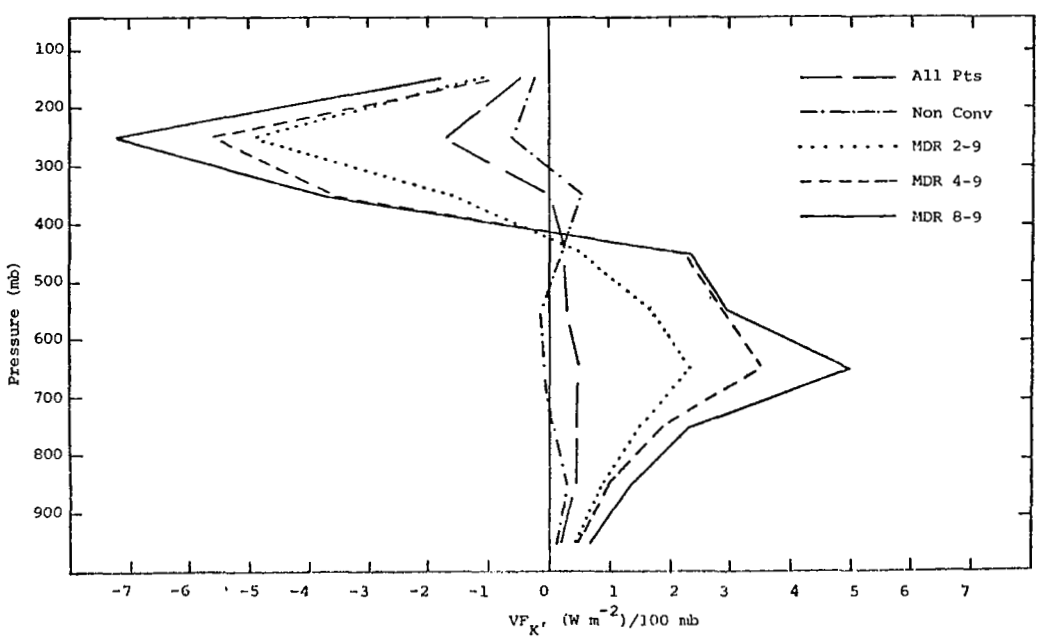

Fig. 38. Vertical profiles of term VF_K for various ranges of MDR values.

iv. Dissipation of kinetic energy. Transfer of kinetic energy to subgrid scales of motion occurs below 800 mb in all five categories (Fig. 39). Above 800 mb, transfer to larger scales of motion occurs over the entire area and for grid points associated with nonconvective regions. The profiles for the categories of convection show maximum transfer of energy to the larger scales at about 650 mb and transfer to subgrid scales above 550 mb. Differences between categories of convection are pronounced near 650 mb and above 300 mb. Since vertical profiles shown previously for limited volumes enclosing the squall lines did not yield consistent results between the two cases for term D, the present results, which are similar to those observed for the squall line of 25 April (Fig. 18, p. 60), are encouraging. Although physical processes producing the observed profiles of term D are not completely understood, subgrid processes of all types are large in areas of convection. Several hypotheses to explain the values have been given previously.

v. Time derivatives of kinetic energy. All five categories show losses of kinetic energy (Fig. 40), but the most intense convection is characterized by considerably larger losses above 500 mb than the others. Values of $\frac{\partial K}{\partial t}$ are nearly zero at 750 mb for MDR values from 8 to 9 while they are more negative for the other categories of convection.

Another approach to the time derivative question is to compute the total derivative which indicates changes following a parcel instead of the local derivative which indicates changes at a fixed point. The data in this section are used to compute an average "synoptic-scale total derivative" of kinetic energy, $\frac{DK}{Dt}$, for each MDR category. The total derivative can be expressed symbolically as

$$\frac{DK}{Dt} = -C_K + D, \qquad (26)$$

which indicates that changes in kinetic energy of a "synoptic-scale parcel" are due to cross-contour conversion of energy and dissipation of energy. Smith (1973b) called the sum $-C_K + D$ the net internal source or sink of kinetic energy. Figure 41 reveals relatively small values of $\frac{DK}{Dt}$ for the entire AVE area and for grid

Table 11. Average energy budget for all grid points with MDR values 4 to 9. The number of grid points is 193.

Pressure Layer mb	K 10^5 J m^{-2}	$\frac{\partial K}{\partial t}$ W m^{-2}	HF_K W m^{-2}	VF_K W m^{-2}	$-C_K$ W m^{-2}	D W m^{-2}	G W m^{-2}	C_K W m^{-2}	PW W m^{-2}	HF_Π W m^{-2}	VF_Π W m^{-2}	C_A W m^{-2}
200-100	4.8	-2.8	1.9	-1.0	1.1	-3.0	-41.8	-1.1	279.9	1369.8	-390.3	17.4
300-200	5.8	-2.4	8.9	-5.6	3.1	-2.2	10.0	-3.1	162.7	3878.2	-3308.8	-189.6
400-300	4.2	-0.2	3.4	-3.5	3.0	-3.3	91.4	-3.0	-151.9	2212.3	-2743.4	433.4
500-400	3.2	-0.4	1.5	0.2	3.1	-1.8	121.0	-3.1	-92.5	593.6	-917.6	-451.7
600-500	2.6	-0.6	0.1	2.9	2.7	-0.2	80.0	-2.7	-102.0	-805.8	448.5	-383.8
700-600	1.8	-0.8	0.1	3.5	2.0	0.8	23.8	-2.0	-12.4	-1523.5	1480.0	-276.5
800-700	1.2	-0.6	0.0	1.9	0.6	0.6	0.2	-0.6	-7.7	-1649.5	1622.3	-179.9
900-800	0.9	-1.1	-0.6	1.0	1.6	-2.3	-76.9	-1.6	-178.1	-2546.8	1922.0	-97.4
sfc-900	0.4	-0.6	-0.5	0.5	2.2	-2.8	-104.2	-2.2	-308.1	-2442.5	1361.5	-24.3
Vertical total	24.9	-9.5	14.8	-0.2	19.3	-14.2	103.8	-19.3	-410.2	-914.3	-525.8	-2019.3

Table 12. Average energy budget for all grid points with MDR values 8 to 9. The number of grid points is 65.

Pressure Layer	K	$\frac{\partial K}{\partial t}$	HF_K	VF_K	$-C_K$	D	G	C_K	PW	HF_Π	VF_Π	C_A
mb	10^5 J m^{-2}	W m^{-2}	W m^{-2}	W m^{-2}	W m^{-2}	W m^{-2}	W m^{-2}	W m^{-2}	W m^{-2}	W m^{-2}	W m^{-2}	W m^{-2}
200-100	5.4	-5.1	5.7	-1.9	7.8	-9.0	-70.1	-7.8	478.9	2239.8	-563.3	33.1
300-200	6.6	-7.5	14.0	-7.2	4.2	-4.8	11.2	-4.2	231.5	5073.9	-4263.9	-259.5
400-300	4.5	-2.9	8.6	-3.6	5.0	-2.9	111.5	-5.0	-89.7	3140.1	-3454.0	-553.7
500-400	3.2	-1.7	5.8	0.3	6.4	-1.9	137.1	-6.4	-45.2	1549.2	-1707.4	-592.7
600-500	2.4	-0.8	2.5	2.8	4.4	0.1	88.3	-4.4	-123.8	-435.4	2.0	-536.5
700-600	1.6	-0.3	0.7	5.0	2.3	3.2	35.8	-2.3	-4.6	-1623.6	1607.4	-410.8
800-700	0.9	-0.1	-0.4	2.3	0.2	1.7	3.6	-0.2	-23.9	-2247.8	2163.8	-284.9
900-800	0.8	-0.8	-1.8	1.4	1.0	-2.2	-123.1	-1.0	-315.1	-4160.8	3055.2	-162.0
sfc-900	0.3	-0.5	-1.0	0.7	1.5	-2.3	-160.7	-1.5	-374.4	-3784.2	2470.4	-37.3
Vertical total	25.7	-19.6	34.2	-0.2	32.7	-18.3	33.5	-32.7	-266.3	-248.8	-689.9	-2804.3

to potential energy occurring in the 800- to 300-mb layer. While this phenomenon was observed to some extent for the squall line of 25 April (Table 6, p. 64), it is not apparent in the MDR averages of either category. Maximum conversion to kinetic energy is observed near the ground and near the top of the atmosphere in both studies.

Low- and middle-level horizontal inflow of kinetic energy is seen in the results of M&K while a much more shallow layer is seen for the current study. In fact, values of HF_K for MDR 4 to 9 are near zero below 500 mb. Maximum horizontal outflow near 300 mb is common to both studies, but the value given by M&K is about 1/2 that observed for MDR values 4 to 9 and about 1/4 that observed for MDR values 8 to 9. M&K reported a vertical total of -8.88 W m^{-2} (inflow) while the value for the most intense convection of this study is 34.2 W m^{-2} (outflow).

Profiles of term VF_K are quite similar between the two studies below 400 mb, but are considerably different above that level. The differences are probably due to the method in which vertical motion was computed and due to dissimilar synoptic conditions.

Values of term D are comparable between the two studies below about 500 mb; this is especially true of the average obtained for MDR values 8 to 9. Larger negative dissipation at the surface was reported by M&K, however. M&K showed transfer of energy from subgrid to grid scales of motion occurring in the 800- to 300-mb layer while this feature extends only to 500 mb for the category of most intense convection of this study. Both studies indicate maximum transfer of kinetic energy to subgrid scales of motion in the 200- to 100-mb layer, but the value of M&K was about three times larger than that observed for MDR values 8 to 9. A major conclusion by M&K was that areas of thunderstorms can dissipate more energy than is created and therefore must import the remainder, but current results do not support such a conclusion. Values for term $\frac{\partial K}{\partial t}$ were not given by M&K; they were stated to be small.

General agreement exists between the present results and those of McInnis and Kung although there are interesting differences. No complete budgets of the total potential energy or available

potential energy of volumes enclosing convective areas occur in the literature to this author's knowledge.

g. Energy budget summary

Average kinetic and total potential energy budgets (Figs. 44-45, respectively) of limited volumes enclosing the squall lines at three stages in their life cycles are given in schematic form to summarize the complex energy processes described in this report. The limited volumes used here are identical to those described previously; their dimensions are given in Table 5 (p. 54) and Table 8 (p. 68). Values for the development stage are an average of those observed in the vicinity of the first squall line case at 1800 GMT on 24 April and the second case at 0000 GMT on 24 April while values for the mature stage are an average of those observed at 0600 GMT on 24 April and 25 April. The average of values for the limited volumes enclosing the convection at 1200 GMT on 25 April and 1500 GMT on 24 April is used for the dissipation stage. Since the budgets for each individual squall line have already been discussed in great detail, only general comments are given in this section.

During the development stage of the squall line, the limited atmospheric volume is characterized by horizontal inflow and vertical outflow of kinetic energy near the level of the jet stream, and horizontal outflow and vertical inflow below that level. K-conversion to kinetic energy, transfer of kinetic energy to subgrid scales of motion, and negative values of term $\frac{\partial K}{\partial t}$ occur throughout the vertical extent of the limited volume. Diabatic cooling is indicated below 400 mb while heating is indicated in the 400- to 100-mb layer. A-conversion to potential energy occurs in the 700- to 400-mb layer, but conversion to kinetic energy occurs above and below that layer. Boundary fluxes of total potential energy are relatively small at this stage of development.

Magnitudes of most energy processes are much larger during the mature stage of the squall line than the development stage. Diabatic heating is pronounced in the middle troposphere and is almost certainly the cause of the other changes in energy processes.

A-conversion and K-conversion to kinetic energy are found in all layers of the atmosphere with the maximum value of C_A occurring in the 700- to 400-mb layer and the maximum value of $-C_K$ occurring in the 400- to 100-mb layer. The processes of horizontal inflow and vertical outflow of kinetic and total potential energy in the lower levels of the atmosphere, together with horizontal outflow and vertical inflow aloft carry large quantities of kinetic and total potential energy up and out of the convective areas. Transfer of kinetic energy to subgrid scales of motion occurs in all layers but is somewhat smaller during this stage than the development stage. Local changes of kinetic energy are small and negative in all layers of the atmosphere.

Most energy processes decrease in magnitude as the squall line dissipates. Diabatic cooling is observed near the ground and near the level of the jet stream, but diabatic heating is observed in the 700- to 400-mb layer. A-conversion and K-conversion to kinetic energy continue at this stage, but magnitudes are smaller than during the mature stage in most layers of the atmosphere. Total potential energy still is concentrated horizontally in the lower atmosphere, transported aloft, and exported near the jet stream, but magnitudes of these processes also are smaller. Horizontal export of kinetic energy occurs in all layers of the atmosphere during the dissipation stage while vertical export of kinetic energy occurs below 400 mb and vertical import occurs above that level. Kinetic energy continues to be transferred to subgrid scales of motion, but magnitudes are slightly smaller at this stage than the mature stage. Values of $\frac{\partial K}{\partial t}$ are positive in the middle troposphere but are negative above 400 mb and below 700 mb.

While random errors in input data and computational uncertainties are known to exist, it should again be emphasized that the trends of the results and the nature of the inferred processes can be considered with great confidence. This conclusion is suggested by the systematic nature of the results, comparisons with other investigators, and the good balance of the potential energy budget.

Random error estimates of this study and those of Vincent and Chang (1975) and Kornegay and Vincent (1976) also are useful in this regard.

6. CONCLUSIONS

Synoptic-scale budgets of kinetic and total potential energy for volumes enclosing intense convection have been studied in this report. The availability of 3- and 6-h synoptic-scale data from the AVE IV experiment enabled temporal resolution of features that would ordinarily be lost.

Several conclusions are drawn from the present research:

1) Systematic temporal changes occur in most terms of the energy budget equations for relatively small volumes that enclose intense convection. These changes are related to the life cycle of the enclosed convection.

2) The kinetic energy budget of a volume enclosing a squall line at peak intensity is characterized by large values of K-conversion to kinetic energy. The processes of horizontal inflow and vertical outflow in the lower levels, together with horizontal outflow and vertical inflow aloft transport kinetic energy up and out of the convective areas. Transfer of kinetic energy to subgrid scales of motion occurs in the volume, while local changes in kinetic energy are relatively small.

3) The total potential energy budget of a relatively small volume enclosing a squall line at peak intensity is characterized by large values of latent heat release in the middle troposphere. Values of A-conversion are large, but values of conversion due to cross-contour flow are much smaller indicating large interaction of the relatively small volumes with the surrounding atmosphere. Total potential energy is concentrated horizontally in the lower levels of the atmosphere, transported aloft, and then exported near the jet stream. Only small local changes of total potential energy occur, however.

4) These results and those of other investigators suggest strongly that the systematic energy changes are due to latent heat release associated with convection. It is impossible, however, to determine what energy changes would have occurred under similar synoptic conditions but without the convection.

5) Some of the synoptic-scale energy processes associated with the squall line at peak intensity are as large or larger than those observed in the vicinity of mature cyclones. Relatively small areas of intense convection, therefore, can have a large effect on larger surrounding atmospheric volumes.

6) While errors in input data and in computational procedures lead to errors in the energy terms, these errors are not large enough to change conclusions based on those terms. Average energy budgets for areas as small as 8.0×10^{11} m^2 are reasonable, and spatial fields of energy budget terms show good time continuity and vertical consistency.

7) Values of energy processes are related to the intensity of convection at individual points. The energy budgets of points associated with nonconvection differ greatly from those where convection is observed.

8) Results of this investigation are in general agreement with those of other studies, but since marked variability likely exists between individual areas of intense convection, more research of this nature should be conducted.

7. RECOMMENDATIONS FOR FURTHER RESEARCH

Further studies of the type presented can contribute to a better understanding of the energetics of convective systems and their interaction with other scales of motion. Since the time and length scales of convective systems are relatively small, special observational networks should be established to provide data for these experiments. Data from projects SESAME and HIPLEX and future AVE experiments should be especially useful.

REFERENCES

Anthes, R. A., and D. R. Johnson, 1968: Generation of available potential energy in Hurricane Hilda (1964). Mon. Wea. Rev., 96, 291-302.

Aubert, E. J., 1957: On the release of latent heat as a factor in large-scale atmospheric motions. J. Meteor., 14, 527-542.

Barnes, S. L., 1964: A technique for maximizing detail in numerical weather map analysis. J. Appl. Meteor., 3, 396-409.

Barr, S., W. K. Widger, Jr., I. A. Miller, and R. Stanton, 1971: Objective subsynoptic upper level analysis. J. Appl. Meteor., 10, 410-417.

Brousaides, F. J., 1975: The radiosonde hygristor and low relative humidity measurements. Bull. Amer. Meteor. Soc., 56, 229-233.

Bullock, B. R., and D. R. Johnson, 1971: The generation of available potential energy by latent heat release in a midlatitude cyclone. Mon. Wea. Rev., 99, 1-14.

Chien, H., and P. J. Smith, 1973: On the estimation of kinematic parameters in the atmosphere from radiosonde wind data. Mon. Wea. Rev., 101, 252-261.

Danard, M. B., 1964: On the influence of released latent heat on cyclone development. J. Appl. Meteor., 3, 27-37.

_____, 1966: On the contribution of released latent heat to changes in available potential energy. J. Appl. Meteor., 5, 81-84.

Fankhauser, J. C., 1969: Convective processes resolved by a mesoscale rawinsonde network. J. Appl. Meteor., 8, 778-798.

_____, 1971: Thunderstorm-environment interactions determined from aircraft and radar observations. Mon. Wea. Rev., 99, 171-197.

Foster, D. S., and R. M. Reap, 1973: Archiving of manually-digitized radar data. Techniques Development Laboratory Office Note 73-6, National Weather Service, Silver Springs, Md., 12pp.

Fucik, N. F., and R. E. Turner, 1975: Data for NASA's AVE IV experiment: 25-mb sounding data and synoptic charts. NASA TM X-64952, George C. Marshall Space Flight Center, Alabama, 458pp.

Fuelberg, H. E., 1974: Reduction and error analysis of the AVE II pilot experiment data. NASA CR-120496, George C. Marshall Space Flight Center, Alabama, 131 pp.

Gall, R. L., and D. R. Johnson, 1971: The generation of available potential energy by sensible heating: A case study. Tellus, 23, 465-482.

Gommel, W. R., 1973: A kinetic energy study of hurricane Celia, 1970. Ph.D. Thesis, Department of Geosciences, Purdue University, West Lafayette, Indiana, 153 pp.

Kornegay, F. C., and D. G. Vincent, 1976: Kinetic energy budget analysis during interaction of tropical storm Candy (1968) with an extratropical frontal system. Mon. Wea. Rev., 104, 849-859.

Krishnamurti, T. N., and W. J. Moxim, 1971: On parametrization of convective and nonconvective latent heat release. J. Appl. Meteor., 10, 3-13.

Kung, E. C., 1967: Diurnal and long-term variations of the kinetic energy generation and dissipation for a five-year period. Mon. Wea. Rev., 95, 593-606.

_____, 1970: On the meridional distribution of source and sink terms of the kinetic energy balance. Mon. Wea. Rev., 98, 911-915.

_____, 1973: Note on design of an optimized computation scheme for kinematic vertical motion fields. Mon. Wea. Rev., 101, 685-690.

_____, 1974: An analysis of kinetic energy balance over the Marshall Islands area. Proc. Internat. Tropical Meteor. Meeting, Nairobi, Kenya, Amer. Meteor. Soc., Part I, 72-80.

_____, and P. J. Smith, 1974: Problems of large-scale kinetic energy balance--A diagnostic analysis in GARP. Bull. Amer. Meteor. Soc., 55, 768-777.

Lenhard, R. W., 1973: A revised statement of radiosonde accuracy. Bull. Amer. Meteor. Soc., 54, 691-693.

McInnis, D. H., and E. C. Kung, 1972: A study of subsynoptic scale energy transformations. Mon. Wea. Rev., 100, 126-132.

Ninomiya, K., 1971a: Dynamical analysis of outflow from tornado-producing thunderstorms as revealed by ATS III pictures. J. Appl. Meteor., 10, 275-294.

_____, 1971b: Mesoscale modification of synoptic situations from thunderstorm development as revealed by ATS III and aerological data. J. Appl. Meteor., 10, 1103-1121.

O'Brien, J. J., 1970: Alternate solution to the classical vertical velocity problem. J. Appl. Meteor., 9, 197-203.

Oort, A. H., 1964: On estimates of the atmospheric energy cycle. Mon. Wea. Rev., 92, 483-493.

_____, and J. P. Peixóto, 1974: The annual cycle of the energetics of the atmosphere on a planetary scale. J. Geophys. Res., 79, 2705-2719.

Peixóto, J. P., and A. H. Oort, 1974: The annual distribution of atmospheric energy on a planetary scale. J. Geophys. Res., 79, 2149-2159.

Petterssen, S., 1956: Weather Analysis and Forecasting. Vol. I. Motion and Motion Systems. New York, McGraw-Hill Book Co., 428 pp.

_____, and S. J. Smebye, 1971: On the development of extra-tropical cyclones. Quart. J. Roy. Meteor. Soc., 97, 457-482.

Read, W. L. 1976: Vorticity imbalance and stability in relation to convection. M.S. Thesis, Department of Meteorology, Texas A&M University, College Station, Texas, 110 pp.

Scoggins, J. R., and O. E. Smith, 1973: Data for the first NASA atmospheric variability experiment (AVE I), Part I: Data tabulation. NASA TM X-2938, Goerge C. Marshall Space Flight Center, Alabama, 681 pp.

Shuman, F. G., 1957: Numerical methods in weather prediction: II. Smoothing and filtering. Mon. Wea. Rev., 85, 357-361.

Smith, P. J., 1969: On the contribution of a limited region to the global energy budget. Tellus, 21, 202-207.

_____, 1970: A note on energy convesions in open atmospheric systems. J. Atmos. Sci., 27, 518-521.

Smith, P. J., 1971: An analysis of kinematic vertical motions. Mon. Wea. Rev., 99, 715-723.

_____, 1973a: Mid-latitude synoptic scale systems: Their kinetic energy budgets and role in the general circulation. Mon. Wea. Rev., 101, 757-762.

_____, 1973b: The kinetic energy budget over North America during a period of major cyclone development. Tellus, 25, 411-423.

_____, and S. P. Adhikary, 1974: The dissipation of kinetic energy in large-scale atmospheric circulations. Rev. Geophys. Space Phys., 12, 281-284.

_____, and L. H. Horn, 1969: A computational study of the energetics of a limited region of the atmosphere. Tellus, 11, 193-200.

Tracton, M. S., 1973: The role of cumulus convection in the development of extratropical cyclones. Mon. Wea. Rev., 101, 573-593.

Vincent, D. G., 1974: Parameters related to the mean state of available potential energy of the tropical Atlantic. Proc. Internat. Tropical Meteor. Meeting, Nairobi, Kenya, Amer. Meteor. Soc., Part I, 81-89.

_____, K. E. Bossingham, and H. J. Edmon, Jr., 1976: Comparison of large scale vertical motions computed by the kinematic method and quasi-geostropic ω-equation. Preprints of Papers, Sixth Conf. on Weather Forecasting and Analysis, Amer. Meteor. Soc., Albany, 357-364.

_____, and L. N. Chang, 1975: Kinetic energy budgets of moving systems: Case studies for an extratropical cyclone and hurricane Celia, 1970. Tellus, 27, 215-233.

_____, W. R. Gommell, and L. N. Chang, 1974: Kinetic energy study of hurricane Celia, 1970. Mon. Wea. Rev., 102, 35-47.

Ward, J. H., and P. J. Smith, 1976: A kinetic energy budget over North America during a period of short synoptic wave development. Mon. Wea. Rev., 104, 836-848.

West, P. W., 1973: Atmospheric energetics as related to cyclogenesis over the eastern United States. NASA CR-2189, Marshall Space Flight Center, Alabama, 103 pp.

Wiin-Nielsen, A., 1968: On the intensity of the general circulation of the atmosphere. Rev. Geophys., 6, 559-579.

Williams, K. T., 1970: A statistical analysis of satellite-observed trade wind cloud clusters in the western north Pacific. Atmos. Science Paper No. 161, Colorado State University, Fort Collins, 80 pp.

Wilson, G. S., and J. R. Scoggins, 1976: Atmospheric structure and variability in areas of convective storms determined from 3-h rawinsonde data. NASA CR-2678, National Aeronautics and Space Administration, Washington, 118 pp.

Young, H. D., 1962: Statistical Treatment of Experimental Data. New York, McGraw-Hill Book Co., 172 pp.

APPENDIX

Rawinsonde Stations Participating in AVE IV Experiment

Station Number	Location
208 (CHS)	Charleston, South Carolina
211 (TPA)	Tampa, Florida
213 (AYS)	Waycross, Georgia
220 (VPS)	Apalachicola, Florida
226 (CEN)	Centerville, Alabama
232 (BVE)	Boothville, Louisiana
235 (JAN)	Jackson, Mississippi
240 (LCH)	Lake Charles, Louisiana
248 (SHV)	Shreveport, Louisiana
255 (VCT)	Victoria, Texas
260 (SEP)	Stephenville, Texas
261 (DRT)	Del Rio, Texas
265 (MAF)	Midland, Texas
304 (HAT)	Hatteras, North Carolina
311 (AHN)	Athens, Georgia
317 (GSO)	Greensboro, North Carolina
327 (BNA)	Nashville, Tennessee
340 (LIT)	Little Rock, Arkansas
349 (UMN)	Monette, Missouri
363 (AMA)	Amarillo, Texas
402 (WAL)	Wallops Island, Virginia
405 (IAD)	Sterling, Virginia (Dulles Airport)
425 (HTS)	Huntington, West Virginia
429 (DAY)	Dayton, Ohio
433 (SLO)	Salem, Illinois
451 (DDC)	Dodge City, Kansas
456 (TOP)	Topeka, Kansas
486 (JFK)	Fort Totten, New York (Kennedy Airport)
518 (ALB)	Albany, New York
520 (PIT)	Pittsburgh, Pennsylvania
528 (BUF)	Buffalo, New York
532 (PIA)	Peoria, Illinois
553 (OMA)	Omaha, Nebraska
562 (LBF)	North Platte, Nebraska
606 (PWM)	Portland, Maine
637 (FNT)	Flint, Michigan
645 (GRB)	Green Bay, Wisconsin
654 (HUR)	Huron, South Dakota
655 (STC)	St. Cloud, Minnesota
662 (RAP)	Rapid City, South Dakota
11001 (MFS)	Marshall Space Flight Center, Alabama
22002 (FSI)	Fort Sill, Oklahoma

NASA- Langley, 1977